Journal of ISAS

An open access peer reviewed quarterly e-journal by
Indian Society of Analytical Scientists

Cover page images(5)- courtsey Pixabay.com

<u>Message from Dr R. Chidambaram</u>

Dear Dr. Chandrachoodan,

I am very happy to note that ISAS, for the first time in India, is bringing out a Journal in Analytical Sciences, named as Analytica India. Analytical sciences are essential for many areas including healthcare and biology, environmental monitoring, forensics, and of course, research in chemistry, physics and other disciplines.

I am sure that Analytica India, as it will be managed by highly experienced and reputed Indian scientists from DAE and ISRO, and other leading Indian academicians, will maintain the highest standards in terms of content and quality,

I send my best wishes to Analytica India for becoming a popular journal of high international repute.

Regards

R. Chidambaram
AICTE Distinguished Chair Professor &
Chairman (Honorary),
School of Advanced Studies in Nuclear Science & Technology, BARC

Message from Dr Anil Kakodkar

Dear Dr. Chandrachoodan,

I am very happy to note that ISAS has embarked upon, for the first time in India, the responsibility of running a high quality Journal 'Analytica India' in the field of analytical sciences.

I am sure that it will be of the best standard in content and quality and bridge a key gap through the efforts of active scientists from DAE and ISRO, along with other reputed Indian academicians.

I wish that Analytica India soon becomes a very popular Indian Technical Journal of International reputation.

With best regards,

Anil Kakodkar
Chairman, Atomic Energy Commission &
Secretary, Department of Atomic Energy (former)

June 09, 2022

Dear Dr. Chandrachoodan,

I am very happy to note that ISAS has embarked upon, for the first time in India, the responsibility of running a Journal in Analytical Sciences, named as Analytica India.

I am sure that it will be of the best standard in content and quality, as it is managed by highly experienced and reputed Indian Scientists from DAE and ISRO, along with reputed Indian academicians.

I wish that the Analytica India soon become a very popular Indian Technical Journal of International reputation.

Thanking you & with best regards,

Yours sincerely,

(K.N. Vyas)

Dr. P.P Chandrachoodan
President, ISAS

डॉ. अजित कुमार मोहान्ती
Dr. Ajit Kumar Mohanty

भारत सरकार
Government of India

निदेशक, भाभा परमाणु अनुसंधान केंद्र
Director, Bhabha Atomic Research Centre
सदस्य, परमाणु ऊर्जा आयोग
Member, Atomic Energy Commission

MESSAGE

Analytical science having footprint across all the domain of science & technology, plays a key role in healthcare diagnostics, environmental monitoring, forensics, chemical biology, pharmaceuticals, chemical engineering, synthetic chemistry and sustainability sciences. With the continuous developments of various advance instruments and also the methodologies of analysis, the arena of quality control which is an essential component of various field assumes great significance. Advances in scientific fields demands faster, efficient, economical, sensitive, selective, accurate, and simple analytical techniques. In this context, the introduction of journal 'Analytica India' by Indian Society of Analytical Scientists is very timely. This will definitely help the researchers to share their research and innovations with scientific community and also help the analysts to adopt the latest analytical techniques in their respective fields.

I am sure that 'Analytica India' with its highly qualified and experienced editorial team members will be of the desired standard in content and quality.

I wish that Analytica India soon become a very popular Indian technical journal noticed internationally.

Ajit Kumar mohanty

(Dr. Ajit Kumar Mohanty)

Message from President ISAS

Congratulations to the **Internationally Reputed Indian Analytical Scientists**, who have contributed to the tremendous All Round technical growth of India,and who are also the strength behind the organisation of this **Journal of ISAS**, titled as **Analytica India.**

I wish the Analytica India a grand popularity amongst the Indian National and International scientific fraternity, both in terms of Content and Quality, as well as Relevance and Acceptability.

I wish to acknowledge the yeomen efforts put in by the Advisory Committee and the Editorial Committee of the ISAS Journal, as well as appreciate the prudence and Wisdom expressed by the Executive Committee of Indian Society of Analytical Scientists, for embarking upon a much needed Indian Journal on this topic.

Further, I wish to gratefully acknowledge the highly appreciative and supportive Messages to Analytica India, given by the contemporary leaders and achievers of great land marks of Self Reliance in Indian Science and Technology Scenario, like Dr R. Chidambaram, Dr Anil Kakodkar, Dr KN Vyas and Dr AK Mohanty, included in this issue of Analytica India.

I wish well for Analytica India to become a very reputed International Journal, very soon.

(Dr. P. P. Chandrachoodan)
President, ISAS.

Message From Dr. Raghaw Saran

Vice President, ISAS (India)

Chief Advisor and Publisher, `Analytica India'

Friends, I am very much humbled to publish and present to you all the very first inaugural issue of Vol.1(1), July 2022, an open access peer reviewed e-journal, all settled with the name `Analytica India' but suddenly, to our utmost dismay, it was brought to our notice that the name was already registered trademark of some other organisation leaving us with the only sensible logical solution of changing the name to an already registered name available to us. The matter was quickly resolved by changing the name from Analytica India to **Journal of ISAS.** After all a stitch in time saves nine and friends, after all what is there in a name, rose is after all a rose only. Dedication of the whole team behind the publication of journal is absolutely the same. It's indeed a great dream come true moment to all the executive members of ISAS and also to all the members associated with the process of publishing the journal.

The inconvenience caused to one and all, due to changed name, subscribing authors, reviewers, sponsors is deeply regretted. Above all, our sincere most apologies to the great leaders of scientific world, Chairman, AEC, Secretary to the govt. of India, DAE (Former and present), Director BARC who had blessed our Journal with inspiring and motivating messages, due to discomfort caused by the change of name of the journal to **Journal of ISAS**. All concerned, directly or indirectly, may please note that name of the journal mentioned as Analytica India stands changed to **Journal of ISAS** with immediate effect (as resolved by the competent authority) and the use of Analytica India, as name of ISAS journal is totally withdrawn from the messages from dignitaries or in any other form.

So far ISAS, in general was confined to conferences, theme meetings, half day seminars and various other activities across ten chapters of ISAS. During pandemic, we resorted to the webinar mode and organised 75 talks, one on every Saturday evening, delivered by eminent speakers from wide cross section of scientific, technology and industrial community pertaining to various parts of the country. Recently, we organised two conferences, IASC-2022 (national) and NHCHTCS-22 (*international*) respectively, at Kerala and Nagpur. But still we were restless to realize our long-cherished desire of have our own journal. The matter was proposed by our President and was happily agreed by Dr. Nilima Rajurkar, Chairman, ISAS Pune Chapter, to be Editor in Chief for the journal. Subsequently, our journey began with the rocket speed consisting of formulations of the journal, various committee members and many more aspects, the result of which is **Journal of ISAS**' a journal open to you all, freely, today.

Needless to mention that during conferences, the interactions amongst scientific community are of time bound nature and to some extent not that long lasting, hence partially fructified. On the contrary, journal, that too e journal, with no fees for publishing at the end of authors and also for readers, researchers, totally being free, can be a permanent platform to have continued interactions. Also, the pace with which the science is progressing, analytical sciences assume newer dimensions so rapidly that analytical figures of merit, once thought impossible, is becoming reality. Creative thinking in analytical sciences and then bringing it to the application end is possible just because of new, constant researches across the globe, free access to knowledge, and all, assuming a real dimension today. This is mainly due to like-minded people working hard to innovate new ready to use applications, through off line, online interactions and data publication with high pace daily in various journals. The present attempt by ISAS to publish our own ISAS Journal, **Journal of ISAS** is one such milestone to encourage, motivate younger generation scientists affiliated to various universities, institutions and industries, We also aim to integrate our younger generation researchers across the country and also globally with ISAS playing a pivotal role with the expertise available with it in form of executive member scientists, advisors and editors for journal who have expertise in various areas of analytical sciences for over three decades at least.

I am very confident that communicating research papers in '**Journal of ISAS**' journal, provides an opportunity for your paper to get reviewed by experts with par excellence expertise in respective fields ensuring the high quality of papers. I am happy to let you know that we have already received papers sufficient even for the next issue.

My whole hearted gratitude to our ISAS President for keeping faith in me and bestowing the team to shoulder the responsibility of a very exciting journey towards the task of completion of the first inaugural issue of the journal '**Journal of ISAS**'. I am very much thankful to the Editor in Chief, Analytica India' for carrying out the highly strenuous job of bringing the manuscripts, meticulously to the 'acceptance' level scientifically as per journal's guidelines, who is well backed by strong team of advisors, editors, reviewers, EC members of ISAS, layout designers and printing press personnel. I wish to express my sincere thanks to Dr V. Balram for his continued support. My special thanks to all our sponsors for supporting us by the way of advertisements in the current issue of the journal

Our gratitude needs no bound for the kind inspiring motivational messages blessing us to move ahead incessantly on the new path from Chairman, Atomic Energy Commission, Secretary to the Department of Atomic Energy, Govt. of India (former and present) and Director, BARC, for the journal. Deeply gratified to you all Sir!

I wish to place on record, my special thanks to one and all who have contributed directly or indirectly, towards bringing out this issue of our journal. Lastly and most importantly to all the authors for sending the manuscripts to us. As is well known that the manuscripts published in the journal will always be permanent. I on behalf of my all-vibrant team members of journal and EC members of ISAS would be happy to keep the promise to you all towards taking the level of the journal to greater heights by way of acquiring ISSN, doi, UGC approval, etc. very soon and incorporating novel research articles from various domains of analytical sciences across the country and globe to be an equal partner in all round development of science leading to betterment of mankind.

Dr. Raghaw Saran

Editorial

It is with immense pleasure, pride and enthusiasm, I invite you to read the inaugural issue of our Journal "Journal of ISAS". It represents the collective thinking of a group of innovative individuals from different disciplines of scientific fields with whom I am privileged to work. In this inaugural issue you will find an array of works right from cost effective techniques for waste water treatment to an exhaustive review on widely used technique of ICPMS and its applications. Quite a lot of efforts have been put in the development of this journal and I am sure you will see them reflected in this volume and its subsequent impact on the scientific community. "Journal of ISAS" will be always innovative providing a special space for scholarly works representing the integration of all branches of science.

I must give special thanks to Dr. P.P. Chandrachoodan, President ISAS who had the vision to embark a new venture of starting our own scientific journal. His ability to draw together diverse talents and his confidence in board members brought this journal to fruition. It has been an interesting journey right from the inception of journal to making a dream true. I would like to express my sincere gratitude towards Dr. Raghaw Saran, Vice president ISAS and Chairman, Advisory board of Journal of ISAS for his constant guidance, inspiration and support at each stage of journal progress. I wish to express my special thanks to Editorial board members: Dr. Vijayalaxmi Adya and Dr. Vinay Bhandari for their continuous cooperation in this journey. Without the guidance, support, and feedback of the Editorial and Advisory board members and reviewers, it would have been impossible to offer the selections you will see in this issue. I congratulate all the researchers who contributed their work in this inaugural issue. I would like to put on record my sincere thanks to Kailash Gharat, Shivani Kantak and Vaibhav Parse for their technical support.

I am very much grateful to all the dignitaries for their blessings to the journal in the form of inspirational and motivational messages.

Dr. Nilima Rajurkar
Editor in Chief, Journal of ISAS
..

Contents

Inductively Coupled Plasma-Tandem Mass Spectrometry (ICP-MS/MS) and Its Applications

V. Balaram

CSIR-National Geophysical Research Institute, Hyderabad -500 007, India

Email:balaram1951@yahoo.com

Abstract

During the last about 10 years, the inductively coupled plasma tandem quadrupole mass spectrometry (ICP-MS/MS) technique with reaction cell is being utilized for the analyses of several trace elements/isotopes at very low concentration levels in a variety of matrices including geological, environmental, biological, medical, nuclear, agriculture, food, material and metallurgical sciences. Both solution nebulization, as well as direct analysis of samples by laser ablation (LA-ICP-MS/MS), are utilized for sample introduction. In fact, ICP-MS/MS technique with collision reaction cells eliminated the need for laborious chemical separations using methods such as ion-exchange or solvent extraction procedures to eliminate/minimize spectral and matrix interference effects as these interferences are removed using online chemical reactions within the instrument itself (chemical resolution). In addition, the technique is hyphenated with chromatographic techniques such as GC and HPLC for a variety of applications. The detection limits for several elements in the periodic table lie in the pg/ml-fg/ml range, and the technique compares favourably with the expensive, complex, and superior high resolution-ICP-MS (HR-ICP-MS), both in terms of the detection limits as well as the ability to remove the most complex interferences. Thus, the ICP MS/MS made the determinations of elemental as well as isotopic concentrations very simple and easy even in complex materials with several novel quantification approaches. This article provides an overview of these new developments during the last decade along with several applications in all areas of science and technology.

Key words: ICP-MS/MS, LA-ICP-MS/MS, GC-ICP-MS/MS, collision reaction cell, reaction gas, speciation.

Introduction

From the time the first publication[1] on inductively coupled plasma mass spectrometry (ICP-MS) by Houk et al. in 1980 and the first commercial instruments released in 1983, the ICP-MS technology has become more efficient and more powerful over the years with a lot of significant instrumental developments leading to the development of powerful instruments such as ICP-time-of-flight-MS (ICP-TOF-MS), high resolution-ICP-MS (HR-ICP-MS) and multi collector-ICP-MS (MC-ICP-MS) incorporating a variety of technologies for the interference removal such as cool plasma, collision/reaction cell technology (CCT), dynamic reaction cell (DRC) technology, collision reaction interface (CRI), kinetic energy discrimination (KED), tandem mass spectrometry (ICP-MS/MS)/triple quadrupole ICP-MS, and multi-quadrupole ICP-MS with each technique having its strengths and limitations[2,3]. Several companies have developed quadrupole-based ICP-MS instruments equipped with extra quadrupole-, hexapole- or octopole- containing cells that can be pressurized with a gas (e.g., H_2, O_2, NH_3) or a combination of these gases to remove interferences with reasonable success. But despite these developments in ICP-MS technology, the removal of spectroscopic interferences has been a continuous problem in several cases all these years. Though most of the interferences can be removed by utilising HR-ICP-MS instrumentation, its higher cost and the instrument complexity prohibit its abundant usage. In addition, there is also a limitation (maximum ~10,000R) on the resolution of commercial HR-ICP-MS instruments. But the recently developed ICP tandem mass spectrometry or ICP-MS/MS brought a remarkable change in the ways to manage and effectively eliminate even the most complex interferences in ICP-MS studies. Zhu et al.[4] recently reviewed the trends, advances, and a few applications of ICP-MS/MS, based on the studies published mainly from January 2018 to July 2021. But this article aims to provide a comprehensive overview of the ICP-MS/MS from its development to its current status, emphasizing its growing applications in different areas during the last decade.

Instrumentation

ICP-tandem mass spectrometer or ICP-MS/MS is a new type and the latest generation ICP-MS instrument. The main difference between ICP-MS/MS and the traditional ICP-MS system is the introduction of an additional quadrupole (Q1) before a collision reaction cell (CRC). Sample introduction and all other related aspects remain more or less the same. When a particular m/z is fixed in Q1, only that m/z is allowed to enter into the CRC, as a result, more

efficient interference correction even for the most complex matrices is possible in the CRC before the analyte is finally detected by the analyzer quadrupole (Q2) (Fig. 1a). For example, for the determination of iron (^{56}Fe) in a rock matrix when 56 mass is chosen, all other masses will be rejected by Q1, and ions having only m/z 56 will be allowed to enter the CRC. As a result, ^{56}Fe$^+$ and ^{40}Ar^{16}O$^+$ only will enter the CRC. In CRC, the ion, ^{40}Ar^{16}O$^+$ reacts with gas like H$_2$ and breaks, and as a result, only ^{56}Fe will only be allowed to pass through the analyser quadrupole (Q2) and detected without any interference by the *on-mass* mode[5]. In another example, Ti$^+$ is made to react with a mixture of hydrogen and oxygen and converted to TiO$^+$ and determined by the *mass-shift* mode which eliminates all interferences on Ti$^+$ ions. One firm uses an octopole-based reaction system (ORS^3) for CRC and this instrument is named as triple quad ICP-MS. When the *mass-shift* mode is selected, Q1 filters only the selected m/z ratio which will enter into the CRC filled with reaction gas. Under selected optimum conditions analyte ions will react efficiently with gas molecules while the interfering ions will not react at all. This allows the analyte ion to be converted into a reaction-product ion with a different m/z ratio than the original ion which had interference problems. The new m/z formed after the reaction in the CRC is then selected in Q2 and detected. When the on-mass mode is selected, the same m/z is fixed on both quadrupoles and spectral interferences are removed by making the interfering ion to react efficiently with the reaction gas. As a result, interfering polyatomic species will be converted into new species with a m/z ratio different than the one of the analytes and will not get detected by the second quadrupole. The choice between these two different modes depends on the reaction efficiency. Recently Fu et al.[6] proposed N$_2$O as a universal reaction gas to overcome spectral interferences since N$_2$ has a lower O atom affinity (1.6 eV) than the O atom (5.2 eV), and also N$_2$O was a more effective O atom transfer gas than O$_2$. In addition, when N$_2$O was selected as the reaction gas, high sensitivities and low limits of detection (LODs) were obtained by mass shift methods for several analytes. In an attempt to understand the need for an internal standard in ICP-MS/MS studies, Bolea-Fernandez et al.[7] made a study both *on-mass* as well as a *mass-shift* mode on 17 elements covering a wide range of masses (24–205 amu) and ionization energies (3.89–9.39 eV), and concluded that the internal standard must also be detected in the same way as analyte masses for obtaining the best results.

Performance characteristics and other advancements

Balcaen et al.[8] provided the details of the development of ICP-MS/MS and its performance characteristics with examples of a few applications. Sample introduction by all possible methods: i) sample solution nebulisation, ii) laser ablation sampling (LA-ICP-MS/MS), iii) sample introduction through GC (GC-ICP-MS/MS), and iv) sample introduction through LC/HPLC (LC/HPLC-ICP-MS/MS) are possible for a variety of applications (Fig. 1b-e). The major advantage is that the existing single quadrupole ICP-MS solution nebulisation methods and most of the collision and reaction methods used can be simply transferred to ICP-MS/MS applications without significant modifications. The combination of separating techniques such as GC or LC or HPLC when coupled with ICP-MS/MS, becomes an important analytical tool for diverse applications. In fact, GC-ICP-MS has proven to be very useful for classical organometallics analysis (i.e., Sn, Pb, Hg, and As) in environmental-, biological- and industrial-related samples[9]. The analysis is relatively easy as the interferences are removed only using online chemical reactions. The two-quadrupole arrangement helps to drastically reduce the chemical noise levels, leading to much better detection limits that fall in the sub-ng/g-pg/g range for most elements in the periodic table. Fig. 2: presents a comparison of limits of detection for various elements/isotopes between ICP-MS/MS and HR-ICP-MS. It can be seen that for the majority of the elements, the detection limits of ICP-MS/MS are approaching those obtainable by HR-ICP-MS. Additionally, a number of elements can be determined simultaneously under the same set of instrument settings without compromising the accuracy and precision of the results.

Applications

Despite the fact that ICP-MS/MS technique is only a decade old, it has become very popular because of its versatility, capability to resolve even the most complex interferences, and offer lower detection limits and accuracy of determination[10]. Following are some of the application studies reported during the past decade in a wide range of scientific fields.

i) Geological

Geological, geochemical, and mineral exploration studies require the determination of major, minor, trace, and ultra-trace elements in different types of geological materials[11]. Isotope geochemical and geochronological studies require the accurate and precise determination of

isotopic concentrations and isotopic ratios of different elements[12]. Zimmermann et al.[13] optimised a new and total digestion protocol (50 mg aliquots, microwave digestion, 5 mL HNO_3, 2 mL HCl, 1 mL HBF_4) for the analysis of 48 elements in different sediment reference materials by ICP-MS/MS. Zhi-fei et al.[14] used oxygen reaction mode with ICP-MS/MS to eliminate Zr and Mo ion interference on Cd, for its determination in soil samples. Attapulgite clay is a water-rich magnesium aluminosilicate mineral with a layered chain structure. The different geneses of the deposit results in a different composition of trace elements in attapulgite clay. Li and Li-15 determined several trace elements in attapulgite clay samples by ICP-MS/MS by NH_3/He as reaction gases[15]. Whitty-Léveillé et al.[16] made a comparative study of sample dissolution and instrumental analytical techniques for the determination of rare earth elements (REE) in mineral matrices and some related reference materials. The combination of the high digestion temperatures (1050°C) and using $LiBO_2$ as a flux was found to be the most effective strategy for the sample digestion compared to open-vessel acid and microwave digestions, and the REE data provided by ICP-MS/MS was in excellent agreement with the certified values compared to those obtained by conventional single quadrupole ICP-MS and microwave plasma atomic emission spectrometry (MP-AES). This was mainly because of the perfect elimination of the spectral interferences by tandem ICP-MS, which is not possible by conventional single quadrupole instruments. MP-AES is already an inferior technique compared to ICP-MS, especially for the determination of REE in geological materials[17]. Zhu et al.[18] determined REE concentrations in natural waters by ICP-MS/MS directly without any separation or preconcentration. Oxygen as the reaction gas was used for eliminating spectral interferences. REE data in SLR-4, the natural river water reference material (NRC-CNRC), obtained by ICP-MS/MS are presented in comparison with other well-established analytical techniques such as conventional single quadrupole ICP-MS, HR-ICP-MS, isotope dilution-HR-ICP-MS, along with certified or compiled values (Table 1). The precisions and accuracies achieved for different REE at different concentrations are sufficient to identify the natural variations or anomalies of Ce, Eu, and Gd in the REE distribution patterns in natural waters.

Yang et al.[19] measured ng/g contents of Rh and Pd in Cu-rich minerals by LA-ICP-MS/MS, using a mixture of ammonia (NH_3)/He (10%/90%) reaction gas, respectively, to attenuate $CuAr^+$ interfering species on ^{103}Rh and ^{105}Pd. According to the authors, when compared with that of a single quadrupole ICP-MS, the most accurate and precise measurements of Rh at less than 10 ng/g and Pd at ~ 100 ng/g in Cu-rich minerals were achieved by LA-ICP-MS/MS

at an optimized NH_3/He reaction gas flow rate. LA-ICP-MS/MS was used for *in-situ* dating of K-rich minerals, e.g., micas and K-feldspar, by the Rb–Sr isotopic system. Online chemical separation of Rb and Sr is possible by the reaction of Sr with O_2 in the reaction cell leading to the formation of SrO^+ and Rb doesn't react. Use of O_2 reactions provide stable analytical conditions sufficient for precise and accurate determination of Rb/Sr and Sr/Sr isotopic ratios using 80-micron laser ablation spots. It was also found that by using N_2O or SF_6 as a reaction gas for *mass-shifting* of ^{87}Sr to avoid interference on ^{87}Rb, sensitivity improved by ~10 and ~8 times, respectively, compared to the use of O_2[20]. Re-Os dating of molybdenite by LA-ICP-MS/MS was reported recently by Hogmalm et al.[21]. A major advantage of *in-situ* LA-ICP-MS/MS dating is the direct analysis of molybdenite in thin-sections and epoxy mounts, which allows analysis of sub-millimeter grains in a microtextural context. The Rb/Sr isotopic system, one of the most established geochronological methods and is a useful tool for constraining the timing of magmatic and metamorphic events through geological history. It is based on the radioactive β^- decay of ^{87}Rb to ^{87}Sr, with a half-life of 48.8 billion years[22]. The precision of this technique is largely dependent on the laser system and ICP–MS/MS conditions used. Traditionally, $^{87}Rb/^{86}Sr$ and $^{87}Sr/^{86}Sr$ isotopic ratios were measured by thermal ionization mass spectrometry (TIMS) or more recently by MC-ICP-MS[23]. However, these approaches require isotopic spiking and time-consuming chemical separations of Rb and Sr from the sample matrix. LA-ICP-MS/MS was used to date the Cu-Au mineralization event in the Arabian Shield, Saudi Arabia using the *in-situ* Rb-Sr dating technique. These studies indicated that the development of the Umm Farwah shear zone occurred at 651 ± 20 Ma, followed by the emplacement of Mount Ablah pegmatite dated at 625 ± 19 Ma. Subsequent greisenisation of local igneous rocks took place between 613 Ma and 589 Ma, followed by a younger reactivation event(s) dated between 580 Ma and 530 Ma during which period the Cu-Au mineralisation was believed to form in the Mount Ablah region[24]. Another interesting study is the dating of apatite mineral, which is an accessory mineral in various igneous, metamorphic and clastic sedimentary rocks, by the U-Pb method. However, ^{204}Pb is difficult to measure using ICP-MS instruments because of the isobaric interference of ^{204}Hg on ^{204}Pb. Even HR-ICP-MS cannot resolve the overlap of ^{204}Hg on ^{204}Pb, as this requires a resolution of 500,000 as commercial HR-ICP-MS can go maximum up to 10,000R. In such situations, one needs to utilize alternative approaches such as the use of ICP-MS/MS as it can allow the online chemical separation by using NH_3 which reacts efficiently (> 98%) with Hg while isotopes of Pb are not affected. Gilbert and Glorie[25] proved that the Hg interference on ^{204}Pb can be efficiently removed using NH_3 as the reaction gas for

LA-ICP-MS/MS analysis, and used the ^{206}Pb/^{204}Pb and ^{207}Pb/^{204}Pb ratios for accurate common Pb corrections. Simpson et al.[26] used LA-ICP-MS/MS for the direct *in-situ* geochronological studies of garnet, apatite, and xenotime minerals with several advantages such as very rapid and no chemical separations required. Despite all these advantages, there are still problems with this technique for the successful application of the LA-ICP-MS/MS for isotopic ratio determinations. For example, the Rb-Sr dating studies are currently poorly quantified and unconstrained 'elemental fractionation phenomena' and 'matrix effects', as well as the general lack of suitable chemically/mineralogically well-characterized reference materials (i.e., mineral-specific standards) that are homogeneous at the micro-scale level.

ii) *Marine sciences*

Precise data of trace elements/isotopes in ocean waters, sediments, and biological species in marine environments are required for understanding various marine geochemical aspects such as the sources and processes that define the distribution of different elements/isotopes in marine environments and biogeochemical cycling. Sulphur isotopic concentrations both in marine waters as well as in sediments are useful for tracing seawater intrusion in coastal systems in addition to several other applications such as providing insights into the early earth sulphur cycle, paleo-redox conditions of the ocean-atmosphere system, and ancient microbial/abiotic processes. Determination of sulphur isotopes in complex natural liquid or solid samples by conventional gas source isotope ratio mass spectrometry (GS-IRMS) is complicated, time-consuming, and relatively expensive. Leyden et al.[27] utilised ICP-MS/MS for the accurate and precise determination of sulphur isotope abundances (i.e., ^{34}S/^{32}S ratios, expressed as δ^{34}S) in coastal waters proving that this method can meet the growing applications of sulphur isotopes. Interaction of seawater with oceanic lavas at low temperatures (10's of $\circ$C) away from mid-ocean ridges plays a significant role in the major element composition of seawater. The secondary minerals that form during these processes are important for understanding this process properly. Laureijs et al[28] dated celadonite from altered upper oceanic crust using LA-ICP-MS/MS using CH_3F as a collision reaction gas. Based on these studies, the authors concluded that the environmental conditions within the first ~20 My after-crust formation will control the intensity of alteration and chemical exchanges between seawater and basalt. Jackson et al.[29] determined the concentrations of Mn, Fe, Ni, Cu, Zn, Cd and Pb in seawater using offline extraction, and ICP-MS/MS.

iii) *Nuclear*

Plutonium (Pu) isotopes, especially ^{239}Pu and ^{240}Pu with half-lives of 24,110 years and 6561 years, respectively, are among the most important and dangerous transuranic nuclides in the environment due to their high radiotoxicity and long retention time in the environment. Pu is released to the environment mainly through atmospheric nuclear weapons testing, nuclear accidents, and nuclear fuel reprocessing plants. Xing et al.[30] used three different digestion methods (acid leaching with 8 M HNO_3, aqua regia, and lithium metaborate fusion) for the accurate determination of Pu in soils by ICP-MS/MS using NH_3/He as cell gas. Determination of low-level plutonium in high uranium samples is challenging because of the abundance sensitivity (tailing of ^{238}U to m/z = 239 and 240), isobaric and polyatomic ions interferences (e.g., $^{238}U^1H^+$). Hou et al.[31] combined ICP-MS/MS with a dynamic collision/reaction cell and eliminated the interference of uranium hydrides ($^{238}U^1H^+$ and $^{238}U^1H^{2+}$) using CO_2 as reaction gas by converting hydrides to oxides of uranium ions (UO^+/UO_2^+) but still keeping the intensity of the Pu^+ signal. The tailing interference of $^{238}U^+$ (abundance sensitivity) was eliminated significantly by suppressing the $^{238}U^+$ signal. This method enabled accurate determination of $<10^{-15}$ g/g level plutonium isotopes in environmental samples even in a uranium debris sample with a U/Pu atomic ratio of up to 10^{12}. The presence of fission products including numerous isotopes of lanthanides released from nuclear power plants and nuclear weapons testing can impact the environment. ICP-MS/MS was used as a tool to evaluate variations in isotopic ratios of selected lanthanides as tracers for the assessment of nuclear anthropogenic contamination in the environment[32].

Both ^{135}Cs and ^{137}Cs, enter the environment due to anthropogenic nuclear activities. Zheng et al.[33] used ICP-MS/MS and N_2O as collision gas to significantly reduce the isobaric interferences ($^{135}Ba^+$ and $^{137}Ba^+$) and polyatomic interferences ($^{95,97}Mo^{40}Ar+$, $^{119}Sn^{16}O^+$, and $^{121}Sb^{16}O^+$) to determine ^{135}Cs and ^{135}Cs/^{137}Cs isotope ratio at global fallout source environmental samples. Analysis of concrete is of significant importance for nuclear decommissioning as some concrete structures are exposed to high neutron fluxes, resulting in activation products. For example, neutron activation of stable ^{40}Ca (96.94% abundance) will lead to the production of ^{41}Ca [half-life; $(9.94 \pm 0.15) \times 10^4$ years][34]. Measurement of ^{41}Ca by conventional ICP-MS is prevented by multiple interferences, some of which cannot be removed by offline chemical separations. ICP-MS/MS technique with NH_3, H_2, and He as

collision gases proved to be most effective in accurately detecting and determining ^{41}Ca in concrete samples. More details are provided by Russell et al.[35].

iv) *Petroleum industry*

Petroleum products can be analyzed using ICP-MS/MS by direct injection of petroleum products after solvent dilution. For the determination of heavy elements (Z>70) in organic matrices, the ICP-MS/MS was less sensitive than the HR-ICP-MS. For light elements (Z<40), the sensitivity was similar or better using ICP-MS/MS (Figure 2). For elements such as Si, S, Ca, Fe, which have severe interference problems, but by using He, O_2 or H_2 as reaction gases, ICP-MS/MS gave similar or better detection limits (LOD) than the HR-ICP-MS in medium resolution[36]. Though silicon plays a crucial role in many fields such as food, semiconductor, steel, and oil industries, monitoring its concentration in the petroleum industry during the refining process is important due to its poisoning effect and decreasing its activity on hydrogenation catalysts which will have a great economic impact. Silica can be determined by a number of techniques like inductively coupled optical emission spectrometry (ICP-OES) and ICP-MS, but the situation becomes more complex when speciation analysis is required as gasoline samples may contain around 200 different hydrocarbon compounds. Sánchez et al[37] used GC-ICP-MS/MS for the analysis of different petroleum derivatives. Hydrogen was used as a reaction gas in the octopole reaction cell (ORC) to eliminate the interference of $^{12}C^{16}O^+$ and $^{14}N^{14}N^+$ on $^{28}Si^{+}$. Cyclic siloxanes (D3-D6) were confirmed as the main silicon compounds present in coker naphtha samples. Such silicon speciation studies in real coker naphthas will allow the development of trapping systems to remove these compounds before hydrotreating catalysts. GC-ICP-MS/MS was also used to determine the sulphur-containing petroleum derivatives[38]. Chlorinated compounds (HCl or organic chlorides) in crude oils can create problems during refinery operations. Cl is a known challenging element to be determined by quadrupole ICP-MS. Nelson et al.[39] developed a method for the accurate determination of chloride in crude oils by direct dilution using ICP-MS/MS. Complex interferences including sulphur-based interferences were effectively eliminated using H_2 cell gas and mass-shift mode. Amais et al.[40] determined P, S, and Si in biodiesel, diesel, and lubricating oil by ICP-MS/MS using oxygen gas as a reaction gas for eliminating interferences. Phosphorus, S, and Si are challenging elements to be determined by quadrupole-based ICP-MS due to severe polyatomic interference.

Environmental

The platinum-group elements (PGE: Pt, Ir, Os, Pd, Rh, and Ru) consist of six elements; those are among the least abundant in the continental crust and have similar physical and chemical properties. Recent studies are showing that the concentrations of Pt, Pd, and Rh are constantly increasing in the environment because of the use of these elements in autocatalytic converters in all automobile vehicles for the reduction of harmful carbon monoxide, nitrogen dioxide, and unburnt hydrocarbon emissions. Their emissions, distribution, migration in different environmental compartments, and their bioavailability are posing one of the biggest human health risks[41,42]. Measurement of PGE and Re in environmental samples, such as soils and water is extremely difficult because of their low-level concentrations. In addition, severe isobaric and polyatomic interferences make their determination by conventional ICP-MS difficult. Mitra et al.[43] determined PGE and Re in road dust samples using ICP-MS/MS after sample decomposition by high-pressure asher (HPA) at a pressure of 130 bars and a temperature of 220∘C, and also adopting a cation exchange procedure for the separation of PGE and Re from the sample matrix, and for complete removal of potentially interfering species arising from Cd, Hg, Zr, Hf, Mo, and W, and with isotope dilution (ID) as a calibration strategy. Table 2 presents the PGE and Re data obtained in a road dust reference sample and a base metal sulphide bearing komatiite sample in comparison with certified values and the values obtained by a nickel sulphide fire-assay ICP-MS procedure[44].

Determination of elemental as well as isotopic concentrations of uranium and thorium is important in monitoring the quality of drinking water, and other environmental issues such as nuclear emergency responses[45]. Ni et al.[46] determined Th (^{230}Th, ^{232}Th) and U (^{234}U, ^{235}U, ^{238}U) isotopes in small volume (20 mL) of water matrices using ICP-MS/MS. Detection limits going down to pg/ml – fg/ml levels for these elements. Amaral et al.[47] described a novel strategy to determine As, Cr, Hg, and V in drinking water by ICP-MS/MS with the detection limits in pg/ml at the 99.7% confidence level. Small volume digests of Antarctic atmospheric particulates (PM_{10}) and of soils, from Australia and South America as potential source areas for atmospheric particulates reaching East Antarctica, were analyzed by ICP-MS/MS. For the introduction of low-volume samples, a setup consisting of a syringe-driven pump that allows it to work at low and stable sample introduction flow rates was utilized. The method requires 240 µL of the sample only, introduced at a sample uptake rate of 20 µL/min,

and allows the straightforward measurement of the $^{87}Sr/^{86}Sr$ isotope ratio without prior Rb/Sr separation[48].

Monitoring pesticide residues in food products is important especially from the point of the health of infants and children, as the quantity of food they ingest per kilogram of body weight is relatively high. Nelson et al.[49] used the GC-ICP-MS/MS method with oxygen as a reaction gas for the selective, sensitive detection and determination of specific hetero-atoms of phosphorus, sulphur, and chlorine-containing pesticides in various food matrices. Zhang et al.[50] used GC-ICP-MS/MS with a *mass-shift* mode for the indirect determination of polybrominated diphenyl ethers in fish tissue using bromine oxide ion. The highest sensitivity was found using N_2O as the reaction gas when compared to other gases such as O_2 and $H_2,$ and He. Klencsár et al.[51] determined the total contents of drug-related Cl and Br in human blood plasma using HPLC-ICP-MS/MS. Hydrogen was used as a reaction gas for monitoring the $^{35}ClH_2^{2+}$ reaction product at a mass-to-charge ratio of 37. Br could be measured by "*on mass*" mode at a mass-to-charge of 79. HPLC was used for the separation of the drug-related entities from the substantial amount of inorganic Cl. It is well known that molybdenum oxides affect Cd determination by conventional ICP-MS. By using ICP-MS/MS, Amais et al.[52] eliminated Mo oxide-based interferences and determined both Cd and Mo using an octopole reaction system (ORS^3) pressurized with oxygen gas in milk powder after microwave-assisted digestion using diluted HNO_3 and H_2O_2.

vi) Biological and medical

Element constitution and distribution in body tissues and fluids have increasingly become key pieces of information in life sciences and medicine, and trace elements may be successfully used as disease biomarkers. Titanium is an inert and biocompatible metal, and its elastic modulus is similar to that of the natural human bone, making it an ideal metal for human implants, such as dental implants and other artificial implants, along with various surgical reconstruction techniques. It is also a highly corrosion-resistant metal because of the thin and stable protective oxide layer spontaneously formed on its surface[53]. However, very minor degradation of all types of metal implants in the human body is observed and the worn metal particles and/or ions get released into body fluids such as serum and urine. Fu et al.[54] used ICP-MS/MS to determine ultra-trace concentrations of Ti in human blood serum using a mixture of H_2 and O_2 as a reaction gas in the CCT for converting Ti^+ to TiO^+ and determined in the *mass-shift* mode by eliminating all spectral interferences. These authors also

successfully cross-checked the results by HR-ICP-MS. Virgilio et al.[55] evaluated ICP-MS/MS protocols using oxygen in the octopole reaction system for the accurate and precise determination of As, Cd, Cr, Ni, Pb, and V in phytotherapy medicines. Two plant-certified reference materials (apple leaves and tomato leaves) were used to check the accuracy. Use of both *on-mass* and *mass-shift* modes for different analytes demonstrated as efficient strategies to correct for spectral overlaps and provided accurate determinations. Despite significant breakthroughs in the understanding, prevention, and treatment of cancer, the disease continues to affect millions of people worldwide. A potential solution to this challenge may lie in nanomedicine, including the use of various nanomaterials for the diagnosis and treatment of cancer[56]. In this context, superparamagnetic iron oxide nanoparticles (SPIONs) are widely tested as tools for drug delivery, magnetic hyperthermia, magnetic resonance imaging, and catching tumor cells[57]. Complete physicochemical characterization of properties of SPIONs is extremely important for safe biomedical applications in vivo. Single particle-ICP-MS/MS (SP-ICP-MS/MS) studies allowed fast and straightforward monitoring of the changes in the structure of SPIONs upon interaction with serum proteins thereby helping to shortlist the investigational nanomaterials before in-depth preclinical testing[58]. Gd has been used in a chelated form as a contrast agent in magnetic resonance imaging (MRI) measurements[59,60], though new research finds direct evidence of gadolinium deposition in biological tissues which can be harmful to patients and is a major concern. However, no data are available in human beings or animals to show adverse clinical effects due to the gadolinium deposition in the brain[61,62]. Clases et al.[63] presented a novel analytical method based on LA-ICP-MS/MS to detect the retention of Gd from contrast agents for MRI in brain and skin tissue samples of patients. Gadolinium was monitored in *mass-shift* mode and this resulted in an improved detection limit. Radium (Ra) is a naturally occurring metal found in uranium and thorium ores in trace quantities. It can cause harmful health effects to humans by getting incorporated into biochemical processes because of its radioactivity and chemical reactivity. Chronic exposure to higher levels of radium over a long period of time may result in an increased incidence of anemia. If radium is swallowed through water or with food, most of it will promptly leave the body in the feces. Xiao et al[64] developed a method for monitoring ^{226}Ra in urine using ICP-MS/MS.

vii) *Agriculture*

The mineral fertilizers are used in agriculture for the proper growth of the crops and to increase the yield during agricultural practices. These mineral fertilizers contain macronutrients (Ca, Mg, N, P, and S), micronutrients (such as Fe and Si), REE, and, in some cases, toxic elements (As, Cd, Hg, and Pb) in their composition. In order to understand the environmental effects and legislations established for controlling agricultural products, it is necessary to analyze mineral fertilizers and agricultural gypsum for toxic elements. Machado et al.[65] evaluated the application of ICP-MS/MS for the determination of As in agricultural inputs with high REE contents. The use of MS/MS in *mass-shift* mode was effective to remove doubly charged interferences from REE on As. When operating in single quadrupole mode, recoveries ranged from 59 to 151%; while values obtained by MS/MS mode varied from 81 to 105% when 0.30 mL/min O_2 was introduced into the ORS reaction cell, demonstrating the usefulness of MS/MS mode. Wang et al[66] developed a method to determine the content of 30 trace elements in rice from different production areas in China using the ICP-MS/MS method. Different gases such as H_2, O_2, He, and NH_3/He, both *on-mass* and *mass-shift* modes were used under optimized conditions. China is a vast country with diverse climatic and geographical conditions, and the crops have different biological characteristics and physical and chemical indices. Principal component analysis of the multielement content of rice samples was used to provide a method basis for rice origin traceability. Molybdenum is an important micronutrient for the plant's growth and the ideal concentration range for this micronutrient in plants is 0.2–2.0 μg/g. However, there are some species in which Mo concentrations as low as 0.02 μg/g, which are enough to maintain vital functions, Mo contents higher than 1000 μg/g can be potentially toxic and hence monitoring of Mo becomes important. Barros et al.[67] determined Mo concentrations in plant materials such as tomato, apple and spinach leaves, and wheat and rice flour, with excellent selectivity, sensitivity, and accuracy by ICP-MS/MS with an octopole reaction system and pressurized oxygen gas and the *mass-shift* mode to remove K-based interferences after microwave digestion using H_2O_2.

viii) *Food safety*

Different government agencies and the World Health Organization (WHO), are putting efforts to standardize food testing practices around the world. Both the world's population and food production are growing at a significant rate and currently, there is a greater need to

be more careful to prevent food contamination. For example, though the intake of fluorine at low concentrations is considered essential, it can become toxic through elevated intake of water or food, which can result in fluorosis and in renal, gastrointestinal, and immunological disorders. Guo et al.[68] developed a method for the determination of total fluorine in foods by ICP-MS/MS using NH_3 as reaction gas with a *mass-shift* strategy. Nelson et al.[49] used GC-ICP-MS/MS with oxygen as a reaction gas for the selective, sensitive detection, and determination of specific hetero-atoms of phosphorus, sulphur, and chlorine-containing pesticides in various food matrices. Although seafood has several advantages for human nutrition, it can accumulate high levels of potentially toxic elements (such as arsenic and mercury) in its tissues, which may represent a risk to human health. Schmidt et al.[69] utilized LC-ICP-MS/MS for the As speciation analysis [AsB, As (III), DMA, MMA, and As (V)] in several types of seafood such as shark, shrimp, squid, oyster, and scallop. Since its development, ICP-MS/MS has been used to analyze several types of food materials including fruit wines, fruit juices, medicinal plants, and bone tissue samples from lambs, piglets, and calves[70-73].

ix) *Material science*

Molybdenum's strength and stability at higher temperatures make it attractive to several high technology applications such as petroleum refining, and optoelectronic devices. Some applications require ultrapure molybdenum, and ICP-MS/MS was utilized for the determination of 28 ultra-trace impurities in molybdenum metal by using H_2, NH_3/He as reaction gases by both *on-mass* and *mass-shift* mode[74]. Fu et al.[75] used ICP-MS/MS for the determination of metallic impurities in (Mg (TFSI)$_2$) electrolytes for rechargeable magnesium batteries using N_2O as a reaction gas. No significant difference was observed between the ICP-MS/MS and HR-ICP-MS results at a 95% confidence level. Soft magnetic ferrite, the most important magnetic material, possesses many excellent magnetic properties and is used in various fields such as electronics, and mobile communications. The impurity elements in soft magnetic ferrite significantly affect the magnetic performance of the materials and hence there is a need to monitor its purity. Fu et al.[71] developed a method for the accurate determination of harmful, and doping elements in soft magnetic ferrite powders using ICP-MS/MS. Thus, this analytical technique with several applications in material scientific studies in recent times proved to be very versatile.

x) *Speciation analysis*

The quantitative determination or qualitative assessment of different chemical species requires the development of sufficiently sensitive, and selective methods. Speciation analysis is a key aspect of modern analytical chemistry, as the toxicity, environmental mobility, and bioavailability of different elements are known to depend strongly on an element's chemical species. Thus, speciation analysis offers deeper insight into molecular mechanisms and pathways of disease by determining the speciation of an element, particularly in the environment and health-related studies. For example, organomercury compounds, such as methylmercury (CH_3Hg^+), are more toxic than inorganic forms of mercury (Hg^{2+}). Chromium (Cr^{3+}) is considered a micronutrient whereas Cr^{6+} is classified as carcinogenic[76]. In general, a separation method like HPLC when coupled to an element-specific technique like ICP-MS is best utilized for speciation analysis. ICP-MS/MS was used for the ultra-sensitive speciation analysis of tellurium by coupling to manganese and iron-assisted photochemical vapor generation (PVG)[17]. Te^{4+} was selectively determined by direct PVG and validated for speciation analysis of Te in water samples of different origins such as freshwater, well water, seawater, and contaminated water[77]. In another interesting example is the determination of different arsenic species by LC-ICP-MS/MS in seafood. Seafood is one of the major sources of dietary exposure to As. As species arsenobetaine (AsB) tends to be the major species in fish, mollusk, and crustacean products. The As speciation analysis showed that in addition to AsB, AsC, dimethylarsenate (DMA), monomethylarsenate (MMA), and the inorganic As species arsenate and arsenite, a total of 15 unknown As peaks were present across the various seafood products, highlighting the diverse amount of As species that people are getting exposed to via this diet[78]. A few more examples of speciation can be found in other sections of this article such as environmental applications and food safety.

xi) *Current application trends*

The literature on the ICP-MS/MS during the last 10 years reveals that solution nebulization is the most popular method of sample introduction, followed by laser ablation, GC, and LC/HPLC in that order. On the other hand, when looking at the number of applications points of view, geological, biological, medical, environmental, and food safety in that order, are the most reported during the last decade. But the technique seems to be popular even in other areas such as marine, nuclear, petroleum, agricultural, material sciences, and speciation

analysis (Fig.3). Table 3 presents a few more striking and exciting applications of ICP-MS/MS in recent literature.

Conclusion and future

The ICP-MS/MS instrumentation has taken the conventional ICP-MS technology to the next level through its capability of interference-free elemental/isotopic determination of the majority of the elements in the periodic table including the challenging elements such as P, S, Si, Cl, As, Se, and Br, by resolving even very difficult interferences and providing accurate data at ng/g-pg/g levels required in a variety of science and technology applications with matching performance with that of expensive HR-ICP-MS in many cases and even excelling in some cases. ICP-MS/MS offers high sensitivity taking the detection limits for several elements to pg/ml or better, with excellent accuracy and precision. Due to the outstanding capability of eliminating all kinds of spectral interferences, ICP-MS/MS is able to find wide applications in multiple research areas such as geological, environmental, biological, medical, nuclear, and agricultural sciences. Another important aspect is this instrument is less expensive compared to HR-ICP-MS, relatively easy and less complex to handle, and has less recurring maintenance expenditure. GC-ICP-MS/MS and HPLC-ICP-MS/MS have been established as the best instrumental choices for speciation analysis, and also for the extremely sensitive and robust analysis of highly interfered elements present in numerous potential targets in complex sample matrices such as pesticides and petroleum-related products. ICP-MS/MS technology enabled the determination of femtogram-level plutonium isotopes in environmental samples. The lower purchase cost of the ICP-MS/MS makes this a useful instrument, a valuable addition for laboratories aiming to expand their analytical capabilities. Future developments may focus on some of the drawbacks of the current systems particularly related to isotope ratio determinations such as 'elemental fractionation phenomena' and matrix effects, as well as the general lack of suitable chemically/mineralogically well-characterized reference materials that are homogeneous at the micro-scale level.

Acknowledgements

daughter, T. Naga Lavanya (London, UK) is thanked for helping in the improvement of the quality of the figure.

Figures:
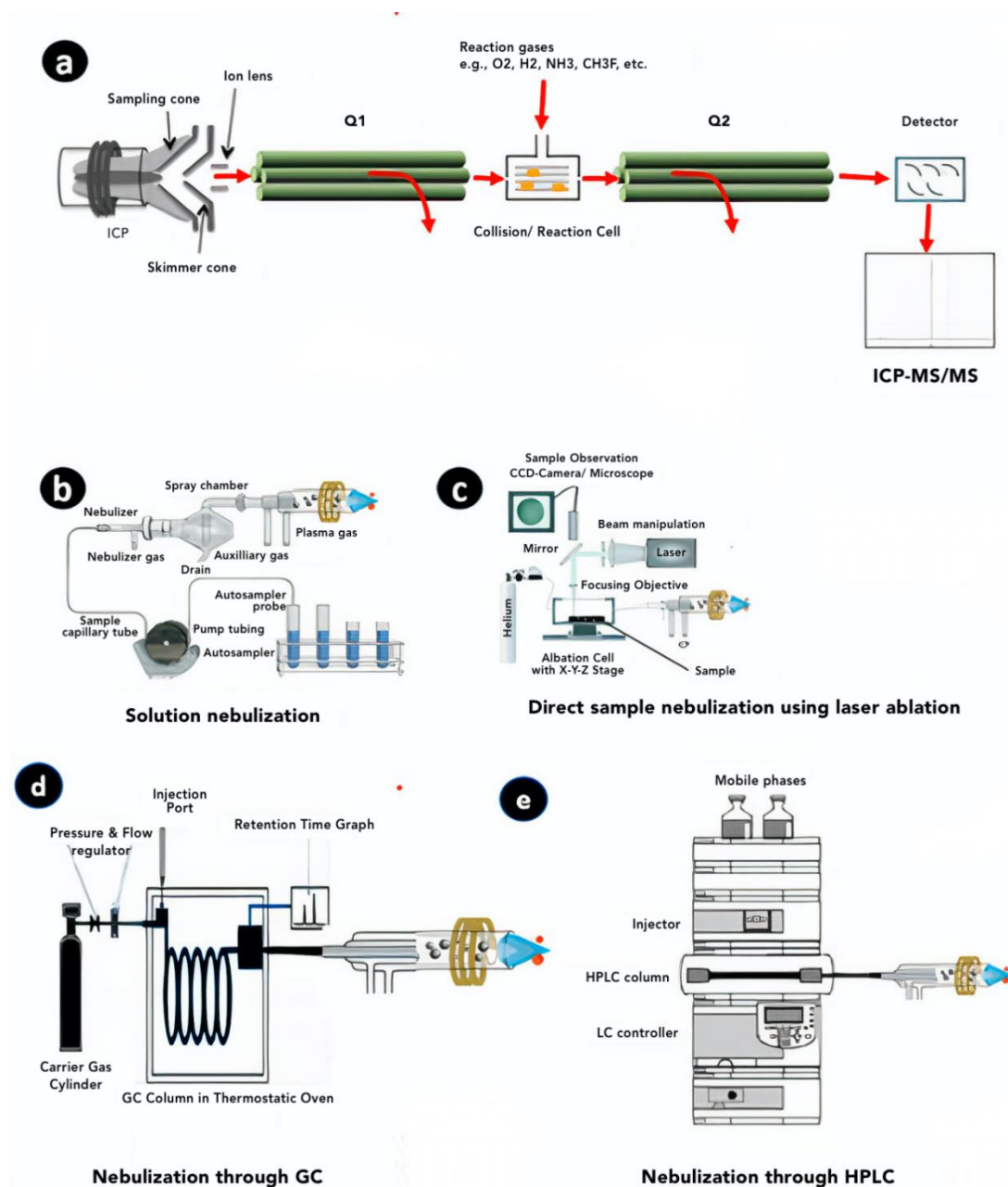
Fig. 1: Schematic diagram of a) a typical ICP-MS/MS instrument, b) with sample introduction by solution nebulization set-up, c) direct sample nebulization by laser ablation, d) sample introduction through GC, and e) sample introduction through LC/HPLC (Author's design).
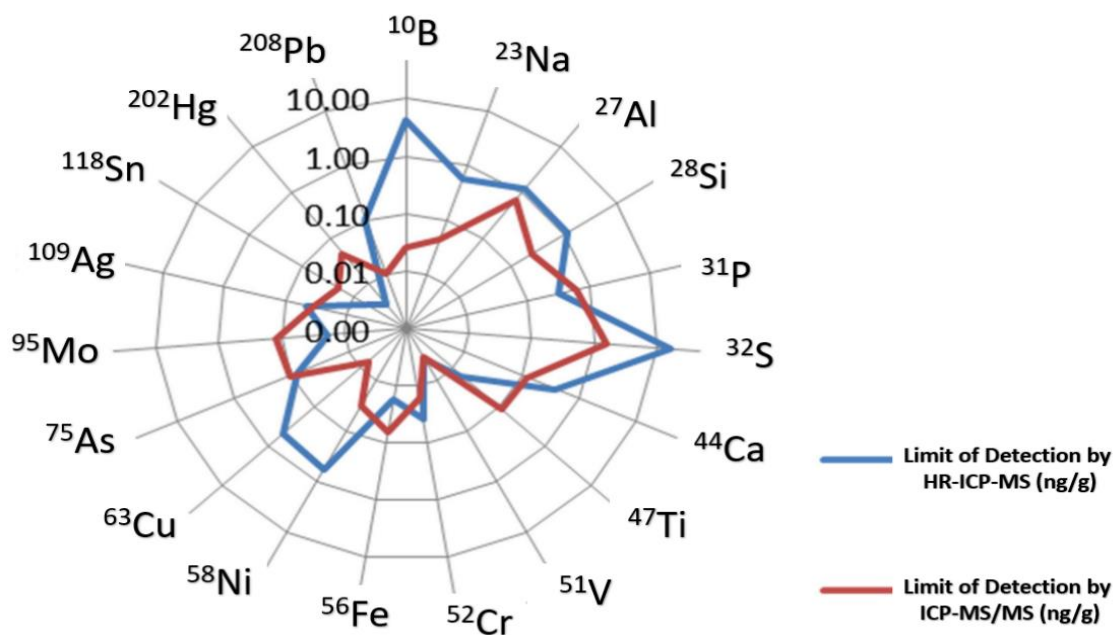
Fig. 2: Comparison of limit of detection for various elements/isotopes between ICP-MS/MS and HR-ICP-MS[36].
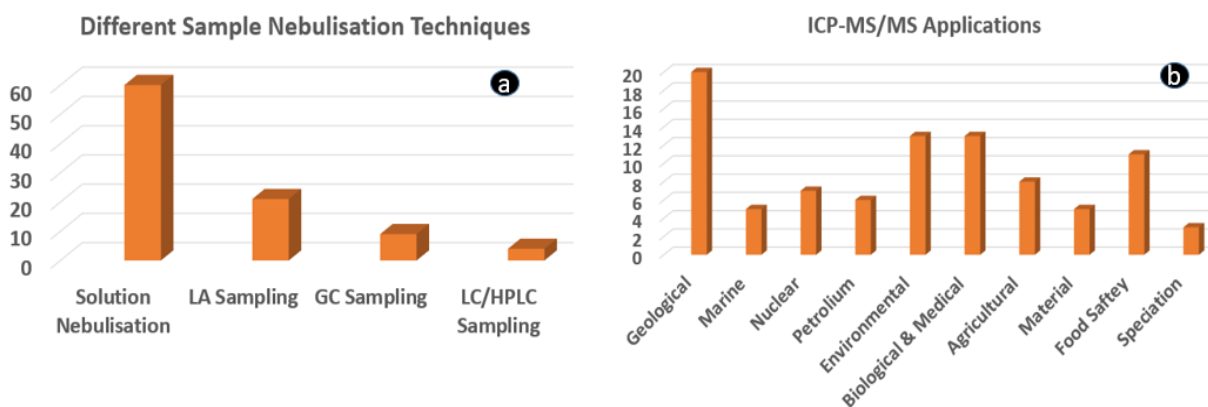
Fig. 3: Trends in the application of different modes of sample nebulization methods (a), and various areas of applications (b) of ICP-MS/MS in the literature during the last decade.

Tables:

Table 1: The analytical results of REE in water reference material, SLRS-4 obtained by different well-established analytical techniques in comparison with those obtained by ICP-MS/MS

REE	Concentration (ng/mL)				
	ICP-MS/MS[18]	ICP-MS[92]	HR-ICP-MS[93]	ID-HR-ICP-MS[9]	Compiled value[95]
La	294.5 ± 3.2	302.2 ± 7.3	279±12	290.3±6.4	287±8
Ce	357.5 ± 3.2	378.4 ± 8.2	369±15	364.1±3.5	360±12
Pr	70.9 ± 0.4	73.6 ± 1.5	75.4±8.0	70.6±2.3	69.3±1.8
Nd	274.2 ± 3.2	277.4 ± 5.7	261±9	270.3±2.8	269±14
Sm	58.5 ± 1.9	59.3 ± 1.4	54.3±5.0	57.2±0.3	57.4±2.8
Eu	8.06 ± 0.41	8.09 ± 0.61	8.4±0.8	8.00±0.7	8.0±0.6
Gd	33.86 ± 1.46	35.13 ± 1.01	38.3±6.0	33.80±0.36	34.2±2.0
Tb	4.27 ± 0.20	4.50 ± 0.23	4.1±0.5	4.30±0.12	4.3±0.4
Dy	22.82 ± 0.75	23.91 ± 0.66	21.7±3.0	23.60±0.16	24.2±1.6
Ho	4.39 ± 0.19	4.86 ± 0.11	4.2±0.5	4.60±0.18	4.7±0.3
Er	13.21 ± 0.46	13.53 ± 0.70	11.4±3.0	13.10±0.06	13.4±0.6
Tm	1.75 ± 0.11	1.91 ± 0.04	1.8±0.2	1.80±0.02	1.7±0.2
Yb	11.73 ± 0.36	12.03 ± 0.51	10.6±2.0	12.30±0.07	12.0±0.4
Lu	1.76 ±0.09	1.86 ± 0.11	1.7±0.4	1.95±0.02	1.9±0.1

Table 2: Concentrations of PGE and Re (ng/g) in road dust reference samples obtained by ICP-MS/MS in comparison with those obtained by NiS fire-assay-ICP-MS and certified values

CRM/ Element		BCR 723			OKUM	
	ICP-MS/MS[43]	NiS FA-ICP-MS[41]	Certified value	ICP-MS/MS[43]	Consensus value	
Ru	0.67±0.25	-	0.85± 0.29	3.75±0.17	4.66±0.56	
Rh	10.39± 0.80	14.4 ± 1.5	12.80±1.2	1.54±0.03	1.74±0.63	
Pd	6.00±0.23	9.2 ± 1.6	6.0±1.8	11.59±0.32	11.50±1.0	
Re	6.49±0.52	-	6.65±0.09	0.52±0.0	0.50±0.04	

Os	0.42±0.16	-		0.46±0.10	0.57±0.04	0.85±0.12
Ir	0.36±0.1	-		0.53±0.58	0.64±0.02	1.00±0.13
Pt	81.56±3.53	83.3 ± 4.9		81.3±3.3	10.32±0.48	11.79±1.46

BCR 723 is a road dust certified reference material; OKUM is a base metal sulphide bearing komatiite

Determined values are average of 4 (ICP-MS/MS) and 6 (NiS FA-ICP-MS) determinations.

Mixed acid dissolution in HPA-S, matrix removal by cation-exchange column followed by ICP-MS/MS determination[43].

Table 3: Some important applications of ICP-MS/MS from the recent literature.

Matrix	Elements determined	Sample digestion	Remarks	Reference
Fruit juices	Al, V, Cr, Mn, Fe, Co, Ni, Cu, Zn, As, Se, Cd, Hg, and Pb	After dilution, acidified with HNO_3, Li, Sc, Ge, Y, In, Tb, and Bi were used for online corrections of matrix effects and signal drift	ORS^3 was used with the mixed reaction gases O_2/H_2 and $NH_3/He/H_2$ for eliminating the spectral interferences	71
Atmospheric particulate matter (PM)	67 elements including important aerosol source markers such as P, S & Si.	Microwave digestion with HNO_3, HCl & HF	O_2 reaction mode for analysis of Ca, P, S, and Si, and no-gas or KED mode by He collision on SQ mode for the rest of the 63 elements.	96
Drug-related chlorine and	Br and Cl	After collection, the samples were stored	H_2 reaction gas was used in the	51

bromine contents in human blood plasma		at -20°C until analysis. The suspension was centrifuged the volume of the supernatant was reduced by solvent evaporation under N_2 flow.	collision/reaction cell during HPLC-ICP-MS/MS method	
Medicinal plants	As, Cd, Cr, Ni, Pb, and V	Microwave-assisted digestion using HNO_3 and H_2O_2	MS/MS mode, the use of O_2 as reaction gas combined with and *on-mass* mode were used	55
Smolina samples obtained from the durum wheat	57 elements including phosphorus and sulfur	Not available	Recoveries of the elements were found in the range of 92-108% for the digested CRM	97
Metalloids in complex food	B, Si, As, Se and Sb	Not available	ORS³ system, O_2 reaction gas, *on-mass* and mass shift mode was utilized	98
NIST salmon reference materials	Sr and S isotope ratios		O_2 as reaction gas and mass shift were utilized.	99

References

1. R. S. Houk, V. A. Fassel, G. D. Flesch, H. I. Svec, A. L. Gray and C. E. Taylor, Anal. Chem., 52, 2283, 1980.

2. V. Balaram, Current Trends Mass Spectrom., 16 (2), 8, 2018.

3. V. Balaram, Geol. J., 56 (5), 2300, 2021.

4. Y. Zhu, T. Ariga, K. Nakano and Y. Shikamori, At. Spectrosc. 42(6), 299, 2021.

5. V. Balaram, Rapid Commun Mass Sp., 35(10), 2021.

6. L. Fu, G. Huang, Y. Hu and F. Pan, Anal Chem., 94(7), 3035, 2022.

7. E. Bolea-Fernandez, A. Rua-Ibarz, M. Resano and F. Vanhaecke, J. Anal. At. Spectrom., 36(6), 1135, 2021.

8. L. Balcaen, E. Bolea-Fernandez, M. Resano, and F. Vanhaecke, Anal. Chim. Acta, 894, 7, 2015.

9. J. García-Bellido, L. Freije-Carrelo, M. Moldovan, J. R. Encinar, Trends Anal. Chem., 130,115963, 2020.

10. V. Balaram, Spectrosc., 31(10), 40, 2016.

11. V. Balaram, J. Geol. Soc. India, 97, 331, 2021.

12. V. Balaram, S. S. Sawant, Minerals, 12(4), 394, 2022.

13. T. Zimmermann, M. von der Au, A. Reese, O. Klein, L. Hildebrandt and D. Pröfrock, Anal. Meth., 12, 3778, 2020.

14. Z. Zhi-fei, R. Xiao-rong, L. Ce, G. Zhao, S. Juan-e and G Hua, J. Rock and Mineral Anal., 40(1), 95, 2021.

15. T. Li and A. Li, J. Rock Min. Anal., 2021, 40(2), 196, 2021.

16. L. Whitty-Léveillé, K. Turgeon, C. Bazin and D. Larivière, Anal. Chim. Acta. 961, 33, 2017.

17. V. Balaram, Microchem. J., 159(18), 105483, 2020.

18. Y. Zhu, K. Nakano, Y. Shikamori and A. Itoh, Spectrochimica Acta Part B: At. Spectrosc., 179, 106100, 2021.

19. Z. Yang, S. E. Jackson, L. J. Cabri, P. Wee, H. P. Longerich and M. Pawlak, J. Anal. At. Spectrom., 235, 534, 2020.

20. K. J. Hogmalm, T. Zack, A. K. O. Karlsson, A.S. L. Sjöqvis and D. Garbe-Schönberg, J. Anal. At. Spectrom., 32(2), 305, 2017.

21. K. J. Hogmalm, I. Dahlgren, I. Fridolfsson, and T. Zack, Mineralium Deposita 54, 821, 2019.

22. I. M. Villa, P. De Bievre, N. E. Holden and P. R. Renne, Geochim. Cosmochim. Acta, 164, 382, 2015.

23. V. Balaram, W. Rahaman and P. Roy, Geosystems and Geoenvironment, 1(2), 100019, 2022.

24. A. A. Redaa, Thesis submitted to the Department of Earth Sciences, School of Physical Sciences, The University of Adelaide, Australia, 310, 2022.

25. S. Gilbert and S. Glorie, J. Anal. At. Spectrom., 35, 1472, 2020.

26. A. Simpson, S. Gilbert, R. Tamblyn, M. Hand, C. Spandler, J. Gillespie, A. Nixon and S. Glorie, Chem. Geol., 577, 120299, 2021.

27. E. Leyden, J. Farkas, S. Gilbert, J. Hutson and L. M. Mosley, Talanta, 235, 122708, 2021.

28. C. T. Laureijs, L.A. Coogan and J. Spence, Chem. Geol., 579, 120339, 2021.

29. S. L. Jackson, J. Spence, D. J. Janssen, A. R. S. Ross and J. T. Cullen, J. Anal. At. Spectrom. 33, 304, 2018.

30. S. Xing, M. Luo, N. Yuan, D. Liu, Y. Yang, X. Dai, W. Zhang and N. ChenAt. Spectrosc., 42(2), 62, 2021.

31. X. Hou, W. Zhang and Y. Wang, Anal. Chem., 91(18), 11553, 2019.

32. C. Labrecque, P. J. Lebed and D. Larivière, J. Environ. Radioactivity, 155, 15, 2016.

33. J. Zheng, L. Cao, K. Tagami and S. Uchida, Anal. Chem., 88(17), 8772, 2016.

34. G. Jörg, Y. Amelin, K. Kossert and C. L. V. Gostomski, Geochim. Cosmochim. Acta, 88, 151, 2012.

35. B. Russell, H. Mohamud, M.G. Miranda, P. Ivanov, H. Thompkins, J. Scott, S. Goddard, J. Anal. At. Spectrom., 36(4), 845, 2021.

36. F. Chainet, A. Desprez, S. Carbonneaux, L. Ayouni, M.L. Milliand and C. P. Lienemann, Fuel Processing Technology, Elsevier, 188, 60, 2019.

37. R. Sánchez, F. Chainet, V. Souchon, S. Carbonneaux, C. P. Lienemann and T. J. L. Todoli, J. Anal. At. Spectrom., 35, 2387, 2020.

38. L. Freije-Carrelo, J. García-Bellido, F. Calderon-Celis, M. Moldovan and J. R. Encinar, Anal. Chem., 91(11), 7019, 2019.

39. J. Nelson, L. Poirier, F. L. Linares, Determination of Chloride in Crude Oils by Direct Dilution using Inductively Coupled Plasma Tandem Mass Spectrometry (ICP-MS/MS). J. Anal. At. Spectrom., 34, 1433, 2019.

40. R. S. Amais, A. D. Virgilio, D. Schiavo and J. A. Nóbrega, Microchem. J., 120, 64, 2015.

41. R, Mathur, V. Balaram, M. Satyanarayanan, S. S. Sawant, S. L and Ramash, Environ. Earth Sci., 62, 1085, 2011.

42. V. Balaram, Handbook of Environmental Materials Management, C.M. Hussain (Ed), Springer Nature Switzerland AG, 1, 2020.

43. A. Mitra, I. S. Sen, C. Walkner and T. C. Meisel, Acta Part B: At. Spectrosc., 177, 106052, 2021.

44. V. Balaram and K. S. V. Subramanyam, Advances in Sample Preparation, 1, 100010, 2022.

45. V. Balaram, A. Rani and D. P. S. Rathore, Geosystems and Geoenvironment,1(2), 100043, 2022,

46. Y. Ni, W. Bu, X. Ding, K. Xiong, H. Wang, C. Yang, S. Hu and W. Men, J. Anal. At. Spectrom., 37, 919, 2022.

47. C. D. B. Amaral, R. S. Amais, L. L. Fialho, D. Schiavo, T. Amorim, A. R. A. Nogueira and J. A. Nóbrega, Anal. Meth., 7(3), 1215, 2015.

48. S. Bertinetti, E. Bolea-Fernandez, M. Malandrino, B. Moroni, B., Cappelletti, D., Grotti, M and F. Vanhaecke, J. Anal. At. Spectrom., 37, 103, 2022.

49. J. Nelson, H. Hopfer, V. Silva, S. Wilbur, J. Chen, K. S. Ozawa, P. L. Wylie, J. Agr. Food Chem., 63, 4478, 2015.

50. C. Zhang, X. Li, H. Li, Y. Chen, T. Ma, X. Li and Q. Zhang, Anal. Chim; Acta. 1075, 38, 2019.

51. B. Klencsár, E. Bolea-Fernandez, M. R. Flórez, L. Balcaen, F. Cuyckens, F. Lynen and F. Vanhaecke, J. Pharmaceutical Biomed. Anal., 124,112, 2016.

52. R. S. Amais, D. B. C. Amaral, L. L. Fialho, D. Schiavo and J. A. N´obrega, Anal. Methods, 6, 4516, 2015.

53. H. Matsuno, A. Yokoyama, F. Watari, M. Uo, T. Kawasaki, Biomaterials 22 (11), 1253, 2001.

54. L. Fu, H. Xie, J. Huang, X. Chen and L. Chen, Anal. Chim. Acta, 1165, 338564, 2021.

55. A. Virgilio, R. S. Amais, D. Schiavo, J. A. Gomes Neto and J. de Araújo Nóbrega. Anal. Lett., 50(5), 842, 2016.

56. S. Naz, M. Shamoon, R. Wang, L. J. Zhang, J. Zhou, J. Chen,. Int. J. Mol. Sci., 20, 965, 2019.

57. S. Mukherjee, L. Liang, O. Veiseh, Pharmaceutics, 12, 147, 2020.

58. J. Sikorski, M. Matczuk, A. Kaminska, J. Kruszewska, M. Trzaskowski, A.R. Timerbaev, M. Jarosz, Int. J. Mol. Sci, 23, 1088, 2022.

59. C. S.K. Raju, A. Cossmer, H. Scharf, U. Panne, D. Lück, J. Anal. At. Spectrom. 25, 55, 2010.

60. V. Balaram, Geoscience Frontiers, 10(4), 1285, 2019

61. R. J. McDonald, J. S. McDonald, D. F. Kallmes, M. E. Jentoft, D. L. Murray, K. R. Thielen, E. E. Williamson and l. J. Eckel, Radiology 275 (3), 772, 2015.

62. V. Gulani, F. Calamante, F. G. Shellock, E. Kanal and S. B. Reeder, The Lancet Neurology, 16(7), 564–2017.

63. D. Clases, S. Fingerhut, A. Jeibmann, M. Sperling, P. Doble and U. Karst, J. Trace Elem. Med. Biol., 51, 212, 2019.

64. G. Xiao, Y. Liu and R. L. Jones, Radiat Prot Dosimetry, 1, 2022.

65. R. C. Machado, V. Alex, C. D. B. Amaral, D. Schiavo, J. A. Nóbregaa and A. R. Nogueira, J. Braz. Chem. Soc., 27(11), 2076, 2016.

66. Y. Wang, X. Yuan, L. Liu, J. Ma, S. Fan, A. Y. Zhang and Q. Li, J. Food Qual., 5536241, 2021.

67. J. A. V. A. Barros, A. Virgilio, D. Schiavo and J. A. Nóbrea, Microchem. J., 133, 567, 2017.

68. W. Guo, L. Jin, S. Hu and Q. Guo, J. Agric. Food Chem. 65(16), 3406, 2017.

69. L. Schmidt, J. A. Landero, D. L. R Novo, F.A. Duarte, M. F. Mesko, J. A. Caruso, E.M.M. Flores, Food Chem., 255, 340, 2018.

70. F. C. Pinheiro, C. D. B. Amaral, D. Schiavo and J. A. Nóbrega, Food Anal. Methods, 10, 992, 2017.

71. L. Fu, S and Shi, Food Chem. 299, 125172, 2019.

72. L. Fu, S. Y. Shia and X.Q. Chen, Food Chem., 245, 692, 2018.

73. L. Dospatliev and M. Ivanova, Bulgarian Chem. Commu., 52(2), 203, 2020.

74. F. Liang, S. Shu-yun, T. You-gen and W. Hai-yan, Spectrosc. Spectral Anal., 38(8), 2588, 2018.

75. L. Fu, S. Y. Shi and J. C. Ma, Chinese J. Anal. Chem., 47(9), 1382, 2019.

76. J. L. M. Viana, A. A. Menegário, A. H. Fostier, Talanta, 226, 122119, 2021.

77. E. Jeníková, E. Nováková, J. Hraníček and S. Musil, Analytica Chimica Acta, 1201, 339634, 2022.

78. A. A. Roberts, Ph. D thesis submitted to the School of Public Health Department of Environmental Health Sciences, State University of New York, US, 2020

79. A. L. Gray, Analyst, 110 (5) 551, 1985.

80. S. J. Jiang, R. S. Houk and M. A. Stevens, Anal. Chem., 60(11), 1217, 1988.

81. N. Bradshaw, E. H. Hall, N. E. Sanderson, J. Anal. At. Spectrom. 4 (8) 801-803, 1989.

82. A. J. Walder and P. A. Freedman, J. Anal. At. Spectrom. 7(3), 571, 1992.

83. F. A. Byrdy and J. A. Caruso, Environ. Health Perspectives, 103 (1), 21, 1995.

84. G. K. Zoorob, J. W. McKiernan and J. A. Caruso, Mikrochim. Acta. 128 (3-4), 145, 1998.

85. J. T. Rowan and R. S. Houk, Appl. Spectrosc. 43(6), 976, 1989.

86. D. J. Douglas, Canad. J. Spectrosc. 34, 3, 1989.

87. P. P. Mahoney, S. J. Ray, G. M. Hieftje and G. Li, J. Am. Soc. Mass Spectrom. 125,125, 1997.

88. G. D. Schilling, F. J. Andrade, J.H. BarnesIV, R.P. Sportline, M.B. Denton, C. J. Barinaga, D.W. Koppenaal, G.M. Hieftje, Anal. Chem. 79, 7662, 2007.

89. S. D. Fernández, N. Sugishama, J. R. Encinar and A. Sanz-Medel, Anal. Chem., 84(14), 5851, 2012.

90. E. Kroukamp and F. A. Shakra, Spectrosc., 35(9), 16, 2020.

91. D. Bevan, C. D. Coath, J. Lewis, J. Schwieters, N. Lloyd, G. Craig, H. Wehrs, T. Elliott, J. Anal. At. Spectrom. 36(5), 917, 2021.

92. M. G. Lawrence, A. Greig, K. D. Collerson and B.S. Kamber, Appl. Geochem. 21, 839, 2006.

93. C. H. Chung, I. Brenner and C. F. You, Spectrochim. Acta Part B. 64, 849, 2009.

94. T.C.C. Rousseau, J. E. Sonke, F. Chmeleff, J. Candaudap, F. Lacan, G. Boaventura, P. Seyler, P and C. Jeandel, J. Anal. At. Spectrom. 28, 573, 2013.

95. D. Yeghicheyan, J. Carignan, M. Valladon, M. B. Coz, F. L. Cornec, M. Castrec-Rouelle, M and E. Serrat, A Geostand. Geoanal. Res., 25(2-3), 465, 2001.

96. Arıa, A., Arıa, P. E. Gaga, E. O. Talanta, 208, 120350, 2020

97. Arı A, Ertürk Arı P, Ermişer D, Cındık B, Yalçın E, Gaga EO. Biol. Trace Elem. Res. 2021.

98. Wang, B., Wu, F and Yang, H, Chinese Journal of Analytical Chemistry, 100120, 2022.

99. Christopher, S. J., Ellisor, D.L and Davis, W.C, Talanta, 231, 122363, 2021.

Electrochemical Impedance Spectroscopy for the determination of oxide ion conductivity

Naeemakhtar Momin[1], J. Manjanna[1,*]

1 . Dept. of Chemistry, Rani Channamma University, Belagavi-591156, Karnataka, India
Email: jmanjanna@rediffmail.com

Abstract

The properties of oxide ion conductors depend upon the structure, compositions, nature of interface, dopant and defects dissemination. The electrochemical impedance spectroscopy (EIS) is emerged as strong tool for disentangling the intricacies of oxide ion conductors, and their capacities by using the different frequencies reliance for the isolations into their constituent's parts. Consequently, the electrical homogeneities in oxide ion conductors used for SOFC applications like anode/electrolyte/cathode, grain, grain boundary (GB) conductivity, area specific resistance of fuel cell and temperature coefficient of resistance can generally be examined effectively by utilizing the EIS.

Keywords: Electrochemical Impedance Spectroscopy; Solid Oxide Fuel Cells; Electrolyte; Oxide ion conductivity

Introduction

The fuel cell technology has emerged to be an alternative potential in the present energy crisis as it is capable to drench high-performance energy output of environmental benefits over other energy devices. Fuel cells as a significant part comprise customary solid oxide fuel cells (SOFCs), giving largely account to the recent innovation advancement and expected to emerge as major technological distribution for energy generation till 2030[1]. The elective procedures of determining electrical properties are impedance spectroscopy, wherein measurements are done over wide range of frequencies to characterize the different regions of the materials with respect to their relaxation time or time constant[2]. Impedance spectroscopy is moderately simple to utilize and is appropriate to a wide assortment of materials and issues. It has gone through significant advancements as of late with the accessibility of programmed gear fit for spreading over numerous times of recurrence in a solitary scope. A distant memory are the times of adjusting R and C (or L) circuits utilizing invalid strategies, where it could require a few minutes to get a particular reading. The principal reason for this review is

to show the value of impedance spectroscopy for the characterization of SOFC electrolytes[3-6]. It is quickly turning into a fundamental strategy in the advancement of novel materials for energy applications due to the fact that it empowers the by and large electrical properties of a material to be isolated into their elemental components, which can then be deliberately, considered or changed[7-10].

Electrochemical Impedance spectroscopy (ESI)

The EIS is a technique used for the electrical characterization of electroceramics. The a.c. current is applied to the sample over a wide range of frequencies to record the response of the sample[11-13]. The EIS is employed to study the properties of ionic conductors, dielectric materials, semiconductors, solar cells, fuel cells, batteries and corrosion etc. In 1967 Bauerle[14] introduced the EIS technique to determine the oxygen ion conductivity in solid electrolytes[15]. The information about the electrode process and contribution of grain and GB conductivity to the total conductivity can be obtained using the EIS technique. The parallel RC elements represent the different regions of the materials. The product of the resistance and the capacitance of the element in the region is a characteristic time constant[16]. Thus, the regions can be identified as the frequency of maximum loss (ω_{max}), with capacitance calculations using eq. (1).

$$\tau = RC \; ; \; \omega_{max} RC = 1 \qquad\qquad (1)$$

Because of the geometrical relation between the capacitance, thickness and surface area of the sample, the magnitude of the capacitance is related to the phenomenon in the sample. Typical impedance spectrum is represented as negative of the imaginary impedance component (Z'') versus real impedance (Z') and termed as Nyquist plot. The equivalent electrical circuits were used to fit the experimental data to represent the physical behavior of the materials. In mixed conductors, the probable behavior is comprised of ionic and electronic[17]. Since ions could have travelled through various components and respective impedance could be related to it. The electrical behaviors of the materials can be analyzed by plotting different plots such as complex plane impedance and capacitance, spectroscopic plots of capacitance, electric and impedance modulus. The total ionic resistance would be the sum of the grain and grain boundary resistance, if the grain and GB effects appear in impedance spectra.

The series model to the current pathway.

$$R_i = R_b + R_{gb} \qquad\qquad (2)$$

$$R_b = R_{b,i} \times R_{b,e} / R_{b,i} + R_{b,e} \tag{3}$$

$$R_{gb} = R_{gb,i} \times R_{gb,e} / R_{gb,i} + R_{gb,e} \tag{4}$$

Huggins[18] has proposed complex impedance plots of pure ionic conductors and pure electronic conductors shown below to obtain the transport number from the complex impedance plane. The plots for mixed conductors without grain and grain boundaries are also shown in Fig.1 and 2 respectively.

The ionic and electronic resistance of the material is represented by the real axis of the complex impedance spectra[19]. The resistance and transport number for ionic and mixed conductors can be calculated using the above-mentioned equation (eq. 4). For the high electron transfer number, the semi-circle arc at high frequency would be larger than at low frequency. For high ionic transport numbers, the semi-circle arc at high frequency is smaller than at low frequency[20].

The complex impedance of a sample is measured as a function of frequency and depicted in the form of Nyquist plots. Generally, the a.c impedance spectrum of solid ionic conductors shows three different contributions. The arc, at high frequencies, is attributed to grain (bulk) behavior, at intermediate frequencies, attributed to grain-boundary (GB) behavior, and at lower frequencies belongs to electrode behavior which is regarded to be more complex due to the appearance of multiple arcs. Due to different relaxation time constants for individual polarizations of conductors at a constant temperature, all the arcs will not appear simultaneously, and hence with a rise in temperature grain and GB arcs at high frequencies tend to disappear, and only total electrode contribution (arc) will be observed at high temperature[21]. The other reason for this behavior could be similar relaxation time of charge carriers inside the grain and GB, hence with the increase in temperature, the semicircle arc of grain and GB contributions were overlapped and difficult to distinguish. To distinguish the grain, GB, and electrode, contributions equivalent electrical circuit model [R(QR)(QR)] had been employed, which is shown in Fig.3. This equivalent circuit consists of the grain resistance (R_g) and two RC circuits in series for GB (R_{gb}) and the other for electrode polarization (R_e). A constant phase element (CPE= Q) is applied instead of a capacitor. This constant phase element is equivalent to the distribution of the capacitor in parallel. The element R_g, $R_{gb} \| Q$ represents the ionic conductivity through grain and grain boundary[22]. The total resistance of the electrolyte is calculated by using the eq. (5).

$$R_{total} = R_g + R_{gb} \tag{5}$$

Where R_g and R_{gb} be the grain and GB resistance, respectively

The total conductivity is obtained by using eq. (6).

$$\sigma = t/RA \qquad\qquad (6)$$

where t be the thickness of the pellet, R is the resistance, and A is the total surface area.

The capacitance values were computed using the equation $\omega RC = 1$, where ω is the angular frequency (=$2\pi f$, f is the frequency in Hz) and R is the arc magnitude. Grains have a capacitance of pF, whereas GB has a capacitance of nF [23-25].

Arrhenius equation is used to show the influence of temperature on conductivity [26] eq. (7).

$$\sigma T = A_o \exp^{\left(\frac{-E_a}{KT}\right)} \qquad\qquad (7)$$

where σ, A_o, T, E_a and K are the conductivity, pre-exponential constant, temperature, activation energy, and Boltzmann constant, respectively.

As a typical case the reported oxide ion conductivity of $Ce_{1-x}La_xO_{2-\delta}$ ($0 \leq x \leq 0.1$), LDC samples were determined using EIS techniques [24]. For a.c. impedance measurement, the silver paste was applied on both sides of the LDC pellet samples and baked at 600 °C for 1 h for electrical connection. The electrochemical impedance spectrometer (CH Instrument, Inc CHI604D USA) was used to record the Nyquist plots at different temperatures from 350 − 750 °C in the frequency range of 1 − 10 MHz with an a.c. signal of 10 mA. The obtained data were fitted to the corresponding equivalent circuits [R(QR)(QR)] using the ZSimpWin software to obtained the polarization resistance for grain and grain boundary (GB) as shown in the below Fig. 4.

The fitting parameters of 0.5 LDC sample at 700 °C are given here as typical case in Table. 1.

From the above plots (Fig. 5) it has been clearly observed that, the semicircles of grain and grain GB were found to be overlapped and depressed. This depression of semicircles might be due to varying sizes and distribution of grain inside the samples. The total conductivity (σ_t) was calculated using the eq. (6). The obtained Nyquist plots of 0.05 LDC sample after fitting are shown in Fig. 5[24]. Based on the obtained results the total ionic conductivity of 0.05 LDC samples at 700 °C was computed using the eq. (6) and was found to be 8.32×10^{-3} S cm^{-1}. Thus, the EIS techniques provide facile route for the determination of ionic conductivities for SOFC materials. The capacitance values were found to be in the range of $10^{-12} − 10^{-8}$ F, which indicates the conduction process through grain and grain boundary, respectively. The work on the characterization of materials for SOFC applications has gained momentum and now it is evident that with the help of EIS an abundance of data might be

gotten. Future improvements are probably going to include the isolation and characterization resonance/relaxation phenomenon and determination of ionic and electronic components[25, 26].

Conclusions

This brief outline of electrochemical impedance spectroscopy (EIS) portraying the convenience of materials characterizations is related to energy applications. The measurement of grain and grain boundary (GB) resistance are important parameter of SOFCs electrolytes and therefore determination of ionic conductivity for SOFCs are prime concern. Thus, in this review we utilize the way that materials have quantifiable electrical properties to permit us to concentrate determination of oxide ion conductivity of the materials for SOFCs.
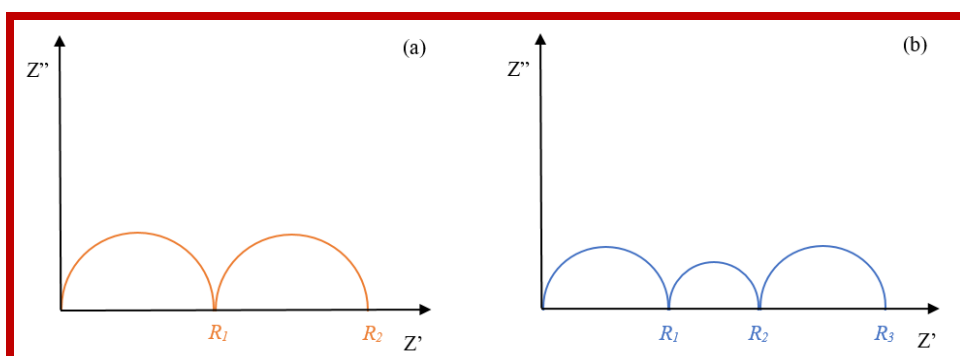
Acknowledgements

Figures:
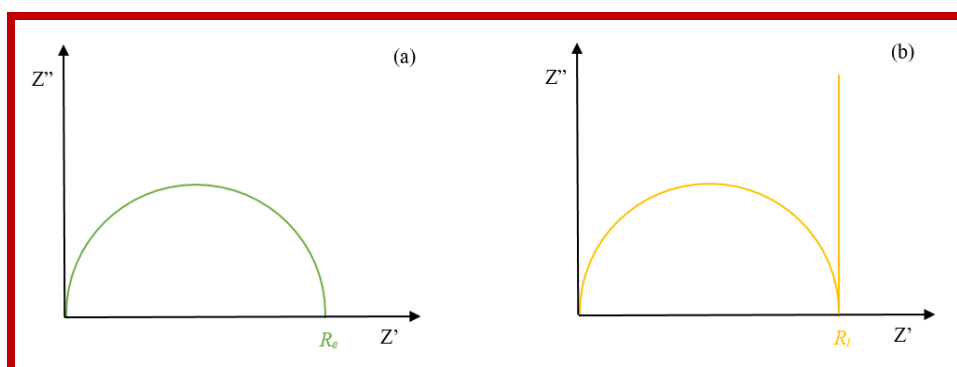
Fig. 1: Complex impedance plane of a purely electronic (a) and ionic conductor (b) [18].

Fig. 2: Complex impedance plane of mixed conductor with 2 elements(a) and 3 elements(b).
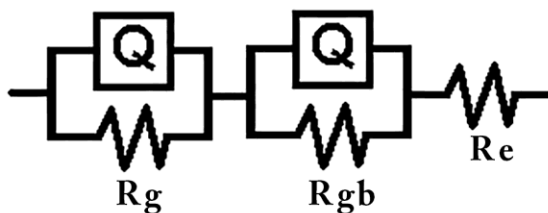
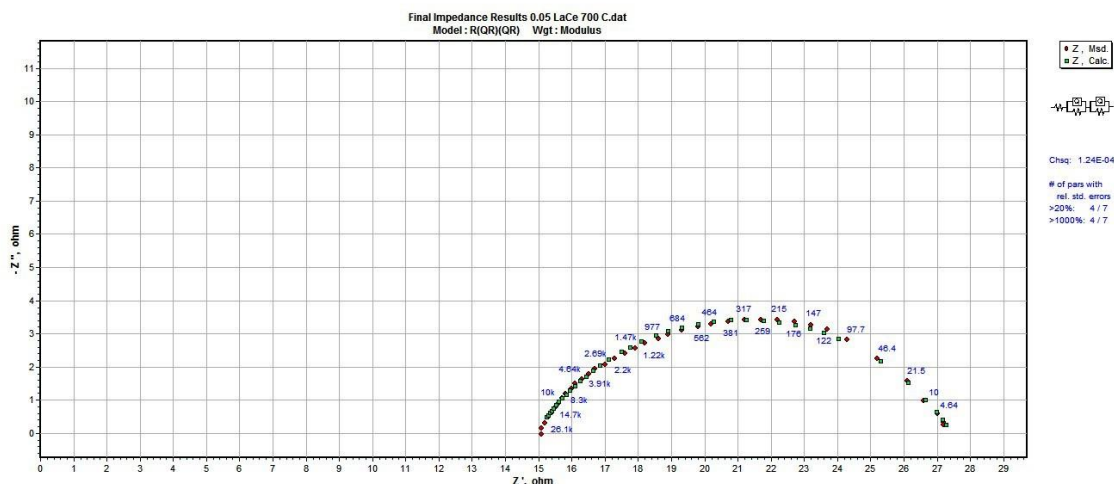**Fig. 3**: electrical model used to fitting arcs [R(QR)(QR)].

Fig. 4: Shows 0.05 LDC data fitting arcs with [R(QR)(QR)]circuit in ZSimpWin software.
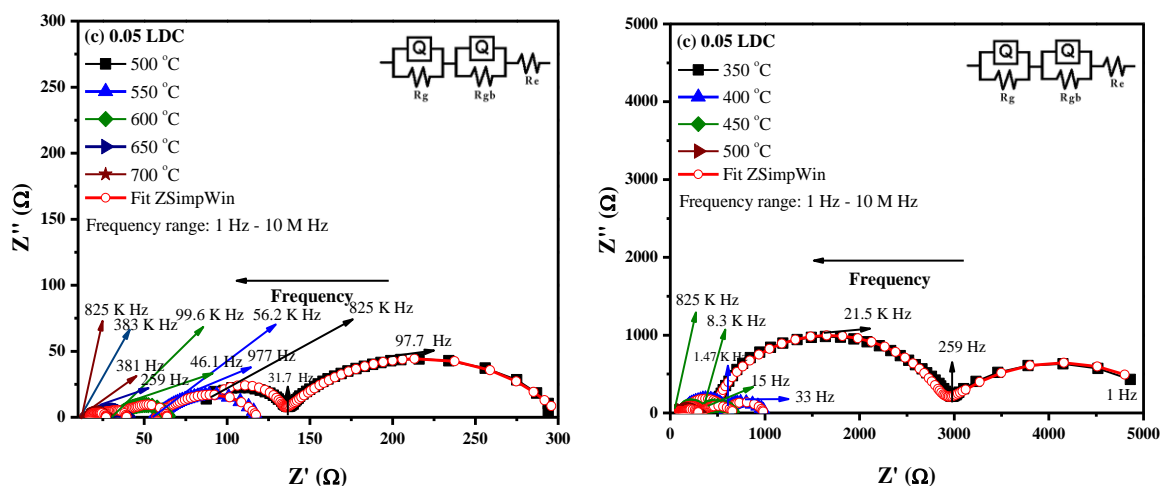

Fig. 5: Nyquist plots for 0.05 LDC measured between temperature range of $350-750$ °C.

Tables:

Table 1: Nature of resistances and transport numbers for electronic, ionic, and mixed conduction.

Conduction	Resistance	Electronic Transport Number t_{ele}	IonicTransport Number t_{ion}
Electronic	Re	1	0
Ionic	Ri	0	1
Mixed	Re × Ri / Re + Ri	Ri / Re	Re – Ri / Re

Table 2: EIS data analysis results of 0.05 LDC sample at 700 °C from ZSimpWin software

Index	Parameter	Start	End
1	R	14.9	10.81
2	Q-Yo (CPE)	0.06227	0.0006227
3	Q-n (Frequency Power)	0.8	0.6361
4	R_{gb}	12.55	12.55
5	Q-Yo (CPE)	8.97E-14	6.218E-18
6	Q-n (Frequency Power)	0.8	0.3789
7	R_g (Resistance)	0.01	4.09
Where, R is the resistance in Ω, Q-n is the frequency power in n and Q-Yo is the constant phase element (CPE) in S. s^n.			

References:

1. N. Jackson, R. Morgan, D. Brett, Fuel Cell Technology Roadmap, automotive council UK, version 1.0, 2020.

2. A. Orera, P.R. Slater, Chem. Mater., 22 (3), 675, 2010.

3. H. Yahiro, T. ohuchi, K. Eguchi, H. Arai, J. Mater. Sci., 23 (3), 1036,1988.

4. K. Eguchi, T. Setoguchi, T. Inoue, H. Arai, Solid State Ion., 52(1-3), 165, 1992.

5. J. Zhang, L. Lei, F. Zhao, F. Chen, M. Han, Electrochim. Acta., 340, 135898, 2020.

6. J. Nielsen, J. Hjelm, Electrochim. Acta. 115, 31, 2014.

7. M. Gödickemeier, D.W. Eth, Mixed Ionic Electronic Conductors for Solid Oxide Fuel Cells Table of Contents, Betrieb., 11348, 1996.

8. M. Zarabian, M. Bartolini, P. Pereira-Almao, V. Thangadurai, J. Electrochem Soc.,164(6), A1133, 2017.

9. J. Zhang, C. Lenser, N.H. Menzler, O. Guillon, , Solid State Ion., 344, 115138, 2020.

10. M. Lang, T. Franco, G. Schiller, N. Wagner, J. Appl. Electrochem., 32(8), 871, 2002.

11. J. Hjelm, M. Sogaard, M. Wandel, M. Menon, M. Mogensen, A. Hagen, ECS Trans., 7(1), 1261, 2007.

12. [R.R. Mosbæk, J. Hjelm, R. Barfod, J.V.T. Høgh, P.V. Hendriksen, Proc. 10th European SOFC Forum B10, PP56, 2012.

13. A.R.C. Bredar, A.L. Chown, A.R. Burton, B.H. Farnum, ACS Appl. Energy Mater., 3(1), 66, 2020.

14. J.E. Bauerle, J. Phys.Chem. Solids., 7 (15), 2657, 1969.

15. H. Nara, T. Yokoshima, T. Osaka, Curr. Opin. Electrochem., 20, 66, 2020.

16. A. West, J. Irvine, D. Sinclair, Adv. Mate., 2(3), 132, 1990.

17. K. Kobayashi, Y. Sakka, T.S. Suzuki, J. Ceram. Soc. JPN., 124(9) 943, 2016.

18. H. Herrera Hernández, A. M. Ruiz Reynoso, J. C. Trinidad González, C. O. González Morán, J. G. Miranda Hernández, A. Mandujano Ruiz, J. Morales Hernández, R. Orozco Cruz, Electrochemical Impedance Spectroscopy, IntechOpen, ,2020.

19. M.E. sayed Ali, O.A. Abdelal, A.A. Hassan, Solid State Ion., 178, 1463, 2007.

20. J. Nielsen, J. Hjelm, Electrochim. Acta., 115, 31, 2014.

21. S. Banerjee, P.S. Devi, D. Topwal, S. Mandal, K. Menon, Adv. Funct. Mater., 17(15), 2847, 2007.

22. A. Ali, R. Raza, M. A. Rafique, B. Wang, B. Zhu, Appl. Phys. Lett., 112(4), 043902, 2018.

23. K.C. Anjaneya, G.P. Nayaka, J. Manjanna, G. Govindaraj, K.N. Ganesha, J. Alloys Compd., 578, 53, 2013.

24. N. Momin, J. Manjanna, L. D'Souza, S.T. Aruna, S. Senthil Kumar, J. Alloys Compd., 896, 163012, 2022.

25. T. hang, J. Ma, Y. Chen, L. Luo, L. Kong, S. Chan, Solid State Ion., 177 (13-14), 1227, 2006.

26. E.M. Köck, M. Kogler, B. Klötzer, M.F. Noisternig, S. Penner, ACS Appl. Mater. Interfaces., 8(25), 16428, 2016.

Crosslinked Chitosan Materials for Adsorptive Removal of Dyes from Aqueous Solutions: A Brief Review

P. M. Nandanwar, S. H. Vithalkar, P. Bakshe, A. Shekhawat and R. M. Jugade*

Department of Chemistry, RTM Nagpur University, Nagpur-440033, India

Email: ravinj2001@yahoo.co.in

Abstract

As a promising adsorbent, chitosan has been found to be extremely useful in its native form as well as in modified forms for the removal of variety of dyes from aqueous medium. Scientific workers have modified chitosan structurally by utilizing its -OH and -NH$_2$ functional moieties in numerous ways to obtain potential material with chemical and physical stabilities. Various modifications of chitosan involve crosslinking, grafting, impregnation and composite formation. Among various established routes of modifications, the most common way is its crosslinking to provide enhanced mechanical strength along with minimizing its solubility in acidic environment. In this paper, we review briefly only the crosslinked chitosan materials reported in last fifteen years by various researchers for adsorption of dyes as pollutants in order to provide clean and safe environment. Various materials formed through crosslinking, the dyes targeted for adsorption, various isotherms studies, kinetics studies and adsorption capacities of these materials have been discussed in details on case wise basis.

Keywords: Chitosan, crosslinked chitosan, adsorption, dyes, adsorption capacity.

Introduction

Bio-sorbents are considered to be ideal candidatures for effective removal of water toxicants since they have characteristic functional groups, large surface area with suitable porosity which leads to high adsorption capacities. The characteristics properties like ease of accessibility, cost effectiveness, mechanical stability and compatibility, its regeneration, non-toxicity towards environment, high selectivity to remove a wide range of water toxicants and simple processing procedures make these materials more attractive[1]. In order to develop an effective bio-sorbent, researchers have focused on natural polymers such as cellulose, chitin

and chitosan to serve as potential adsorbents with magnificent adsorption capacity with minimal synthesis cost. Being abundantly available, chitosan is a low-cost bio-polymer that can be used for water treatment and can be obtained from natural resources. In comparison to majority of commercial adsorbents, chitosan has received attention due to its interesting properties like cationic nature in slightly acidic medium, macromolecular structure and low cost of synthesis.

When compared with cellulose and chitin, the chitosan has two major advantages. Firstly, it is soluble in acidic medium and can be recovered by adding base. This makes its purification and separation possible. Secondly, reactive -NH$_2$ functional group makes it possible to modify chitosan in various ways to achieve desired properties like mechanical and thermal stability and adsorption tendency towards targeted pollutant.

In general, chitosan is an acid-soluble de-acetylated product of chitin. Exoskeleton of sea creatures such as cray fish, lobster, prawn, crab and shrimp are the major sources of chitin which makes it one of the second most abundant polysaccharides worldwide after cellulose. This chitin on deacetylation with alkali leads to formation of chitosan. Chitosan is a linear, semi-crystalline polysaccharide composed of $(1 \rightarrow 4)$-2-acetamido-2-deoxy-β-D-glucan (N-acetyl D-glucosamine) and $(1 \rightarrow 4)$-2-amino-2-deoxy-β-D-glucan (D-glucosamine) units and can be chemically expressed as nontoxic, heterogeneous, linear, cationic and biodegradable polysaccharide with high molecular weight. Depending on the source of chitin, molecular weight of chitosan is typically ranging in between 300-1000 kDa. Although chitin is found naturally in large amounts through many sources, chitosan is only found in nature in limited quantities, such as in some fungi. To meet the industrial as well as research needs, chitosan is typically derived from chitin through chemical modification or enzymatic treatments leading to deacetylation (Fig. 1)[2,3].

The poor solubility and high molar mass of chitin restricts its applicability. On the other hand, presence of amino groups in chitosan increases its solubility in acidic solutions. Also, in near-neutral medium, the free -NH$_2$ group interact with cationic species including metal ions and cationic dyes making it highly useful customer in waste water treatment and purification. Protonation of amino groups of chitosan forms polycations for the formation of ionic complexes with series of anions like bio-macromolecules such as lipid, proteins and DNA along with some synthetic anionic species. In fact, chitosan remains as alone positively charged polysaccharide in nature[4]. In order to form stable covalent bonds during variety of

reactions such as etherification, esterification and reductive amination, chitosan involves both amino and hydroxyl groups. Chitosan has also proved its outstanding ability in biomedical field by acting as an antibacterial and antifungal agent, along with mucoadhesive, analgesic and hemostatic properties. Its biocompatibility can be considered due to biodegradation into nontoxic residues which is highly related to the molecular mass of chitosan and its degree of deacetylation. At least 50% of the free amine form can be observed after its deacetylation. But most commonly used chitosan has more than 80% degree of deacetylation that can be further increased by alkali treatment[5].

Presence of amino and hydroxyl groups on chitosan are capable of forming a variety of interactions including amide and ester bonding as well as Schiff base formation. Schiff base is a weak base and insoluble in water and organic solvents, but usually soluble in acidic solutions. The most influencing properties such as mechanical strength, chemical stability, swelling, aqueous permeability, and solubility can be achieved through crosslinking of chitosan[6].

In various adsorption applications, different crosslinkers modify chitosan by favoring bonding with the readily available amino and hydroxyl groups of chitosan. Crosslinking can be achieved through covalent bonding or through ionic bonding. Covalent bonding can be achieved either through -NH$_2$ group or -OH group. The most frequently used crosslinker for -NH$_2$ group is glutaraldehyde while that for -OH group is epichlorohydrin. Ionic crosslinking involves protonation of -NH$_2$ groups and interaction of multivalent anions like tripolyphosphate (TPP). The nature of boding involving these three crosslinkers has been shown in Fig. 2. Use of epichlorohydrin as a crosslinker is of great significance because it preserves reactive -NH$_2$ group that is capable of coordinating with metal ions or can be further modified by impregnation with various organic moieties[7]. Indeed, crosslinking lowers the adsorption characteristics of chitosan, however it has been used to improve mechanical strength of chitosan. Improvement of metal binding capacity as a result of increase in hydrophobicity caused by partial destruction of crystallinity by homogeneous crosslinking of chitosan was observed as compared to heterogeneous crosslinking[8,9].

Dyes are a common class of pollutants released by most of the textile industries. Dyes can be classified in different ways as acid dyes, basic dyes, mordant dyes, direct dyes, vat dyes, reactive dyes, disperse dyes and sulphur dyes. Presence of textile dyes in wastewater discharged by these industries in aquatic environments such as valleys, rivers, sea, oceans and

lack of their biodegradability under normal ecological conditions, can destroy aquatic ecosystem. There are serious ecological consequences such as changing the nature of aquatic environments and reducing photosynthesis compared to aquatic flora. Aesthetic and health problems associated with such water is another aspect of concern. Such water can cause allergies, dermatitis, skin irritations, cancers and mutations in humans. Furthermore, 60 to 70% of azo dyes are toxic, carcinogenic and are refractory to conventional treatment processes because of their resistance to conventional physicochemical destruction and the absence of their biodegradability[10].

Various methods used in textile effluent treatment have been depicted in Fig. 3. Among these, adsorption is the most preferred due to ease of operation, low cost involved and greener aspect associated with it. These methods can be broadly classified as- physical, chemical and biological. Among all these methods, the chemical methods include use of costly chemicals and also the unreacted chemicals may lead to contamination. Biological process using microorganisms and enzymes are superior, but are very slow and time consuming. Physical processes including reverse osmosis, filtration, coagulation/flocculation and adsorption are considered to be most practical methods and are widely used in water treatment. Among them, adsorption is considered to be most cost effective and useful for larger water bodies. Use of biosorbents make the adsorption process more eco-friendly. Regeneration and reusability of biosorbents gives another greener dimension to biosorption process.

Literature review

Among various methods of modifications of chitosan, only those involving crosslinking have been discussed in this paper. A comprehensive review of literature of last 15 years is presented below.

Adsorbent with a high adsorption capacity for anionic dyes was prepared by Chiou et al.[11] and co-workers in 2006. They studied adsorption behavior of MY (metanil yellow) and reactive dye (RB15, reactive blue 15) in aqueous solutions by crosslinked chitosan beads. The adsorption capacities were 1334 mg/g and 722 mg/g respective for these dyes at pH 4. The adsorption mechanism followed Langmuir model and fits well first order kinetics model with dynamic adsorption behavior. Adsorption capacity towards RB15 has been found to be one of the best ever reported in literature for this dye.

Meanwhile, the crosslinked chitosan/oil palm ash composite was applied as an excellent adsorbent for removal of reactive blue 19 dye from aqueous solution by Hasan et al[12]. At pH 6, maximum adsorption was observed for crosslinked chitosan/oil palm ash composite beads. Various adsorption isotherms were studied such as Langmuir, Freundlich, Redlich–Peterson, and Temkin. Among these adsorption isotherms, Redlich–Peterson showed better correlation coefficient than the other models at all temperatures studied. The prepared adsorbent exhibited adsorption capacity of 423.5 mg/g at pH 6 and 30 °C. The pseudo-second order was better describing adsorption kinetics of dye upon crosslinked composite. Thermodynamic data indicate that dye adsorption onto synthesized composite was spontaneous in nature. Near-neutral conditions are the key features of this study that eliminates necessity of further neutralization of water after adsorption process.

Chitosan-EGDE (ethylene glycol di-glycidyl ether) beads were investigated by Kumari et al[13], for the removal of acid red and blue dyes from aqueous solution. Crosslinking with EGDE enhances chemical resistance and mechanical strength of chitosan. Adsorption isotherm showed that Langmuir isotherm model was best fitting as compared to other models. The kinetics studies were carried out to find out order of reaction which followed pseudo-second order kinetics. Adsorption of acid dyes onto chitosan-based adsorbents was a physical adsorption confirmed by FT-IR spectral analysis. After successive examinations, the maximum adsorption capacity for acid red and blue dyes were found to be 59.52 mg/g and 142.86 mg/g at pH 2 and pH 4 respectively. The physical modification to obtain adsorbent in the form of beads make filtration easy after adsorption of dye.

Subsequently, efficiency of chitosan and crosslinked chitosan adsorbents was examined by Kumari et al[14], using batch adsorption techniques for the removal of acid red and blue dyes from aqueous solution. Chitosan has been crosslinked with glutaraldehyde and sulphuric acid. The adsorption equilibrium data very well followed Langmuir isotherm, while the adsorption of both acid dyes best fits with pseudo-first order kinetics. Thermodynamic parameters were studied to find out enthalpy change ($\Delta H°$), free energy change ($\Delta G°$) and entropy change ($\Delta S°$). It was observed that the adsorption process was spontaneous and exothermic. The additional advantage of these crosslinked chitosan–GLA and chitosan–H_2SO_4 adsorbents is that they can be regenerated and reused in multiple cycles.

A decade before, magnetically separable adsorbent, namely magnetic Υ-Fe_2O_3 /crosslinked chitosan composites represented as MΥ-Fe_2O_3/CSCs were synthesized by Zhu et al[15] using

process of micro-emulsion. The adsorbent has been employed for adsorption of methyl orange (MO) from aqueous solution. After successful characterization, it was observed that magnetic Υ-Fe$_2$O$_3$ introduced well in MΥ-Fe$_2$O$_3$/CSCs which maintained magnetic properties in crosslinked composite. Additional dose of Υ-Fe$_2$O$_3$ was given out to saturate magnetization of synthesized material. After adsorption of methyl orange by MΥ-Fe$_2$O$_3$/CSCs, composite was effectively separated from reaction solution by the application of external magnetic field. Adsorption kinetics of methyl orange on the adsorbent followed pseudo-second order kinetics model giving highest adsorption at pH 4.

Later on, adsorption studies of textile dyes EY-4G and S-Blue onto crosslinked chitosan poly(acrylamide) hydrogels has been carried out by Ekici et al[16]. The result of kinetics of CS-PAAM IPN hydrogels is in accordance with second order model. It was observed that interpenetrating polymeric network structure affects network parameters of PAAM hydrogels. The best fitted adsorption isotherm was Langmuir. The maximum adsorption capacities were in between 18.90 mg/g to 63.20 mg/g. From thermodynamic equilibrium, it was clear that the nature of adsorption phenomenon was endothermic. This study shows that in powder, film, or bead form synthesized hydrogel have greater adsorption potential.

Guo et al[17] studied adsorption properties of Reactive dye on crosslinked chitosan beads for various parameters such as concentration of adsorbent, pH, initial dye concentration and temperature of adsorbate. The adsorption modeling was carried out to analyze equilibrium data at different temperatures. Freundlich isotherm was found to fit well. Crosslinked chitosan showed adsorption capacity of 19.613 mg/g to remove reactive dye and proved great adsorption capability even after repeated cycles. In this material, crosslinking leading to formation of spherical beads giving mechanical stability to adsorbent that remains in solid form even in strongly acidic conditions.

The nanoparticles of templated crosslinked chitosan have been investigated by Chen et al[18] using ECH-RB5 and ECH-3R through imprinting process for adsorptive removal of Remazol Black 5 (RB5) and Remazol Brilliant Orange 3R (3R) dyes. The results match with the second order kinetics and Langmuir adsorption models. Dubinnin-Radushkevich model revealed that adsorption process may be physisorption. The maximum adsorption capacities were found to be 5572 mg/g and 5392 mg/g for Remazol Black 5 and Remazol brilliant Orange 3R respectively at pH 3, that are much higher as compared to most of the reported

materials. The most interesting aspect of this material is its enormously high adsorption capacity towards both of these dyes.

Another study on adsorption of methyl orange (MO) from aqueous solutions on protonated crosslinked chitosan was investigated by Huang et al[19]. There was a negligible effect of pH on adsorption of methyl orange. Langmuir model was fitted perfectly well and the maximum monolayer adsorption capacities obtained from Langmuir model was 130.9 mg/g. The adsorption kinetics followed pseudo-second order model. This study is an example of ionic crosslinking process adopted for simple modification of chitosan.

The removal of Direct Red 80 (DR80), Reactive Yellow 25 (RY25) and Acid Blue 25 (AB25) dyes by chitosan-based beads has been investigated by Luk et al[20]. Glutaraldehyde crosslinked chitosan beads achieved complete removal of the three dyes within one hour. It was observed that adsorption with crosslinked beads at pH 5 promotes removal of RY25 and AB25 by at least two folds more than that by non-crosslinked chitosan beads. The adsorption capacity towards RY25 and AB25 are 368.3 mg/g and 443.3 mg/g respectively. DR80 adsorption is achieved at more acidic condition at 610.5 mg/g. Adsorption isotherm fitted Langmuir model and pseudo-second order equation agreed very well with kinetics data. This material has a potential of multi-toxicant removal and these studies could be very well extrapolated to simultaneous removal of organic dyes from a single solution.

Bulut and Karaer[21] reported crosslinked chitosan/bentonite composite for the removal of Methylene blue from aqueous solution. From the observation of kinetics and thermodynamic parameters of adsorption process, it was confirmed to be an endothermic spontaneous adsorption process. Equilibrium experiments fitted well with Langmuir isotherm model and the maximum monolayer adsorption capacity for MB was 95.24 mg/g at 298K. Kinetics studies estimated that the process was rapid and followed second order kinetics. The maximum uptake was achieved in more basic aqueous environment.

Glutaraldehyde crosslinked magnetic chitosan nanoparticles (GMCNs) have been examined for adsorption of FD&C Blue 1 and D&C Yellow 5 dyes from aqueous solutions, by Zhou et al[22]. Results indicated that GMCNs not only exhibited excellent food dyes adsorption, but also showed low cytotoxicity. From study, it was observed that the adsorption capacity of GMCNs for food dyes were affected by initial pH values, initial dye concentrations and temperatures. Adsorption followed pseudo-second order reaction, and equilibrium

experiments were well fitted Langmuir isotherm. GMNCs displayed maximum capacity of adsorption at pH 3.0 at 298K. Spontaneous and exothermic nature of adsorption was demonstrated through thermodynamic studies. Experimental observations indicated that GMNCs can be regenerated and reused through dye desorption in alkaline solution. Magnetization of the material has made separation of composite extremely easy and rapid after adsorption of dye.

Magnetic chitosan nanocomposites (MCNCs) were synthesized by Kadam et al[23] using reduction precipitation technique with glutaraldehyde as a crosslinker. These supermagnetic MCNCs exhibited magnetic saturation of 17.5 emu/g. and showed 90.60% adsorption of Acid Red 2. Experimental data showed that high adsorption of dye on MCNCs was resulted from presence of free amino and hydroxyl groups. It was observed that the optimum pH and adsorbent concentration were 3 and 1.0 g/L, respectively. Adsorption isotherm best fitted according to Redlich-Peterson models. This isotherm model has a linear dependence on concentration in numerator and an exponential function in denomination which altogether represent adsorption equilibrium over a wide range of concentration of adsorbate which is applicable in either homogenous or heterogeneous systems because of its versatility.

Liu and co-workers[24] reported adsorption of anionic azo dye by crosslinked chitosan/bentonite composite. They synthesized crosslinked chitosan (CCS)/bentonite (BT) composite by the intercalation of chitosan in bentonite and crosslinking reaction between chitosan and glutaraldehyde. Crosslinked chitosan/bentonite composite adsorbed Amido Black 10B at pH 2 to a greater extent. Maximum adsorption capacity of CCS/BT composite was 323.6 mg/g at 293 K and pH 2 and best fitted with Langmuir adsorption isotherm. Thermodynamic and kinetics parameters study showed that adsorption of Amido Black 10B by CCS/BT composite was spontaneous and endothermic in nature and followed a pseudo-second order kinetics model. The only limitation of this process was very low working pH that makes post-adsorption process necessary to eliminate excess acidity imparted to solution.

Xuemei et al[25] synthesized crosslinked chitosan hybrid membranes with oxidized starch and silica couple agent (CS/OSR/Silica) had been employed for removals of two direct dyes (Blue 71 and Red 31). With the help of crosslinking, they achieved enhanced thermal stability and swelling property of CS/OSR/Silica hybrid membrane. The adsorption capacity of CS/OSR/Silica membrane was higher at pH 9.82 for two direct dyes at a fixed membrane dosage and dye concentration. Adsorption of dyes onto CS/OSR/Silica membranes follow

pseudo-second order model and experimental equilibrium data fitted well Freundlich isotherm model. The adsorption capacities on CS/OSR/Silica membranes are 67.2 mg/g and 94.4 mg/g respectively for Blue 71 and Red 31 respectively[25]. It is one of the very few materials that act as good adsorbents in alkaline pH range.

Another example of decorated chitosan with Fe_3O_4 nanoparticles followed by crosslinking with Graphene oxide to prepare Fe_3O_4 supported chitosan-graphene oxide composite (Fe_3O_4©-GO) was synthesized by Gul et al[26]. and co-workers for the removal of Methyl violet and Alizarin yellow R dyes. Adsorption kinetics best fitted with pseudo-second order model. Langmuir and Freundlich isotherm were applied to understand the interaction of dye with adsorbent. Adsorption of Methyl violet and Alizarin yellow R dyes onto Fe_3O_4©-GO best fitted with Langmuir isotherm and maximum adsorption was achieved at pH 10 and 6 respectively for Methyl violet and Alizarin yellow R. The enhanced surface area due to mesoporous nature of graphene-magnetite composite has led to enhancement in adsorption capacity.

Hydrothermal treatment of NaOH was carried out by Khanday et al[27] to obtain crosslinked beads of activated oil palm ash zeolite/chitosan (Z-AC/C) composite using activated oil palm ash followed by beading with chitosan. Batch adsorption of methylene blue (MB) and acid blue 29 (AB29) were studied to find out effect of dye concentration, temperature and pH. Adsorption of both dyes on Z-AC/C was better described by Pseudo-second order kinetics and Freundlich isotherm model. The maximum adsorption was found to be 151.51 mg/g for MB and 212.76 mg/g for AB29 at pH 11 and 3 respectively. As working pH are two extreme values, it has not been possible to study simultaneous removal of both the dyes.

In line with the adsorption of methylene blue (MB) and reactive orange 16 (RO 16), crosslinked chitosan/sepiolite composite was employed by Marrakchi et al[28] where sepiolite clay and chitosan were crosslinked using epichlorohydrin. Adsorption studies were carried out for MB and RO16 adsorption onto Crosslinked chitosan/sepiolite composite. It was observed that Methylene blue gives highest adsorption at pH 9 while for Reactive orange 16 maximum adsorption was achieved at pH 3 and their adsorption capacities were found to be 40.986 mg/g and 190.965 mg/g respectively. Various adsorption isotherms were examined such as Freundlich, Langmuir, and Temkin. From adsorption data for both the dyes it was noticed that Freundlich was best fitted model. For both the dyes pseudo-second order kinetics were found to describe adsorption process better than pseudo-first order kinetics.

A novel graphene oxide-based adsorbent (FCGO) from fly ash crosslinked with chitosan and graphene oxide was synthesized by Guanghong et al[29]. It was used for effective removal of anionic and cationic dyes, namely, Acidic Red GR (ARG) and Cationic 5GN (CRX), respectively. The effect of pH upon adsorption was carried out. It was noticed that percentage removal of anionic dye by FCGO decreases with increasing initial pH in acidic Red X-solutions but is not affected at pH higher than 6 while initial pH minimally influences percentage removal of cationic dye. After adsorption of both anionic and cationic dyes by graphene oxide-based adsorbent, final pH becomes close to neutral in acidic medium because of protonation effect. The adsorption kinetics of ARG and CRX follow pseudo-second order kinetics model. Adsorption process fits well with Redlich-Peterson model. The maximum adsorption capacities are 38.87 and 64.50 mg·g-1 for ARG and CRX, respectively. From thermodynamic data, it was noticed that adsorption is a spontaneous and endothermic process.

Jawad et al[30] and co-worker fabricated immobilized crosslinked chitosan-epichlorohydrine thin film (CLCETF) onto glass plate for adsorption of reactive orange 16 (RO16) dye using direct casting technique. Batch adsorption studies were carried out taking contact time, initial dye concentration and pH. From adsorption isotherm it was noticed that adsorption of reactive dye onto CLCETF followed Langmuir model. The adsorption capacity of CLECTF for RO16 was 356.50 mg/g at 27 ± 2∘C. The kinetics parameters demonstrated that the process closely followed pseudo-second order model. From the results, it was clear that immobilized CLECTF can be used as a potential candidate for the treatment of reactive dye without using filtration process.

Crosslinked chitosan(C)/marble powder (M) composites were prepared by Deniz et al[31] from marble powder and chitosan and crosslinked using glutaraldehyde. Adsorption behavior of chitosan/marble powder composite for Dimozol Blue was evaluated. Adsorption behavior of Dimozol Blue onto the chitosan/marble powder composites was carried out to evaluate adsorption kinetics and equilibrium isotherms from aqueous solution. Dimozol Blue dye adsorption on Crosslinked chitosan(C)/marble powder (M) composites was described well by pseudo-second order and Freundlich isotherm models. Study shows maximum adsorption capacity of chitosan/marble powder composites for removing Dimozol Blue to be 234.5 mg/g at pH. The thermodynamic studies revealed that Adsorption process is spontaneous and exothermic and adsorption is physical adsorption was revealed from thermodynamic

equilibrium experiment. The marble powder that gets waste after cutting of marble stones was successfully utilized to enhance the adsorption capacity of chitosan towards Dimazol Blue.

Potential of novel crosslinked chitosan for removal of Congo red dye from an aqueous phase was studied by Zahir et al[32]. Adsorption of dye unto Diammonium tartrate modified Chitosan (DMC) and Urea Diammonium tartrate modified Chitosan (UDMC) examined at different conditions like effect of adsorbent dose, contact time, initial solution pH and temperature. Sips Isotherm model was followed strictly according to adsorption isotherm studies and maximum dye uptake was 1597 mg/g for Diammonium tartrate modified Chitosan (DMC) while 1447 mg/g for Urea Diammonium tartrate modified Chitosan (UDMC). Pseudo second order kinetics model was best fitted. From value of $\Delta H°$ and $\Delta G°$, it is suggested that the process of adsorption is feasible and endothermic nature of Congo red adsorption over both adsorbents. Incorporation of nitrogen containing moieties into chitosan matrix was found to have a positive impact on adsorption efficiency.

Apart from usual adsorbent, antimicrobial terephthaloyl thiourea crosslinked chitosan (TTCCH) hydrogels was investigated by El-Harby et al[33] for Congo red dye removal from its aqueous solution. Hydrogel was synthesized by reacting chitosan with terephthaloyl diisothiocyanate crosslinker. To achieve best adsorption capacity of hydrogel, its structure, dye adsorption parameters were studied. The parameters incudes initial concentration of the dye solution, temperature and time of exposure to dye. The investigation of adsorption kinetics and isotherms informed that the process of adsorption of Congo red dye onto TTCCH was better fitted by pseudo-second order equation and Langmuir equation, respectively. Adsorption of Congo red dye achieved maximum sorption capacity of 44.248 mg/g. which confirmed the process of uptake of Congo red dye on adsorbent is a chemisorption process. Examination of thermodynamic data showed that adsorption reaction was endothermic and spontaneous in nature.

Foam membrane based crosslinked chitosan was discussed by Hu-Cheng et al[34], to remove some colored dyes. Polyurethane foam membrane filled with humic acid-chitosan crosslinked gels (HA-CS-PUF) was synthesized for dye removal by soaking foams into humic acid-chitosan (HA-CS) crosslinked gels and hot-pressing them into membranes. HA-CS-PUF was characterized for structural morphology by SEM, thermal stability was studied by DTA and membrane was characterized for X-ray photoelectron spectroscopy. These studies revealed

that humic acid and chitosan crosslinked through ionic bonding. Different charged dyes were examined for membrane properties. For that purpose, three dyes were selected including positively charged methylene blue (MB), neutrally charged rhodamine B (RB) and negatively charged methyl orange (MO). Adsorption experiment were carried out to tests their maximum adsorption capacities, kinetics parameters and thermodynamics. Study revealed that adsorption process was better fitted with Pseudo-second order and Freundlich model. Maximum adsorption capacities were found to be 10.31 mg/g, 8.26 mg/g and 5.29 mg/g for MB, RB and MO respectively. The highest adsorption of methylene blue, rhodamine B and methyl orange was achieved at pH 10, pH 4 and pH 4 respectively.

New material for adsorption of textile dye Direct orange 2GL was introduced by Dilarri et al[35], and group. They proposed immobilized Saccharomyces cerevisiae in crosslinked chitosan beads to analyze kinetics, isotherm and thermodynamics for adsorptive removal of textile dye. Adsorption studies were carried out according to pH, it was found that Maximum adsorption of Direct orange 2GL dye onto saccharomyces cerevisiae immobilized crosslinked chitosan was achieved at pH 8. Study revealed that Freundlich isotherm was the best fitted model and adsorption process followed Pseudo second order kinetics. The process was spontaneous and endothermic in nature observed according to thermodynamic data.

The example of β-chitosan crosslinked with nitrogen containing polyamine base eg. triethylenetetramine, (BCCT) demonstrated by Chih-Wei et al[36] for adsorption and removal of Reactive Blue 221 (RB221) dye. Results indicated that, with increasing temperature from 303 to 333 K, adsorption rates of adsorbent BCCT for RB221 dye changed from 1.48×10^6 mg/g.min to 1.52×10^{13} mg/g.min. Adsorption of dye at all temperatures followed Elovich model. These results confirmed that crosslinking leads to incorporation of amine groups, thereby promoting ability of BCCT to adsorb dyes under strongly acidic conditions. Adsorption process revealed that Langmuir isotherm was best fitted with maximum adsorption capacity of 625.0 mg/g.

Carboxymethylated and partially crosslinked chitosan (NaCS-GL) was employed as an effective adsorbent, for removal Of Methylene Blue from aqueous solution, by Doshi et al[37]. Carboxylate groups protonates amino groups on surface of NaCS-GL. Initial rate of adsorption of MB onto NaCS-GL controlled by chemical reaction later it governs by intraparticle diffusion. Kinetics study revealed that the process was following pseudo-second order kinetics. Adsorption isotherms best fitted with Sips isotherm and maximum adsorption

capacity was 365.77 mg/g. The Sips model is a hybrid model combining both Langmuir and Freundlich models. Sips model can describe the homogeneous or heterogeneous systems. Spontaneous and exothermic nature of adsorption of methylene on NaCS-GL was revealed by thermodynamic parameters. The highest adsorption of Methylene blue onto partially carboxymethylated and partially crosslinked chitosan was achieved at pH 5.6.

Sulphate crosslinked chitosan (SCC) for removal of Congo red (a benzidine-based anionic diazo dye) was studied by Jeyaseelan and co-workers[38]. Adsorption studies carried out considering pH, contact time, adsorbent dosage, and concentration of adsorbent. Maximum adsorption capacity obtained at pH 3.0 was 91.8 mg/g at which percentage recovery was about 90% and followed Freundlich adsorption isotherm. The process of capture of congo red dye by SCC followed pseudo-second order kinetics. Thermodynamic equilibrium study noticed that process of adsorption is spontaneous and exothermic in nature. Regeneration of SSC was done with NaOH after repeated cycles.

Polymeric hydrogel (N-maleyl chitosan crosslinked P(AA- co-VPA))synthesized from acrylic acid (AA), vinylphosphonic acid (VPA) and N-maleyl chitosan was studied for the adsorptive removal of crystal violet (CV) and methylene blue (MB) dyes from aqueous solutions. In this study, Nakhjir et al[39] examined Langmuir, Freundlich, Temkin and Redlich-Peterson isotherm models. Experimental data was well described by Redlich-Peterson isotherm model. The adsorption kinetics followed pseudo-second order model. Hydrogel polymer showed adsorption capacity of for removal of CV and MB in 50 ppm dye solutions was 64.56 mg/g and 66.89 mg/g, respectively. Data obtained from thermodynamic studies dictated adsorption process was endothermic and spontaneous. In addition to that adsorbent was regenerated after four fold of adsorption-desorption cycle.

Antimicrobial agent, trimellitic anhydride isothiocyanate-crosslinked chitosan hydrogels has been investigated by Mohamed et al[40]. This new adsorbent was applied to Congo red (CR) dye removal from its aqueous solution. Being polycationic hydrogel, the adsorption capacity of this material has been highly influenced for CR dye. Study revealed that the uptake of congo red dye onto trimellitic anhydride isothiocyanate-crosslinked chitosan hydrogels increased significantly with increasing temperature, with decreasing solution pH and with an increase in their contents of crosslinking. The process of adsorption fitted well to pseudo-second order kinetics model and confirmed to Langmuir model. The maximum adsorption capacity of hydrogel was found to be 63.05 mg g^{-1} with removal efficiency of 96.59%. The

process is remarkably controlled by chemisorption phenomenon and it was endothermic in nature according to thermodynamic observation. Its an excellent combination of adsorbent formed with antimicrobial activity leading to removal of chemical as well as biological pollution.

One of established groups of Jawad et al[41] reported an inorganic–organic hybrid nanocomposite bioadsorbent for removal of reactive red 120 (RR120) dye from aqueous environment using hybrid crosslinked chitosan-epichlorohydrin/TiO_2 nanocomposite (CTS-ECH/TNC). Adsorption of reactive dye was carried on synthesized adsorbent, maximum adsorption capacity of CTS-ECH/TNC for RR120 dye was recorded to be 210 mg/g at 303 K. From kinetics and adsorption modelling experiments, it was recommended that, the process well illustrated by pseudo-second order (PSO) kinetics and Langmuir isotherm model. Thermodynamic parameters study confirmed spontaneous and endothermic in nature od adsorption RR120 dye on CTS-ECH/TNC. On the basis of characterization and adsorption studies, the uptake of dye on the synthesized nanocomposite was governed by interactions such as electrostatic attraction, n-π stacking, and H-bonding which proves CTS-ECH/TNC as potential adsorbent for removal of RR120 dye as model of reactive azo dyes from aqueous environment.

Same group of researchers came up with an alternative for adsorptive removal of reactive red 120 (RR120) dye from an aqueous solution[42]. Tunable Schiff's base-crosslinked chitosan-glutaraldehyde (CS-GLA/TNA) was selected for studies. Batch adsorption experiment carried out considering parameters, such as adsorbent dosage (0.01–1.2 g/mL), RR120 dye concentration (30-400 mg/L), solution pH (3–12), and contact time (0–400 min). Different adsorptions modelling along with kinetics of the process were examined and results suggested that the process was well described by Freundlich model and pseudo-second order kinetics model. Maximum adsorption capacity of CS-GLA/TNC for RR120 dye was 103.1 mg/g at 30°C at pH 3 which was the combined effect of various interactions, such as electrostatic attraction, n–π stacking, and H-bonding.

Chitosan crosslinked graphene oxide/carboxymethyl cellulose aerogel globules CS-GO/CMC was administrated toward methylene blue (MB) removal by Hyang et al[43]. The results showed that CS-GO/CMC composite aerogel had extremely high adsorption capacity reported so far in literature was 3190 mg/g. Various parameter such as adsorption isotherms, kinetics and thermodynamics were investigated. Data recommended that adsorption of

methylene blue onto CS-GO/CMC followed Langmuir adsorption model, pseudo-second order model and adsorption was a spontaneous and endothermic process.

To remove two structurally different reactive orange 16 (RO-16) and methyl orange (MO) dyes Jawad and co-workers[44] used crosslinked chitosan with glyoxal (Chi-Gly) and deposited onto glass plate to be a superior adsorbent film using non-conventional adsorption system without filtration process. Further, various adsorption isotherms were investigated, among all those adsorption isotherm of RO-16 and MO by Chi-Gly film were best described by Langmuir isotherm, with maximum adsorption capacities of 1554.3 mg/g and 1451.9 mg/g, respectively. Kinetics modelling data revealed that pseudo- first order kinetics model best fitted. Thermodynamic study informed that adsorption process was spontaneous and exothermic in nature at Chi-Gly at pH ~3. The highest values of uptake of RO-16 and MO by Chi-Gly film involved various interactions such as electrostatic attractions, dipole–dipole hydrogen bonding interactions, Yoshida H-bonding and n-π stacking.

Lyu et al[45] functionalized chitosan with ionic liquid to obtain ionic liquid functionalized crosslinked chitosan (IL-CCS) for removing sunset yellow FCF (SY) from aqueous solutions. Adsorption studies were carried out considering parameters such as initial pH, adsorbent dose and contact time. Investigation showed that there was negligible effect of pH on adsorption capacity of IL-CCS for SY. Maximum uptake of IL- CCS for SY observed was 300.28 mg/g, In addition, results of adsorption isotherm, kinetics and thermodynamics showed that adsorption process could fit with Langmuir model, pseudo- second order model, separately. The exothermic nature of reaction was revealed through thermodynamic parameters.

Graphene oxide/lignosulfonate aerogel (GLCA) crosslinked by chitosan without using any toxic chemicals was investigated by Mingfang et al[46] to test adsorption performance of GLCA to methylene blue (MB) considering factors such as pH, dosage, contacting time, temperature and initial concentration. The results showed that synthesized GLCA uptake MB dye potentially remove 99% MB dye from its 100 ppm dye solution. Calculated capacity of MB dye onto GLCA was 1023.9mg/g, which was highest ever than any other reported value for GO/polymer composites and activated carbon in literature. Thermodynamic data noticed that adsorption of MB on GLCA was spontaneous and endothermic in nature. The adsorptive removal of MB onto GLCA may consider various interactions such as electrostatic attraction, π-π interaction and hydrogen bond between GLCA and MB. In addition to that, adsorbent could be regenerated by washing with HCl solution and ethanol for number of cycles.

Another example of crosslinked chitosan-glyoxal/TiO$_2$ nanocomposite (CCG/TNC) by loading different ratios of TiO$_2$ nanoparticles into polymeric matrix of crosslinked chitosan-glyoxal (CCG) have been used for removal of methyl orange (MO) from waste water. Results obtained by Mohammed et al[47] showed that adsorption of MO on CCG/TNC described by pseudo-first order kinetic. The process was in agreement with Langmuir isotherm model with maximum adsorption capacity of 416.1 mg/g at pH 4. Mechanism of adsorption involved various interactions such as electrostatic attractions, n-π stacking interactions, dipole–dipole hydrogen bonding interactions, and Yoshida H-bonding.

Methylenebisacrylamide (MBA) and acrylic acid (AA), chitosan/polyacrylic acid/bentonite composites (CCS/PAA/BNTs) was synthesized and used for adsorption of malachite green (MG) by Yildirim et al[48]. Experimental data gave good agreement with Langmuir model and followed pseudo-second order kinetics. The highest adsorption capacity calculated was found as 384.62 mg/g for MG adsorption at 318 K at pH 6. MG adsorption was endothermic, caused spontaneous reaction and increased entropy between 298-318 K described by thermodynamic studies. Study revealed that adsorption reactions of MG was physisorption ($\Delta H < 80$ kJ mol^{-1}).

Jawad et al[49] reported blending of coalesced Chitosan (CS) with activated charcoal (AC), followed by crosslinking reaction with epichlorohydrin (ECH) was studied to remove thionine (TH) a model cationic dye, from aqueous solution. Batch adsorption studies of CS-ECH/AC was carried out considering various parameters such as initial concentration, adsorbent dose, time etc. The experimental studies showed good agreement with Freundlich isotherm. The maximum adsorption capacity of CS-ECH/AC for TH dye adsorption was 60.9 mg/g at 303 K. The kinetics followed pseudo-second order model. The values calculated for enthalpy and entropy indicated a spontaneous and exothermic nature of adsorption process. The study proved from characterizations that adsorption mechanism included mostly electrostatic attractions, H- bonding interactions, and π–π interactions. CS-ECH/AC found to be compatible composite for the removal of cationic dyes from wastewater.

Mohammed at al[50] physically modified Chitosan (CS) with fly ash (FA) powder and then chemical crosslinking reaction with tripolyphosphate (TPP) to produce a crosslinked FA composite (CSTPP/FA) was examined as adsorbent for removal of reactive orange 120 (RR120) dye. Adsorption studies noticed that the highest removal (88.8 %) of RR120 dye was achieved by CS-TPP/FA at pH 4. The adsorption equilibrium provide good agreement

with Freundlich model and maximum adsorption capacity of CS-TPP/FA for RR120 dye was found to be 165.8 mg/g at 45 °C. Kinetics uptake was well described by Pseudo second order. Thermodynamic studies concluded that adsorption process was spontaneous and exothermic in nature. CSTPP/FA concluded as an ideal composite adsorbent for removal of textile dyes from aqueous environment on the basis of adsorption parameter study.

Crosslinked Chitosan/β-Cyclodextrin beads have been utilized by Kekes and Tzia[51] to study the adsorption of Indigo Carmine. Adsorption studies were carried out considering various parameters such as dye's initial concentration, pH and temperature, and high concentrations of adsorbent. At lower concentration of dye, it was observed that adsorbent removes Indigo Carmine at faster rate at pH 4. On the basis of adsorption study, equilibrium adsorption data were described well for Langmuir model and maximum adsorption capacity was 1000.0 mg/g. Adsorption of Indigo Carmine was found to follow pseudo-second order. The data obtained from thermodynamic study such as negative values of ΔG^o, ΔH^o and ΔS^o dictated adsorption process is exothermic, spontaneous and favorable at low temperatures.

Chanajaree and co-workers[52] examined removal of two dye species i.e. Malachite Green (MG) and Indigo Carmine (IND) using Glutaraldehyde crosslinked chitosan (CSglu), by computational and experimental methods. Freeze dry method was applied to obtain CSglu beads. It is found from adsorption study that the CSglu beads can remove MG much better than IND. The maximum adsorption capacity was found to be 714.29mg/g for Malachite Green and 303.03mg/g for indigo carmine at pH 6. Adsorption kinetics study described well by pseudo-second order kinetics model for both complexes. Thermodynamic study has been carried out to find out values of ΔH and ΔG. The results suggested that adsorption processes of MG-CSglu are spontaneous and endothermic due to negative value of ΔG and positive value of ΔH, while IND-CSglu is non-spontaneous and exothermic.

Crosslinked oxalic acid/chitosan hydrogel (ChOxb) for adsorption of azo-dyes (Reactive Red 195 RR195) from wastewater was reported by John et al[53]. Batch adsorption performance showed a maximum percentage of removal of 90.6%, at pH 4. The maximum adsorption capacity at pH 4 was 110.7 mg/g. Among various adsorption isotherm studied, results gives good agreement with Redlich-Peterson adsorption isotherm and best fitted with pseudo-second order kinetics. Thermodynamic data suggested that adsorption process is endothermic and spontaneous.

Epichlorohydrin crosslinked chitosan/carbon–clay (CSCC) bio-hybrid was studied as an adsorbent by Marrakchi et al[54] for adsorption of cationic methylene blue (MB) and anionic azo acid blue 29 (AB 29). Batch adsorption of MB and AB 29 on CSCC was carried out considering initial dye concentration, initial pH (3−11), and contact time and adsorption temperature. Results of dyes adsorption onto CSCC described well to pseudo-second order model. The isotherms analysis demonstrated that Freundlich isotherm followed adsorption data, and maximum adsorption capacity was found to be 95.31(mg/g) for MB and 167.35 (mg/g) for AB29.

Potential sorbent for exclusion of Reactive Blue 9(RB 9) dye, nano chitosan, crosslinked with activated carbon obtained from fish scales have been employed by Sundararaman et al[55]. Among different isotherms applied Freundlich isotherm proved to be successful and multilayered adsorption was achieved at pH 6.25 with maximum adsorption capacity was revealed to be 31.25 mg/g. Thermodynamic and kinetics data proved the evidence of involved second order kinetics and adsorption of process of Reactive Blue 9(RB 9) dye on nanocomposite owing to occurrence of spontaneous, exothermic and feasible process.

Various pollutants including bacteria, proteins, fluoride, dyes, and pharmaceuticals have been proposed to be removed by crosslinked chitosan/nitrogen doped-graphene quantum dot nanocomposites (CS/NGQD) synthesized via glutaraldehyde as crosslinker by a research group of Amari[56]. Interestingly, it was demonstrated that the synthesized CS/NGQD showed great uptake of dyes. Adsorption studies revealed that CS/NGQD significantly removes dyes as- 82% for Azo blue, 84% for methylene blue and 94% for orange G. Along with that, study noticed after reusability of adsorbent, the nanocomposite remains efficient for removal of pollutants from water after 5 number of repeated cycles.

For effective simultaneous removal of dyes and metals, Usman et al[57] reported a new adsorbent Nitrilotriacetic acid β-Cyclodextrin-Chitosan (NTA-β-CD-CS) was employed. In process of adsorption, the β-CD cavities play an important role for the uptake of Methylene blue (MB) by host/guest contacts while rest of the functionalities were able to capture metal ions and Methyl orange (MO). Maximum adsorption capacities calculated of NTA-β-CD-CS adsorbent toward MB and MO were 162.6, and 132.5 mg/g, at pH 6 and 3 respectively. Among all adsorption models studied, Sips model was appropriate to define adsorption system and mechanism and worked constantly even after four cycles.

Graphene oxide (GO) crosslinked nanocomposites hydrogels (NCH) of chitosan (CS) and carboxymethyl cellulose (CMC) was synthesized and its application for the removal of cationic and anionic dyes contaminated waste water was explored by Mittal and Alhassan[58]. From the adsorption studies, it was revealed that about 99% dye was adsorbed from the dye solution of MB dye with CS/CMC-NCH at pH 7, whereas, for MO about 88% dye was adsorbed with CS/CMC-NCH at pH 3. Kinetics data explained the adsorption process of both dyes follows pseudo-second order and Langmuir models with the maximum adsorption capacities of 655.98 mg/g for MB and 404.52 mg/g for MO. From the values of change in enthalpy and change in entropy it was suggested that the process of uptake of methyl orange as well as methylene blue onto CS/CMC-NCH was spontaneous and exothermic in nature.

Recently, ultrasound wave-induced synthesis of crosslinked chitosan hydrogels (CAAT) using terephhalaldehyde as crosslinking agent was reported by Garg et al[59]. The adsorption performance for the removal of congo red dye on CAAT revealed that the adsorption of congo red dye on CAAT best fitted the Redlich-peterson isotherm. Kinetics of adsorption strictly follows pseudo-second order model. CAAT hydrogel shown its potential up to six adsorption-desorption cycles after its desorption studies.

We have reported glutaraldehyde crosslinked chitosan-alginate material including the Twizzer-like aniline pendents to enhance the adsorption efficiency towards brilliant green, methyl orange and patent blue V dyes. All the three dyes followed Freundlich model with pseudo-second order kinetics. Adsorption capacities of 235.82, 198.09 and 117.34 mg/g were observed for the three dyes respectively at pH 8, 6 and 3 respectively[60].

A most recent work of our own research group[61] reports chitosan-activated charcoal composite with tripolyphosphate as a crosslinker for the removal of remazol brilliant blue R dye with excellent adsorption capacity of 540.3 mg/g in accordance with Langmuir isotherm model. More than 95% of the dye was removed from 200 mg/L solution of the dye within 60 minutes. The process was observed to be endothermic and entropy-driven in nature. This material is probably the best in terms of adsorption capacity as well as the rate of adsorption. Tripolyphospate crosslinker was found to impart thermal as well as mechanical stability to the composite.

Conclusion

Immense developments and studies have been done on chitosan with focus of evaluating and marketing chitosan as an alternative adsorbent for activated carbon. Major goal behind chitosan to be emerging as adsorbent is that it has to be abundant at lower cost, non-toxic to the nature, its processing should be easier and must remove the dyes effectively from the waste water. The results indicated that chitosan provides greater class of agreement with majority of essential criteria's because of its advantageous nature such as cheaper in cost, maximum adsorption capacity and selectivity, its versatile nature, non-toxicity to environment, compatibility and biodegradability. It is noticed that modified chitosan is found to be potential adsorbents for the removal of dyes from effluents. Functional characteristics along with surface morphology and adsorption application of chitosan significantly influenced by chemical and physical processing. Study revealed that dissolution of chitosan required acidic medium and modified with various crosslinkers (such as glutaraldehyde, epichlorohydrin, tripolyphosphate etc). To improve surface characteristics of chitosan in adsorption applications it could be modified with some common solid adsorbents such as activated carbon, clay and magnetized materials. Although crosslinking is commonly utilized for improving the chemical and mechanical stabilities of chitosan but often decreases adsorption capacity of chitosan/modified-chitosan for the uptake of dyes from the waste water. In this review we noticed that glutaraldehyde and epichlorohydrin are the most commonly used crosslinkers used for the modification of chitosan. Adsorption isotherm modelling revealed that in most of the cases Langmuir isotherm fitted best and the kinetics were well explained by pseudo-second order kinetics. On the basis of properties of chitosan and from the results obtained, we can evaluate chitosan to be a very prominent adsorbent for wastewater treatment. Still, chitosan-based research has scope of improvement, and believed that chitosan and its crosslinked derivatives can largely be employed commercially and its use should not be limited to the laboratory. A comparative account of various crosslinked chitosan materials used for the removal of dyes has been summarized in Table 1.

An important aspect of chitosan-based adsorbents is its potential of regeneration and reusability. Almost all the studies mentioned in this review have shown that the crosslinked chitosan materials could be very effectively used in multiple adsorption-desorption cycles. The number of cycles reported in literature range from 3 to 15. This shows the cost-effectiveness of these materials as compared to other treatment technologies like chemical and biological processes where the recovery of treatment material is not feasible.
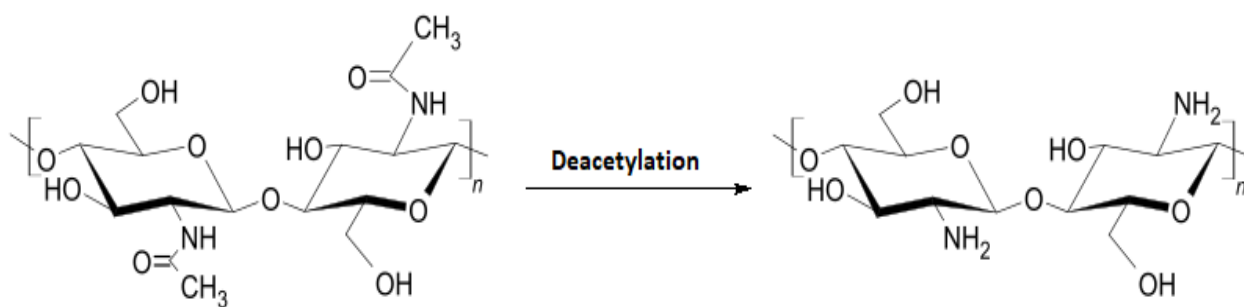
Figures :

Fig. 1: Synthesis of chitosan from chitin

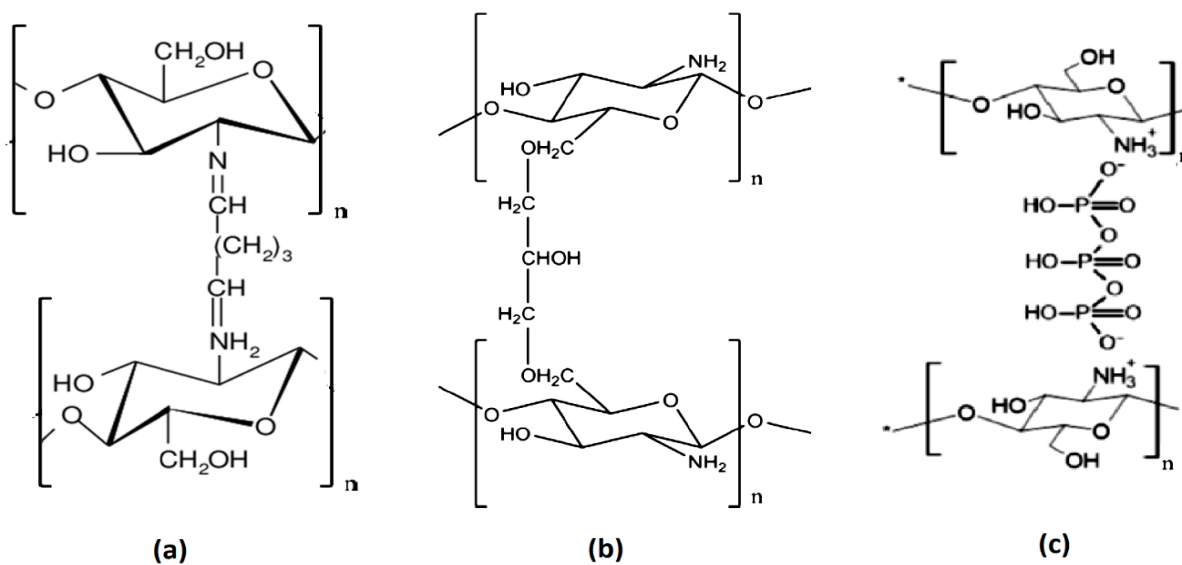(a)   (b)   (c)

Fig. 2: Crosslinking of chitosan using (a) glutaraldehyde (b) epichlorohydrin
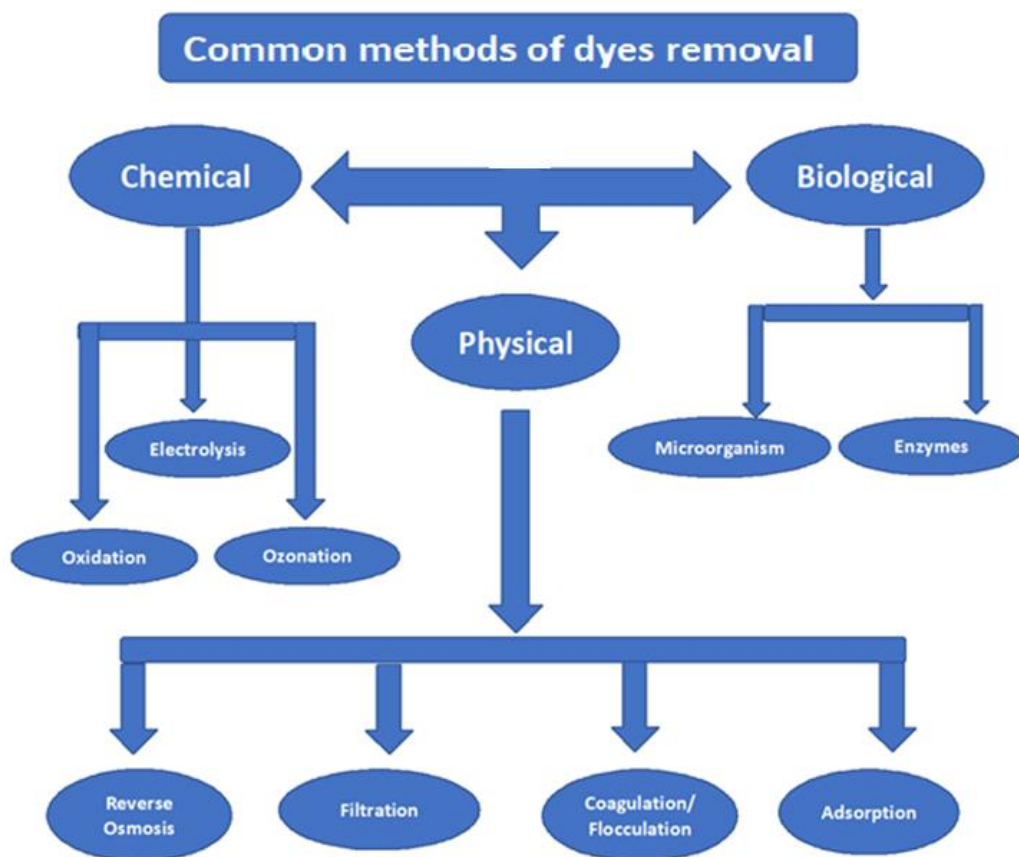(c) tripolyphosphate

Fig. 3: Methods for removal of dyes from water bodies

Table:

Table 1: Crosslinked chitosan reports for adsorption of dyes

Sr. no	Adsorbent	Adsorbate	Adsorption Capacity (mg/g)	pH	Kinetics	Isotherm	Ref
1	Sodium tripolyphosphate crosslinked chitosan beads	i) Metanil yellow ii) Reactive Blue 15	1334 722	4 4	PFO PFO	Langmuir Langmuir	11
2	Crosslinked chitosan/oil palm ash composite	Reactive Blue 9	423.5	6	PSO	Redlich-Peterson	12
3	Ethylene glycol diglycidyl ether crosslinked chitosan	i) Acid Red 37 ii) Acid Blue 25	59.52 142.86	2 4	PSO PSO	Langmuir Langmuir	13
4	i)sulphuric acid	i) Acid blue 25	102.53	6	PSO	Langmuir	14

	crosslinked chitosan beads	ii) Acid Red 37	139.28	4	PSO	Langmuir	
	ii) Glutaraldehyde crosslinked chitosan beads	i)Acid blue 25 ii) Acid Red 37	127.06 166.67	6 4	PSO PSO	Langmuir Langmuir	
5	Magnetically separable Υ-Fe_2O/crosslinked chitosan	Methyl Orange	-	4	PSO	-	15
6	Crosslinked chitosan poly (acrylamide)	i)EY-4GL ii) S Blue	63.20 18.90	-	PSO	Langmuir	16
7	Crosslinked chitosan beads	Reactive dye	19.613	-	-	Freundlich	17
8	Template crosslinked chitosan nanoparticles (epichlorohydrin)	i) Remazol Black 5 ii) Remazol brilliant orange 3R	5572 5392	3 3	PSO PSO	Langmuir Langmuir	18
9	Protonated crosslinked chitosan	Methyl orange	130.9	6.7	PSO	Langmuir	19
10	Glutaraldehyde crosslinked chitosan	i)Direct Red 80 ii) Reactive Yellow 25 iii) Acid Blue 25	610.5 368.3 443.3	2 5.5 5.5	PSO PSO PSO	Langmuir Langmuir Langmuir	20
11	Crosslinked chitosan/bentonite composite	Methylene Blue	95.24	11	PSO	Langmuir	21
12	Glutaraldehyde crosslinked magnetic chitosan nanoparticles	i) FD&C Blue 1 ii) D&C Yellow 5	475.61 292.07	3	PSO	Langmuir	22
13	Glutaraldehyde crosslinked magnetic chitosan	Acid Red 2	90.06	3	-------	Redlich-Peterson	23

	nano composite						
14	Crosslinked chitosan/Bentonite composite	Amido Black 10B	323.6	2	PSO	Langmuir	24
15	Oxidized starch crosslinked chitosan/silica hybrid membrane	i)Blue 71 ii) Red 31	67.2 94.4	9.8 9.8	PSO PSO	Freundlich Freundlich	25
16	Magnetic chitosan crosslinked with graphene oxide	i) Methyl Violet ii) Alizarin yellow R	- -	10 6	PSO PSO	Langmuir Langmuir	26
17	Crosslinked beads of activated oil palm ash zeolite/chitosan	i)Methylene Blue ii) Acid Blue 29	151.51 212 .76	11 3	PSO PSO	Freundlich Freundlich	27
18	Crosslinked Chitosan/sepiolite composite	i)Methylene Blue ii) Reactive orange 16	40.986 190.965	9 3	PSO PSO	Freundlich Freundlich	28
19	Fly ash crosslinked chitosan/graphene oxide composite	i)Acid Red GR ii) Cationic Red X-5GN	38.87 64.50	3 6	PSO PSO	Redlich-Peterson	29
20	Crosslinked chitosan epichlorohydrine thin film	Reactive orange 16	356.50	3	PSO	Langmuir	30
21	Crosslinked chitosan/Marble powder composite	Dimozol Blue	234.5	5	PSO	Freundlich	31
22	i)Diammonium tartarate crosslinked chitosan ii) Urea diammonium tartarate crosslinked	Congo Red	1597 1447	4 5	PSO PSO	Sips	32

	chitosan						
23	Antimicrobial terephthaloyl thiourea crosslinked chitosan	Congo Red	44.248	---	PSO	Langmuir	33
24	Polyurethane foam membrane filled with humic acid-chitosan crosslinked gels	i)Methylene Blue ii)Rhodamine B iii) Methyl orange	10.31 8.26 5.29	10 4 4	PSO	Freundlich Freundlich Freundlich	34
25	Saccharomyces cerevisiae immobilized crosslinked chitosan beads	Direct orange 2GL	-------	8	PSO	Freundlich	35
26	β Chitosan crosslinked with triethylenetetramine	Reactive Blue 221	625.00	2	Elovich	Langmuir	36
27	Partially carboxymethylated and partially crosslinked chitosan	Methylene blue	365.77	5.6	PSO	sips	37
28	Sulphate crosslinked chitosan	Congo Red	91.8	3	PSO	Freundlich	38
29	N-maleyl chitosan crosslinked-acrylic acid and vinyl phosphonic acid	i)Crystal Violet ii) Methylene Blue	64.56 66.89	7 7	PSO PSO	Redlich-peterson	39
30	Novel antimicrobial trimellitic anhydride isothiocyanate crosslinked chitosan hydrogels	Congo Red	60.05	4	PSO	Langmuir	40

31	Crosslinked chitosan epichlorohydrin/TiO$_2$ nanocomposite	Reactive red 120	210	3	PSO	Langmuir	41
32	Tunable Schiff's base crosslinked chitosan-glutaraldehyde	Reactive Red 120	103.1	3	PSO	Freundlich	42
33	Chitosan crosslinked graphene oxide/carboxymethyl cellulose aerogel globules	Methylene Blue	3190	----	PSO	Langmuir	43
34	Crosslinked chitosan glyoxal	i)Reactive orange 16 ii) Methyl orange	1554.3 1451.9	3 3	PFO PFO	Langmuir Langmuir	44
35	Ionic liquid functionalized crosslinked chitosan	Sunset yellow FCF	300.28	No effect	PSO	Langmuir	45
36	Chitosan crosslinked graphene oxide/lignosulfonate composite aerogel	Methylene Blue	1023.9	7	PSO	Langmuir	46
37	Crosslinked chitosan-glyoxal /TiO$_2$ nanocomposite	Methyl orange	416.1	4	PFO	Langmuir	47
38	Crosslinked chitosan/polyacrylic acid/bentonite composite	Malachite Green	384.62	6	PSO	Langmuir	48
39	Mesoporous crosslinked chitosan-epichlorohydrin/activated charcoal	Thionine cationic dye	60.9	7	PSO	Freundlich	49

	composite						
40	Crosslinked chitosan tripolyphosphate, fly ash composite	Reactive orange 120	165.8	4	PSO	Freundlich	50
41	Chitosan/β cyclodextrin crosslinked beads	Indigo carmine	1000	3	PSO	Langmuir	51
42	Glutaraldehyde crosslinked chitosan	i)Malachite Green ii) Indigo Carmine	714.29 303.03	6 6	PSO PSO	Langmuir Freundlich	52
43	Crosslinked chitosan / oxalic acid	Reactive Red 195	110.7	4	Elovich	Redlich-peterson	53
44	Epichlorohydrin crosslinked chitosan / Carbon clay	i)Methylene Blue ii) Azo Acid blue 29	96.08 132.04	11 5	PSO PSO	Freundlich Freundlich	54
45	Nano Chitosan crosslinked with fish scales based activated carbon	Reactive Blue 9	31.25	6.5	PSO	Freundlich	55
46	Crosslinked chitosan/nitrogen doped-graphene quantum dot nanocomposites	i)Azo Blue ii)Methylene Blue iii) Orange G	82% 84% 94%	-	-	-	56
47	Crosslinked Nitrilotriacetic acid β-cyclodextrin chitosan beads	i)Methylene Blue ii) Methyl Orange	162.6 132.5	6 3	PSO PSO	Langmuir Langmuir	57
48	Graphene oxide crosslinked hydrogel nanocomposites of chitosan/carboxymethyl cellulose	i)Methylene Blue ii) Methyl Orange	655.98 404.52	7 3	PSO PSO	Langmuir Langmuir	58
49	Terephthalaldehyde crosslinked	Congo Red	------	--	PSO	Redlich-Peterson	59

		chitosan						
50	Glutaraldehyde-cross-linked chitosan–alginate	i)Brilliant Green ii)Methyl Orange iii)Patent Blue V	235.82 198.09 117.34	8 6 3	PSO PSO PSO	Freundlich	60
51	Tripolyphosphate crosslinked chitosan-activated charcoal composite	Remazol brilliant blue R	530.4	6	PSO	Langmuir	61

(PFO = Pseudo First Order , PSO = Pseudo Second Order)

References:

1. P.R. Yaashikaa, P. Senthil Kumar and S. Karishma, Environ. Res., 212, 113114, 2022.

2. M. Vakili, M. Rafatullah, B. Salamatinia, A. Zuhairi and H. Ibrahim, Carbohydr. Polym., 113, 115, 2014.

3. H. M. Ibrahim and E.M.R. El- Zairy, Concepts, Compounds and the Alternatives of Antibacterials., In Tech Publications, 2015.

4. C. Casadidio, D. Peregrina, M. Gigliobianco, S. Deng, R. Censi and P. Martino, Mar. Drugs, 17, 369, 2019.

5. P. Nechita, Biological Activities and Application of Marine Polysaccharides, 10, 209, 2015.

6. S. Abraham, Rajamanickam D, Science International,6, 18, 2018.

7. A. Anitha, N. Sanoj Rejinold, Joel D. Bumgardner, Shanti V. Nair and R. Jayakumar, Chitosan-Based Systems for Biopharmaceuticals: Delivery, Targeting and Polymer Therapeutics, First Edition. John Wiley & Sons, Ltd, 2012.

8. I. Saheed, O. Da and F. Suah, J. Hazard. Mater., 1, 62, 2020.

9. G. Crini and G. Torri, Wilson E, Environ. Chem. Lett., 17, 1645, 2019.

10. M. Berradi, R. Hsissou, M. Khudhair, M. Assouag, O.Cherkaoui, A. Bachiri and A. Harfi, Heliyon, 5, 1, 2019.

11. M. Chiou and G. Chuang, Chemosphere., 62, 731, 2006.

12. M. Hasan, A. Ahmad and B. Hameed, Chem. Eng. J., 136, 164, 2008.

13. A. Kamari, W. Ngah and L. Liew, J. Environ. Sci., 21, 296, 2009.

14. A. Kamari, W. Ngah, M. Chong and M. Cheah, Desalin., 249, 1180, 2009.

15. H. Zhu, R. Jiang, L. Xiao and W. Li, J. Hazard. Mater., 179, 251, 2010.

16. S. Ekici, G. Güntekin and D. Saraydın, Polym. Plast. Technol. Eng., 50, 1247, 2011.

17. X. Guo, G. Han and Y. Sun, Adv. Mater. Res., 156, 1404, 2011.

18. C. Chen, J. Chang and A. Chen, J. Hazard. Mater., 185, 430, 2011.

19. R. Huang, Q. Liu, J. Huo and B. Yang, Arabian J. Chem., 1, 9, 2013.

20. C. Luk, J. Yip, C. Yuen, C. Kan and K. Lam, J. Fiber. Bioeng. Inform., 7, 35, 2014.

21. Y. Bulut and H. Karaer, J. Dispers. Sci. Technol., 1, 26, 2014.

22. Z. Zhou, S. Lin, T. Yue and T. Lee, J. Food Eng., 126, 133, 2014.

23. A. Kadam and D. Lee, Biores. Technol., 1, 5, 2015.

24. Q. Liu, B. Yang, L. Zhang and R. Huang, Int. J. Biol. Macromol., 72, 1129, 2015.

25. H. Xuemei, D. Mei and L. Hui, Int. J. Biol. Macromol., 0141, 1, 2015.

26. K. Gul, S. Sohni, M. Waqar, F. Ahmad, N. Norulaini and A. Omar, Carbohydr. Polym., 1, 44, 2016.

27. W. Khanday, M. Asif and B. Hameed, Int. J. Biol. Macromol., 6655, 1, 2016.

28. F. Marrakchi, W. Khanday, M. Asif and B. Hameed, Int. J. Biol. Macromol., 6536, 1, 2016.

29. S. Guanghong, Z. Shuang and W. Shisheng, W. Zhiyu, RSC Adv., 1, 10, 2016.

30. A. Jawad and B. Hameed, Int. J. Biol. Macromol.. 95, 743, 2017.

31. S. Deniz and A. Caglayan, Water Sci. Technol., 1, 9, 2017.

32. A. Zahir, Z. Aslam, S. Kamal, W. Ahmad, A. Abbas and R. Shawabkeh, J. Mol. Liq., 7842, 1, 2017.

33. N. El-Harby, M. Shaimaa, A. Ibrahim, and N. Mohamed, Water Sci. Technol., 1, 14, 2017.

34. Y. Hu-Cheng, G. Ji-Lai, Z. Guang-Ming, Z. Peng, Z. Jian, L. Hong-Yu and H. Shuang-Yan, J. Colloid Interface Sci., 505, 67, 2017.

35. G. Dilarri and H. Corso, Environ. Technol., 1, 53, 2017.

36. C. Chih-Wei, M. Tsung, C. Jimmy and C. Ting-Yu, Polymers., 1328, 1, 2018.

37. B. Doshi, A. Ayati, B. Tanhaei, E. Repo and M. Sillanp, Carbohydr. Polym., 13706, 1, 2018.

38. C. Jeyaseelan, N. Chudhary and R. Jugade, Air, Soil Water Res., 11, 1, 2018.

39. M. Nakhjir, G. Marandi, M. Kurdtabar, Int. J. Biol. Macromol., 9741, 1, 2018.

40. N. Mohamed, N. Al-Harby and M. Almarshed, Polym. Bullet., 1, 26, 2019.

41. A. Jawad,· N. Mubarak and A. Abdulhameed, J. Polym.Environ., 1, 14, 2019.

42. A. Jawad, N. Mubarak and Abdulhameed A, Int. J. Biol. Macromol., 732, 142, 2020.

43. T. Huang, S. Yao-wen, Z. Qian, D. Yu-fan, L. Zhi-xuan, G. Fu-zhi, L. Peng-chao and W. Yong, ACS Sustain. Chem. Eng., 7, 8775, 2019.

44. A. Jawad, N. Ahmad, B. Hameed and K. Ismail, Int. J. Biol. Macromol., 135, 569, 2019.

45. H. Lyu, J. Fan, Y. Ling and Z. Xie, Int. J. Biol. Macromol., 126 1023, 2019.

46. Y. Mingfang, H. Wenxing and Z. Li, Int. J. Biol. Macromol., 136 927, 2019.

47. A. Mohammad, A. Abdulhameed and A. Jawad, Int. J. Biol. Macromol., 129, 98, 2019.

48. A. Yildirim and Y. Bulut, Environ. Technol. Innov., 1, 25, 2019.

49. A. Jawad, A. Abdulhameed and S. Mastuli, J. Polym. Environ., 1, 11, 2020.

50. I. Mohammed, A. Jawad, A. Abdulhameed and Mastuli S, Int. J. Biol. Macromol., 15825, 1, 2020.

51. T.. Kekes and C. Tzia, J.Environ. Manag., 262, 110372, 2020.

52. R. Chanajaree, M. Sriuttha, V. Lee and K. Wittayanarakul, J. Mol. Liq., 114507, 1, 2020.

53. P. John, V. Santos and N. Zaritzky, React. Funct. Polym., 155, 104699, 2020.

54. F. Marrakchi, B. Hameed and E. Hummadi, Int. J. Biol. Macomol.,163, 1079, 2020.

55. S. Sundararaman, P. Deivasigamani, N. Gopakumaran, K. Kumar, J. Balasubramaniam and N. Kumar, The institution of Engineering and Technology. 14, 289, 2020.

56. A. Amari, N. Elboughdiri, D. Ghernaout, R. Lajimi, M. Ali, A. Mohamed and F. Rebah, Ain Shams Eng. J., 1, 8, 2021.

57. M. Usman, A. Ahmed, B. Yu, S. Wang, Y. Shen and H. Cong, Carbohydr. Polym., 255, 117486, 2021.

58. H. Mittal and S. Alhassan, Int. J. Biol. Macromol., 167, 1248, 2021.

59. M. Garg, N. Bhullar, B. Bajaj and D. Sud, New J. Chem., 45, 4938, 2021.

60. M. Khapre, S. Pandey and R. Jugade, Int. J. Biol. Macromol., 190, 862, 2021.

61. P. Nandanwar, D. Saravanan, P. Bakshe and R. Jugade, Mater. Adv., In press (Advance article DOI: 10.1039/d2ma00508e) , 2022.

Supercritical Fluid Extraction of Uranium, Plutonium and Thorium:

A Review

Pradeep Kumar

Bhabha Atomic Research Centre, Trombay -40085

E-mail: pradeepk@barc.gov.in

Abstract:

In recent decades, extraction of actinides (U,Pu,Th) employing supercritical CO_2 has drawn attention owing to its inherent potential to minimize liquid waste generation. Supercritical Fluid Extraction (SFE) offers faster extraction with fine control over extraction process by means of varying pressure , temperature conditions. Supercritical Fluids have hybrid properties of liquid and gas. Liquid like solvation and gas like diffusivity enable to penetrate deep inside solid matrix, extracting component of interest, thus capable of extraction from liquid as well as solid matrix. Metal ion is complexed with suitable organic compound, which gets soluble in SC CO_2. SC CO_2 acts as a solvent and after extraction escapes as gas leaving behind extractant. Various types of ligands such organophosphorus compounds, β-diketones, macrocyclic compounds, amides, dithiocarbamates are employed. SFE offers attractive alternative to reprocessing of spent nuclear fuel and radioactive waste. In this paper, research work carried out on the SFE of actinides (U,Pu,Th) has been reviewed.

Key Words: Supercritical CO_2, Uranium, Plutonium, Thorium, Spent Nuclear Fuel

Introduction

Extraction and purification of Uranium from various matrices is of utmost importance in the nuclear industry. Conventional techniques for the separation and purification lead to generation of significant quantity of radioactive liquid waste. Liquid waste consists of used organic solvents and acids. Managing of radioactive waste is cumbersome. In the recent decades, Supercritical Fluid Extraction (SFE) has drawn attention as promising alternative to conventional solvent extraction process owing to its interesting characteristics such as inherent potential to minimize the generation of the radioactive liquid volume and

simplification of the extraction process. Supercritical Fluids (SCF) have hybrid properties of liquid and gas. SCFs can be regarded either compressed gas or expanded liquid. Their properties such as density, diffusivity, viscosity and surface tension are intermediate of liquid and gas. The unique solvating characteristic of SCFs assume significance from extraction consideration. Extraction using supercritical fluids exploits properties of both liquid as well as gas. Liquid like solvating characteristics of SCFs enable dissolution of compounds whereas gas like diffusion characteristics enable higher and faster extraction. Rapid mass transfer and faster completion of reaction is assigned to higher diffusivity than liquids whereas due to low viscosity and surface tension, SCFs can penetrate deep inside the solid matrix, efficiently extracting compound of interest. The SFE process can be finely controlled by tuning pressure and temperature according to desired requirement. Supercritical Fluids offer faster, cleaner and efficient extraction. SFE is regarded as green and clean technology.

Supercritical Fluid was discovered by Cagniard de la Tour in 1822 [1, 2]. He observed that above certain temperature which he named critical temperature, a substance exists in single phase, neither a liquid nor gas. Below critical point, gas can be liquefied by applying pressure, above critical point, the gas cannot be liquified however large pressure might be applied. Our view of this state, now called the "Supercritical State" (a name given to it by Thomas Andrews [3], who elucidated much of its nature), has not changed much in the 200 years since its discovery. This temperature is termed as the critical temperature (T_c) and the corresponding vapor pressure as the critical pressure (Pc). The values of temperature and pressure define a critical point, which is unique to a given substance. Below critical point two phases exist (biphasic system) in equilibrium with each other, above critical point liquid and gas phases merge into single phase called Supercritical Fluid (SCF), a state of continuity. In phase diagram (Fig.1) the vapor pressure versus temperature curve represents the coexistence of two phases, liquid and gas. On moving upward on the curve by increasing pressure and temperature, the liquid goes on becoming lesser dense and the gas more denser. At the critical point, the densities of the two phases become identical, the distinction between the gas and the liquid disappears, and the curve ends at the critical point.

The occurrence of SCF state can be elucidated on the basis of Van der Waals equation of state for real gases[4]. $(P + a/V^2)(V-b) = RT$; where a, b are constants. P, V, T, R are pressure, volume, temperature and gas constant respectively. The equation being is cubic in V, has three values. As shown in Fig.2, for curve-I & II, three values exist, in this region

liquefaction of the gases can occur. At higher temperatures, there exists only one real root (curve-IV), other two being imaginary. At certain intermediate temperature, all the three values of V are identical (curve-III); this temperature is called critical temperature. At this point the P-V curve exhibit a horizontal inflection, hence both the first and second derivatives of the pressure with respect to volume (at constant temperature) are zero.

Conditions of criticality for one–component fluid are [4-6]

$$(\partial P/\partial V)_T = (\partial^2 A/\partial^2 V)_T = 0 \quad\text{————} \quad (1)$$
$$(\partial^2 P/\partial V^2)_T = (\partial^3 A/\partial V^3)_T = 0 \quad\text{————} \quad (2)$$

where 'A' is the Helmholtz free energy. Isothermal thermal compressibility $K_T = (1/\rho)(\partial \rho/\partial P)_T$ is very high near critical point (diverges at critical point). The SCF can be easily compressed near critical point. K_T is proportional to mean squared density fluctuations. Moreover K_T is proportional to $\int r^2 |g(r)-1| dr$, where g(r) called pair correlation function, the ratio of local to bulk density at a distance 'r' away from a fixed molecule as origin. The divergence of K_T at critical point is assigned to the fact that g(r), finite quantity becomes long ranged[20]. The term 'ζ', called correlation length measures the range of density fluctuations. The decay of g(r) near the critical point is described by the equation[7]

$$g(r) \propto \frac{\exp(-r/\xi)}{r} \quad\text{————}\quad (3)$$

For CO_2, $\zeta = 55$ °A at 1 K above T_C and $\zeta = 13$ °A at 10 K above T_c. The average intermolecular distance at critical density is 5.4 °A [7].

This phenomenon remained a matter of curiosity and was discussed in phase diagram, did not find any application in the field of chemistry. Nearly after five decades in 1879, for the first time Hanny and Hogarth[8] reported the solvating properties of supercritical fluids in the Royal Society meeting held at London. In meeting it was a matter of great surprise and curiosity for scientists that how gas can dissolve solids. The application of SCFs remained unnoticed for nearly 8 decades until in 1958 Lovelock[9] recognized the potential of SCF as solvating agent and suggested their use in chromatography as mobile phase enabling faster separation. However first supercritical Chromatography equipment came into existence when in 1962 Klesper et al.[10] achieved separation of nickel prorphyrin from nickel mesoporphyrin dimethyl ester using dichloromethane and monochlorodifluoromethane as supercritical fluids. This triggered exponential growth in separation science using

supercritical fluids. Large number of papers all over the world were published. Seeing the large number of publications, it is not possible to include all of them. We have chosen some prominent papers and review articles. This article is mainly devoted to supercritical fluid extraction of uranium, plutonium and thorium. R.M Smith[11, 12] comprehensively reviewed the work carried out on supercritical fluids in separation science. Limited work has been carried out on SFE of uranium all over the world. The research groups engaged in Uranium SFE can be counted in fingers. Japan, USA, Russia, United Kingdom, France, Korea and India.

Most of review work is focused on SFE of transition metal ions, somewhere uranium SFE is one among various metals. Uranium, Plutonium and Thorium are basic elements used in nuclear reactors. Minimisation of radioactive liquid waste generation is a challenging task. Hence, a need was felt of a review article dedicated to SFE of Uranium, Plutonium and Thorium. Specially reprocessing of spent nuclear fuel using SC CO_2 is desirable.

CO_2 as Supercritical Fluid Gas

A large variety of substances can be employed for preparing supercritical fluid. However majority of research work uses CO_2 as supercritical fluid. It is not surprising that SFE has become synonym with supercritical CO_2 extraction. In very few and special cases and for academic research point of view other substances are investigated. More than 95% publication on SFE employ supercritical CO_2. The nearly monopoly of CO_2 emerged from its moderate critical constants, (critical pressure = 73 atm, critical temperature = 304 K and critical density 0.46 g/mL) which are easy to obtain. Moreover, CO_2 is chemically inert gas, cheap, easily available, nonflammable. Being chemically inert, it does not take part in chemical reaction and   act as an inert solvent. After extraction, at atmospheric pressure it escapes as gas leaving behind the extractant. No solvent residue is left, as in case of solvent extraction where lots of acid or organic solvent is generated. Thus extractant is obtained in pure form. Hence, SFE with CO_2 is termed as "CLEAN" and "GREEN" separation. CO_2 is radiochemically stable and nicely suited for nuclear industry. Moreover CO_2 is non-toxic, recyclable, less expensive. $CO2$ is generally regarded as safe (GRAS) solvent.

Solvent Behaviour of Supercritical CO2

The solvent behavior of CO_2 is similar to dioxane. CO_2 is an excellent example of a simple, nondipolar solvent system. Although CO_2 has a zero dipole moment, it is a charge-separated molecule having significant quadrupole moment. Kauffman[17] attributed dipole-quadrupole interactions with solute molecules responsible for many of the polar attributes of CO_2 and sometimes regarded as a quadrupolar solvent[15-17]. The charge separation with partial negative charges on the electronegative oxygen, considerable partial positive charge on carbon, and the overall electronic structure suggest that CO_2 can act as either a weak Lewis Acid or Lewis Base. This view suggests that CO_2 can solubilize several dipolar and nondipolar molecular systems facilitated by site-specific solute-solvent interactions. Nevertheless, the one should regard CO_2 as a polar molecule with two active and considerably strong bond dipoles. Spectroscopic study in gas-phase suggested a T-shaped dimer (C2v), corresponding to a purely quadrupolar interaction. Jucks et al.[18] demonstrated that, CO_2 dimer has a slipped parallel structure. CO_2 also has trimeric structure which provides insight into the three-body effects in larger CO_2 clusters as well as in liquid or SC- CO_2. Wedia and Nesbitt[19] reported two trimer structures based on IR spectral studies. One of these is a cyclic structure (C3), while the other is noncyclic (C2), with the cyclic trimer being more abundant than the noncyclic trimer. Charge separation in CO2 suggests the oxygen atoms can participate in hydrogen bonding with molecules of electron-deficient hydrogen atoms.

In fact Raveendran and Wallen's[20] by *ab initio* calculations on binary complexes of CO_2 with model carbonyl compounds, revealed existence C-H...O hydrogen bond. Raman spectroscopic studies of room-temperature gaseous mixtures of acetaldehyde and CO_2 provided experimental evidence for the presence of both the LA-LB interaction between CO2 and the carbonyl group[21]. NMR, IR, and Raman spectroscopic studies also support the formation of weak C-H.....O hydrogen bonds with CO_2[15]. Heldebrant and Jessop[22] showed that small molecular analogues of poly(ethylene glycol) are also soluble in SC-CO_2, suggesting that the ether-CO2 interactions result in an enthalpy driven solvation in liquid and SC-CO_2. Similar interactions are responsible for solvation in systems where Wai and coworkers[54] utilized a scheme in which a CO_2-philic Lewis base (tri-*n*-butyl phosphate) acts as a carrier to disperse a CO_2-insoluble Lewis Acid (HNO_3) in SC-CO_2 phase enabling dissolution of an ionic system (uranium dioxide).

Fluorinated compounds have very high solubility in SC -CO_2. Indeed, DeSimone[23,24] coined the term "CO2-philic" for such fluorinated compounds. Darr and Poliakoff [25] have comprehensively reviewed the Metal-organic coordination chemistry in supercritical fluids. Exact mechanism of enhanced solubility of fluorinated compounds is not clearly understood. Raveendran and Wallen[26] investigated in detail the mechanism, concluded the paper with the remark that the mechanism for enhanced solubility of the latter is an open question. Dardin et al.[28] postulated the existence of specific solute-solvent interactions between CO_2 and fluorocarbons based on density- dependent ^1H and ^{19}F NMR studies. Several other experimental groups and theoretical studies disagree and suggested that there are no such CO_2-fluorocarbon-specific interactions in comparison with the hydrocarbon systems[30-34]. Whatever might be the reason, fluorinated compounds are employed for extraction taking advantage of their enhanced solubility.

SFE /SFC of Natural Products

Supercritical Fluid Extraction (SFE) and Supercritical Fluid Chromatography (SFC) have unique characteristics compared to conventional solvent extraction such as fine control over extraction process by precisely tuning pressure and temperature conditions. SCF density can be varied by changing pressure and temperature conditions. SFE and SCF are being employed in separation of natural products. Being non polar, SC- CO2 readily dissolves organic compounds. SFE/SFC has been extensively explored for natural products, more than 95% publications address to natural products, publication on metal SFE are lesser. SFE and SFC are employed for the separation and purification of natural products. The principle of extraction is same for both SFE and SFC. In SFE process, SCF dissolves the compound and transported to a vessel at atmospheric pressure for depressurization where CO_2 escapes as gas or recycled. In SFC process SC CO_2 is employed as mobile phase and separation is performed. Thus, SFE and SFC are complementary separation processes.

Chester et al.[35] reviewed SFE and SFC upto 1998. SFC finds applications in separation and purification of natural products. SFC played an important role to remove fatty acids[36]. Henry and Clement[37] published review article based on 300 papers published between 2003 to 2005. In the paper applications of SFE/SFC in various fields namely food, natural products, pharmaceuticals, environmental applications, energy were discussed in details. Dr. Mamata Mukhopadhyay[38] in her book on SFE has described in detail process and

mechanism of extraction of natural products.

In conventional solvent extraction, the natural product is dissolved or leached by acid and subsequent extraction into organic compound, thus matrix is completely destroyed. In SFE, SC CO_2 act as solvent and extractant, sample matrix is not destroyed and remains as such, also residue of solvent remains CO_2 escapes as gas. Since acid usage is eliminated, many new compounds which are destroyed by acid are discovered.

Instrumentation and Mechanism of Extraction

The SFE/SFC process consists of extraction at high pressure. A schematic diagram of a typical lab supercritical fluid extraction set-up is shown in Fig. 5 [13, 14]. Set-up consists of a CO_2 delivery pump, a modifier pump, extraction vessel, a thermostat, a back-pressure regulator and a collection vessel. Extraction vessel after sample loading is kept in the thermostat whose temperature can be varied from 258 K to ~353 K. CO_2 is delivered to the extraction vessel at a desired flow rate by the CO_2 delivery pump. From the cylinder, CO2 gas is fed to the delivery pump, where CO_2 is liquefied by lowering the temperature to 263 K. The modifier pump is employed to add a desired percentage of the complexing agent to the liquefied CO_2 stream. The CO_2 and complexing agent streams are combined by a T-joint and fed to the extraction vessel. Prior to entry in the extraction vessel, the stream is allowed to

pass through a long spiral coil for acquiring thorough homogeneity. The desired pressure in the   extraction vessel is maintained by opening/closing of a variable stroke needle valve of the back- pressure regulator. The extract coming out of the extraction vessel is collected in the collection tube at atmospheric pressure while CO_2 escapes as gas. For lab scale, pumps used for chromatography can be employed. For large scale, high-capacity pumps are used, extract containing SC CO_2 allowed to expand in a separate chamber and CO_2 can be recycled.

The complexation of metal ions can be carried out in two ways .Online complexation consists of ligand dissolution in SCF and subsequent feeding to extraction vessel. In-situ complexation consists of adding ligand directly to extraction vessel followed by flow of SC-CO_2. The extraction can be carried out essentially in two modes. In the static mode the extraction system is allowed to withstand particular temperature and pressure conditions for certain time period, followed by collection.   In case of dynamic mode, collection is carried out at particular temperature and pressure. The extraction process can be understood by

typical example of uranium SFE by employing TBP. Identical to the conventional solvent extraction process employing TBP, the overall extraction reaction can be expressed by the following formula [13, 14]

$$\text{Kex}$$

$$UO_2^{2+} aq + 2\ TBP_{SF} + 2NO3\ aq^- \xleftrightarrow{} \{\ UO_2(NO_3)_2.2(TBP)\}_{SF} \text{ ---------------(4)}$$
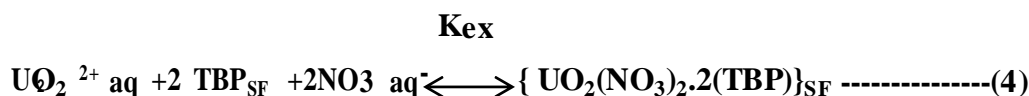
Here, K_{ex} denotes an extraction constant given by following equation:

$$K_{ex} = \frac{[\ UO_2(NO_3)_2.2(TBP)]\ _{SF}}{[U]\ _{aq}\ [TBP]^2_{SF}\ [NO_3^-]^2_{aq}} \text{ ------------------(5)}$$

The extraction reaction involves at least three elemental processes:

(1) Distribution of TBP between aqueous and supercritical CO_2 phase

(2) Formation of complex $UO_2(NO_3)_2.2(TBP)$ in the aqueous phase

(3) Distribution of the complex between aqueous and supercritical CO_2 phase

The K_{ex} can be formulated by the equation :

$$\log\ K_{ex}\ =\log\ K_{D, comp} - 2\log K_{D, TBP} + \log K_f \text{ ----------------(6)}$$

where $K_{D, comp}$, $K_{D, TBP}$ and K_f are the distribution co-efficient of the complex, the distribution co- efficient of TBP and the formation constant of the complex in the aqueous phase respectively.

Distribution ratio of a speciy 'j' is given by equation

$$Log\ K_{Dj} = j\log \rho + Cj - \log Sj,\ _{aq} \text{ \qquad\qquad (7)}$$

Where 'ρ' is the density of supercritical fluid and 'S' is solubility.

SCF density increases with increasing pressure hence according to Chrastil empirical formula, solubility of substance consequently the extraction efficiency is expected to increase. In most of cases, the extraction trend, which is followed for solids. In solution slight deviation above 80 atm pressure is observed. SC- $CO2$ density decreases with temperature however, extraction efficiency is expected to decrease with temperature. Extraction efficiency is influenced by many other factors. Solubility is combination of SC-CO_2 density and volatility of solute. The author has discussed in detail the effects of various parameters [65].

Solubility of Compounds in Supercritical CO$_2$

The fact that SCF can dissolve solids has fascinated chemists since the time of Hanny and Hogarth. A thumb rule is that the dissolving properties of SC- CO$_2$ are similar to n-hexane. Solubility of compounds in SC- CO$_2$ can be predicted by various models. These models are very complicated. However Smart et al.[40] compiled the data in the literature on solubility of 49 organometallic compounds and 15 free ligands in SC -CO$_2$. The highest solubility value reported was 56 g/L[40]. The most soluble metal complexes were fluorine substituted ligands and lowest soluble were phenyl substituted ligands. The data were correlated using a model based on the relationship between ln (solubility) and ln (density) based on the earlier work of Chrastil[39] on correlating the solubility of complex organic molecules in SC-CO$_2$. The model relates the solubility of a solute to solvent density and temperature by equation ln $S = k$ ln $D + C$, where 'S' being the solubility of the solute in g/L, 'D' the density of the SCF in g/L, k a constant for the solute–solvent system indicating the solvation of the solute in the SCF, C is density independent constant which varies with temperature and related to the volatility of the solute. The good agreement between experimental data and the model suggests that such a simple model can be utilized for extrapolation of limited amount of data to a wider temperature and pressure range. The equation predicts a linear relationship between In(S) and ln (D) with a slope proportional to 'k' and intercept 'C'.

Solubility of compound can be measured either by SFE or spectroscopic methods; in SFE by static method and dynamic method. In static method, the SC CO$_2$ is fed to a vessel with sufficient quantity and the system is allowed to reach equilibrium condition under specific pressure and temperature conditions and the amount dissolved is measured by sampling at those conditions. In dynamic mode, SC CO$_2$ is allowed to flow through vessel containing the substance at particular pressure and temperature conditions and the extracted substance is collected in a vessel. In spectroscopic method the cell is maintained at desired pressure and temperature conditions and substance is measured online spectroscopically.

In 1991, Wai et al.[41] was the first to report the solubilities of a number of metal dithiocarbamates in supercritical CO$_2$ determined by UV-VIS spectroscopy using a high-pressure view-cell with quartz window. Erkey at al.[42] developed dynamic method to determine solubility of metal-chelate in SC- CO$_2$. In this technique, the supercritical fluid stream is mixed with an organic solvent stream to form a mixed phase for avoiding solid precipitation and plugging at the outlet. Yankar et al.[44] were the first to carry out NMR

study of Metal Complexes in supercritical fluids by ^{1}H, ^{9}F, and ^{129}Xe resonances, providing information about solution structure at molecular level, ligand substitution and proton position. Organophosphorus compounds are widely used for SFE of actinides, hence knowledge of their solubility in SCF is valuable from extraction point of view. Meguro et al.[45], Japan group in 1998 , deeply studied solubility of various organophosphorus compounds in SC-CO$_2$ such as tributyl phosphate (TBP), diisodecylphosphoric acid (DIDPA), di-(2- ethylhexyl)phosphoric acid (DEHPA), dihexyl-(N,N-diethylcarbamoyl)methylphosphonate (CMP), and octyl(phenyl)(N,N-diisobutylcarbamoyl) methylphosphine oxide (CMPO). The solubility was found to increase with density of SC-CO$_2$ relation consistent with equation $\ln S = k \ln D + C$.

R. Schurhammer and G. Wipff [46] performed molecular dynamics study on the complexation of uranyl nitrate and the dissolution of nitric acid in SC-CO$_2$ by TBP. Study reveals the stronger TBP hydrogen-bonding with HNO$_3$ than with H$_2$O. Nitric acid dissolves in SC-CO$_2$ by TBP, nitric acid alone self aggregates via hydrogen-bonding interactions. The role of water was understood by directly measuring the pH of water in contact with supercritical CO$_2$ by observing the spectra of a pH indicator with a U-VIS spectrophotometer and pH was found in the range of 2.8 to 2.95 under pressure of 70-200 atm and 303-343 K temperature [47].

SFE of Uranium, Plutonium and Thorium

After the application of SCF by Lovelock in 1962, for considerably a long period, supercritical fluids were not employed for metal ion extraction. The reason being that direct extraction of metal ions by supercritical CO$_2$ is highly inefficient owing to charge neutralization requirement and the weak solute– solvent interactions. However, Laintz and Wai [48] in 1992 were the first to report the SFE of metal ion, Cu^{2+} from aqueous solution and from silica surface using SC-CO$_2$ containing Lithium diethyl dithocarbamate(LiFDDC) as complexing agent. This opened a new realm in the field of SFE of metal ions. Subsequently SFE of various metal ions was reported. In the SFE of metal ions, choice of suitable complexing reagent plays vital role. Fascinated by attractive properties of supercritical fluids, after the demonstration of SFE of Cu, the focus was on nuclear field. Very next year in 1993, SFE knocked the door of nuclear industry when the same research group Lin et al.[49] was successful in performing SFE of lanthanides and uranyl ion from solid materials by SC- CO$_2$ containing a fluorinated β-diketone 2,2-dimethyl- 6,6,7,7,8,8,8-heptafluoro-3,5-

octanedione (FOD). The very next year, in 1994, they reported the SFE of thorium and uranium from solid and liquid materials with fluorinated β-diketones and TBP[50]. These studies opened a gateway for application of SFE in nuclear industry. Kumar et al.[52,53] carried out SFE of uranium from tissue paper matrix.

Hong Wu et al.[51] carried out SFE of uranium and thorium from nitric acid solution with organophosphorus reagents. Separation and detection of lanthanide β-diketonates was carried out by adduct formation by supercritical fluid chromatography (SFC) with an open-tubular capillary column and a FID detector. Lanthanide β-diketonates decompose in SCF, but adducts of lanthanide β-diketonates with a neutral donor, tributylphosphine oxide (TBPO) or trioctylphosphine oxide (TOPO), alters their SFC behavior leading to first successful separation of lanthanide complexes of the same β-diketone ligand by SFC using SC- CO_2 as the mobile phase. Wang et al.[56] coined the term "Nuclear Laundry", described the extraction of Co, Cd,Cu, Pb,Zn by using Cyanex 302 and dithiocarbamate. Wai and Wang [57] reported separation of metal chelates and organometallic compounds by SFC and SFE. Smart et al.[58] carried out SFE of toxic metal ions using organophosphorus reagents such as Kelex 100, Cyanex 272, 301 and 302, and D2EHTPA. Toxic heavy metals such as f Cu^{2+}, Pb^{2+}, Zn^{2+}, and Cd^{2+} are extractable from variety of matrices. Kelex 100 was found to be very selective for the extraction of $Cu^{2+.}$

First review article on SFE of metal ions was publishes by Wai's group[43] in 1997 summarising the work on SFE of metal ions for analytical application. Till then SFE of metal ion was nicely matured and quite well understood. Wai's review article described the important parameters controlling SFE of metal species. (1) solubility and stability of chelating agents, (2) solubility of metal chelates, (3) water and pH, (4) temperature and pressure, (5) chemical form of metal species, and (6) matrix. A variety of ligands, including dithiocarbamates, β-diketones, organophosphorus reagents and macrocyclic compounds, can be utilized for SFE of metal species. Some ligands are general complexing agents and others are selective for certain metals. With proper choice of ligand and experimental conditions separation of metal ions can be achieved by SFE. In 2000 Erkey[55] extensively reviewed the SFE of metal ions from aqueous solution including uranium and thorium.

Wai and Wang [57] in 2000 reviewed separation of metal chelated and organometallic compounds by SFC and SFE/GC. Supercritical Fluid Chromatography (SFC) has dual advantages of the high diffusion properties of gas chromatography and solvating properties of liquid chromatography. Since SFC operates at lower temperatures, is nicely suited for

separation of thermally labile compounds. SFC also allows interfacing between supercritical fluid extraction (SFE) and chromatographic analysis of metal-containing compounds. SFC separation of various chelates of transition metals, heavy metals, lanthanides and actinides as well as organometallic compounds of lead, mercury, and tin was reported [58]. The feasibility of separating U from nitric acid solutions of mixed actinides U, Np, Pu, and Am using tri-n-butylphosphate (TBP)-modified SC-CO_2 was investigated [60]. The uranium was separated from plutonium at HNO_3 concentration less than 3M in the presence of acetohydroxamic acid (AHA) or oxalic acid (OA) to mitigate Pu extraction. U separation from Np was successful (<1 M HNO_3) in the presence of AHA, OA, or sodium nitrite to mitigate Np extraction. Americium was not well extracted, hence got separated.

Uranium SFE using diamide derivative was investigated by measuring distribution ratio (D_U) and extraction efficiency of uranium (VI) using N,N,N′,N′- tetrabutyl-3-oxapentanediamide (TBOD)[59]. D_U with TBOD was found superior to that of TBP by 2 orders of magnitude. However Uranium, fission products (Cs, Cd, Mo, Ba), and corrosion products (Ni, Fe, Cr, Co) were extracted with TBOD in SC-CO . Over 90% each of actinides (U,Th) and lanthanides (La, Ce, Gd) were extracted. But, fission products and corrosion products were extracted at a low efficiency of less than 20%.

Ionic liquids are considered to be a relatively recent magical chemical due their unique properties, non-volatility and non flammability . This seems to be promising field in coming future. Much work is not carried out with ionic liquids. Ankita and Tomar[61] studied various amides for solvent extraction of Thorium into 1-butyl-3-methyl imidazolium hexafluorophosphate employing supercritical CO_2 for stripping, higher stripping efficiencies were observed. In the study, highest efficiency was supercritical carbon dioxide modified with DBOA-HNO_3 adduct. Keskin et al.[43] has reviewed the ionic liquids towards supercritical fluid application.. It is noteworthy that SC-CO2 has got solubility in ionic liquids. On the other hand ionic liquids are insoluble in SC-CO2. On passing SC-CO2 through the ionic liquid   with organic compounds, SC-CO2 would selectively extract organic compound. Thus the partnership of volatile and nonpolar SC-CO_2 with nonvolatile and polar ionic liquid offers a novel method to extract organic compounds from ionic liquids using SC-CO_2. Liyang et al.[62]   investigated the possibility SFE of Uranium from TRISO-coated fuel particles using supercritical CO_2 containing tri-n-butyl phosphate. Tristructural-isotropic (TRISO-) coated fuel particles are used in the high temperature gas cooled reactor

as fuel. TRSIO- coated fuel particles have four coating layers of porous carbon, inner dense pyrolytic carbon and silicon carbide for confining the fission products. The study was meant for investigating the possibility of reprocessing of spent nuclear fuel from high temperature gas cooled reactor. The extraction efficiency was higher than 98%.

Inspired by fascinating extraction properties of SC-CO_2 especially as radioactive waste minimisation, the author has also carried out research work on SFE of Uranium, Thorium and few metal ions [63-73]. Various organophosphorus reagents (in 2007) were studied for SFE of Thorium from simulated tissue paper matrix[63]. The solubility trend is TBP>TBPO > TOPO>TBPO, but the extraction trend is quite different indicating the solubility of ligand alone is not the deciding factor. Among phosphates, if aromatic group is replaced by aliphatic group extraction efficiency increases, efficiency with tributyl phosphate (TBP) is higher than that with triphenyl phospahte (TPP). Among phosphine oxide, higher the aliphatic chain length, higher the extraction efficiency. In TPPO, having phenyl group, the efficiency is intermediate to TOPO and TBPO. The trend can be assigned to molecule structure, electronegativity of substituent. Electron withdrawing group decreases electron density on oxygen atom causing less solvation thereby less extraction efficiency, whereas electron donating group increases electron density on oxygen atom causing more solvation thereby enhanced extraction efficiency was observed. Various β-diketones such as acetylacetone (AA), trifluoroacetylacetone (TFA), hexafluoroacetylacetone (HFA), thenoyltrifluoroacetylacetone (TTA) and heptafluorobutanoylpivaroylmethane (FOD) were evaluated and trend observed was TTA > FOD > HFA > TFA > AA[66]. The trend correlates well with the degree of fluorination in the side arms of β- diketones. A combination of TBP and β-diketones further enhances the extraction efficiency. In SC- CO_2, higher fluorination results in higher percentage of enol content, greater dissociation into enolate ion, higher solubility and stability of β-diketones as well as of Th-β-diketone chelates. Highest extraction efficiency with TTA was probably due to the presence of aromatic thenoyl group. Crown ether are versatile class of ion-selective extractant. Various crown ethers were investigated for the SFE of Uranium from acidic medium[67]. HPFOA (Pentdedecfluoro -n-octanoic acid) consisting of several CO2 phillic C-F bonds was used for counter ion production. The nature of substituent attached to ring was found to affect extraction efficiency, Ditertbutldicyclohexano-18-crown-6> Ditertbutldibenzo-18-crown-6> dicyclohexano-18-crown-6> Dibenzo-18-crown-6 [67].

Thus comparison for same size crown ether, electron donating group increases the basicity

of oxygen atoms of ring enhancing binding with metal ion, whereas electron withdrawing group decreases the basicity of oxygen atoms of ring lowering binding with metal ion. The size of crown ether also affect. For same substituent the observed trend in extraction efficiency was Dibenzo-24-crown-8> Dibenzo- 21-crown-7> Dibenzo-18-crown-6, indicated increase in extraction efficiency with increasing ring size.

For nuclear industry, extraction of Uranium from solid matrix is very much desirable, since SFE process minimizes the radioactive waste generation. Supercritical Fluid Extraction of Uranium from U_3O_8 powder and also from various UO_2 solids—powder, granules, green pellet and sintered pellet— obtained from various stages of nuclear fuel fabrication was studied by single medium of TBP–HNO_3 dissolution as well as complexation, thus avoiding free acid usage and minimizing liquid waste generation[68]. With SC- CO_2 alone efficiency was around 70% which increased to ~90% with 2.5% TBP in SC-CO_2 stream and nearly complete uranium extraction (~99%) with 20% TBP. Nearly complete extraction was also achieved with 2.5% TTA in methanol. The optimized procedure tested to remove Uranium from simulated tissue paper waste matrix smeared with uranium oxide solids.

Calixarenes were studied for the SFE of toxic heavy element Cd^{2+} and Pb^{2+} from acidic medium[71,72]. With hexaacetylcalix[6]arene extraction efficiency ~ 90% was obtained and presence of HPFOA was found to enhance the extraction efficiency. Efficient extraction (~93%) of Pb(II) was observed for p-t-butylcalix(4)arene .The method was finally applied to the SFE of Pb(II) from real samples viz. batteries, paints, tobacco and industrial waste released in water.

Supercritical Fluid Extraction (SFE) and purification of Uranium, from crude sodium diuranate (SDU) containing Uranium (53%), Iron (22.2% of U) and rare earth impurities (4% of U), has been studied using adduct of TBP and HNO_3 for Uranium dissolution and extraction[72,73.] This group also studied Uranium SFE from rock phosphates ores containing lean Uranium content (~50-100 ppm). Using SC-CO_2, direct Uranium extraction from rock phosphate ores was studied by employing adducts of trialkyl phosphate (TBP, TiAP and TEHP) and nitric acid . The adduct fulfilled the role of dissolution as well as complexation reagent for U. With these adducts SC-CO_2, direct extraction from yellow cake was studied, and Uranium extraction efficiency >90% was achievable. Crude yellow cake is produced in various chemical compositions such as sodium diuranate (SDU), magnesium diuranate (MDU), heat treated uranium peroxide (HTUP).

N,N-Dialkyl aliphatic amides with varying alkyl groups such as N,N- dibutyl-2-ethyl

hexaamide(DBEHA), N,N- dibutyl-3,3-dimethyl butanmide (DBDMBA), N,N-dihexyl octanamide (DBOA) were studied for SFE of Uranium and Thorium from nitric acid medium and tissue paper matrix[74]. Extraction trend correlated well with structure of amides. Straight chain DBOA was found suitable for Uranium extraction whereas branched chain amide DBEHA was suitable for separation of uranium and thorium. N,N-Dialkyl aliphatic amides were used to extract Uranium into ionic liquid and stripping by SC- CO_2[70]. DBEHA, DBMNA,DHOA,DBPA, DBOA were evaluated for solvent extraction of Thorium from nitric acid medium into the hydrophobic ionic liquid phase, 1-butyl-3- methyl imidazolium hexafluorophosphate. DBOA yielded highest extraction efficiency.

Mohapatra' group[75] studied extraction of Uranium from tissue paper, synthetic soil, and from its oxides (UO_2, UO_3 and U_3O_8) using SC-CO_2 modified with methanol solutions of extractants (TBP) or (DHOA). With TBP, the extraction trend was $UO_3>UO_2>U_3O_8$. Addition of hydrogen peroxide in the modifier enhanced the dissolution/extraction of uranium. DHOA appeared better than TBP. Direct extraction of uranium from sintered oxides UO_2, $(U,Th)O_2$ soil and ore samples using SC-CO_2 containing tri-n-butylphosphate and N,N-di-(2-ethylhexyl) isobutyramide was demonstrated. 80–100% extraction of Uranium from different soil/ore samples was found. The extraction of Uranium from $(U,Th)O_2$ samples was significantly lower for both TBP–HNO_3 (~17%) and D2EHIBA–HNO_3 (~12%) adducts in 2 hour. Employing N,N,N',N'-tetraoctyl diglycolamide (TODGA) this group also carried SFE of trivalent metal ions such as Nd(III), Eu(III) (taken as analogs of Am(III)) from solid oxide (Nd_2O_3), Thorium concentrate, tissue paper/surgical gloves (rubber), and plant waste[76].

Tessy et al.[77] carried out direct in situ supercritical fluid extraction of Neodymium ion from its oxide using thenoyl trifluoro acetone–tri butyl phosphate–methanol in carbon dioxide. Tessy et al.[78] carried out extraction of metals directly from metal oxides by SC- CO_2. Cerium as a candidate, feasibility studies along with TTA as the chelating agent was demonstrated.

Indira Gandhi Centre for Atomic Research (IGCAR) group lead by Sivraman[79-91] has carried out significant work on SFE of actinides (U, Pu, Th) . The group has studied plutonium SFE, very limited work is reported on Plutonium SFE. It is worth mentioning that Plutonium SFE requires glove box adaptation as Plutonium is highly radiotoxic, microgram quantity of Plutonium in body is harmful. Kumar et al.[79] developed a technique for modifier free delivery of ligands in controlled manner for SFE. TBP, TOPO,TTA, D2EHIBA, CMPO

were investigated and the delivery profiles were optimised by investigating parameters such as ligand delivery vessel geometry, temperature, pressure, flow rate of SC-CO$_2$ and ligand content. SFE of Uranium and Thorium was demonstrated from tissue paper matrix, the extraction was comparable with that of making use of methanol or hexane modifier. Kumar et al.[80] used supercritical fluid to remove silicone oil from uranate microspheres prepared by sol-gel process. Silicone oil was extracted completely and the microspheres were found suitable for preparation of UO$_2$ spheres. SFE of Plutonium from tissue paper matrix, teflon, glass and stainless steel was demonstrated by Kumar et al.[81] n-octyl(phenyl)-N,N-diisobutyl carbamoylmethyl phosphine oxide (φCMPO) in methanol was used as modifier and complete extraction of Pu(III) and Pu(IV) in their nitrate was achieved for the first time. SFE of Am(III) using CMPO in methanol resulted in its complete recovery. Sujata et al.[82] (in 2012) demonstrated nearly complete Plutonium extraction from actual Plutonium bearing cellulose matrix waste in 0.1 litre extraction vessel employing (SC-CO$_2$) modified with (φCMPO). Next year(2014) Sujata et al.[83] showed recovery of Plutonium from various polymeric matrices, such as neoprene, polyvinyl chloride (PVC) and surgical gloves using SC-CO$_2$ modified with (φCMPO) in methanol. K. C. Pitchaiah et al.[84] studied SFE of Uranium and Thorium from nitric acid medium employing various organophosphorous compounds. The extractants such as TiAP, TsBP, DAAP, DBBP, DOHP and DOPO were employed for the first time for the extraction of Uranium from HNO$_3$ medium and the results were compared with TBP, CMPO and TOPO. Study revealed that TOPO, CMPO are stronger extractants compared to phosphonates, which in turn are better compared to phosphates for the extraction of Uranium from nitric acid medium. K. C. Pitchaiah et al.[85] studied in detail the influence of co-solvent such as methanol, dichlormethane and n-hexane on the extraction behaviour of Uranium and Thorium with Organophosphorous reagents. The solubility of tri-iso-amyl phosphate (TiAP) in SC -CO2 was determined and employed for selective extraction of Uranium (~95%) from simulated dissolver solution [86]. Pichaiah et al.[88] demonstrated recovery of Uranium and Plutonium from pyrochemical salt matrix using supercritical fluid extraction employing Trioctylmethylammonium chloride as ligand. Typical extraction yield of 95 and 75% was achieved for Uranium and Plutonium respectively. Deepitha et al.[90] determined solubility of pyridine-2,6-dicarboxylic acid in supercritical carbon dioxide and demonstrated removal of Lead and Nickel in simulated matrices. Deepitha et al.[91] measured solubility of on 2-hydroxyisobutyric acid in SC- CO$_2$ and used for actinide extraction.

The evolution of the research work on SFE of actinides (U,Pu,Th) leads for exploring the possibilities of using SC-CO$_2$ in nuclear filed on large scale such as reprocessing of spent fuel or recovery from nuclear waste. B. F. Myasoedov, et al.[92]. Russian research group in 2009 thoroughly investigated recovery of Uranium and Plutonium from simulated spent nuclear fuel (SSNF). For actinide oxides UO$_2$, UO$_3$, U$_3$O$_8$, NpO$_2$, PuO$_2$, Uranium gets nearly quantitative extracted (>~0%) by SC-CO$_2$ containing TBP-HNO$_3$ adduct whereas Pu and Np remains unextracted. From mechanically mixed (UO$_2$ & PuO$_2$), (UO$_2$ & NpO$_2$) only Uranium gets extracted. From solid solutions of UO$_2$ and PuO$_2$ containing 6% and 26 % PuO2, both Uranium and Plutonium nearly quantitative (>90%) extracted. The extraction of Uranium from its dioxide by the TBP-HNO$_3$ adduct dissolved in SC-CO$_2$ was found to be the same as that without SC-CO$_2$.This finding indicates the possibility of elimination or minimization of generation of large volumes of highly toxic aqueous and organic radioactive wastes getting accumulated as a result of the use of conventional technologies of spent nuclear fuel (SNF) reprocessing. They studied direct extraction of the actinides from their solid dioxides by TBP, MIBK and DMDO-HEMA adducts with HNO$_3$, Uranium is nearby quantitatively extracted from the solid actinide compounds (PuO$_2$, NpO$_2$) . In the case of the solid solutions of NpO$_2$ and PuO$_2$ in UO$_2$, Np and Pu are extracted along with Uranium by the TBP-HNO$_3$ and DMDOHEMA- HNO$_3$ adducts practically quantitatively. MIBK extracts U(VI) only, whereas Pu remains in the residue. Thus Uranium can be selectively extracted from the solid solution of PuO$_2$ in UO$_2$ and separated from Pu using the MIBK-HNO$_3$ adduct. U and Pu were separated by counter current chromatography (CCC) under the conditions of concentration gradients both of TBP in the stationary phase and of HNO$_3$ in the mobile phase[93]. The system "30% TBP in white spirit-0.5 M HNO$_3$" enabled Uranium to be concentrated in the stationary phase, while Pu was eluted with a flow of the mobile phase and stepwise elution allowed U and Pu to be practically completely separated. The first Pu fraction contained 98.9% of total Pu and 0.07% of U, and the second U fraction contained 99.93% of total U and 1.1% of Pu. Thus CCC allows separation of U(VI) and Pu(IV) in the form of their complexes with TBP as well as separation of U(VI), Pu(IV), Am(III) and Cm(III) in the form of their complexes with DMDOHEMA[94, 95].

During SFE of the SSNF sample, more than 99% of U goes into the adduct phase along with bulk of ^{95}Zr and ^{95}Nb ($\sim$ 90%), ^{131}I (100%), smaller percentages of ^{103}Ru ($\sim$ 30%), ^{99}Tc and lanthanides ($\sim$ 10%) whereas aqueous phase contains $\sim$ 100% of ^{137}Cs, ^{85}Sr, ^{140}Ba and the bulk of ^{140}La, $^{141-144}$Ce, ^{147}Nd and ^{99}Tc (90%–80%). Uranium separation from

fission products is desirable. In order to achieve separation from fission products the adduct phase containing U and the extracted fission products were separated from the aqueous phase using liquid CO_2 and U is effectively separated by counter current chromatography from the fission products. In the study ^{140}La, $^{141-144}$Ce, ^{147}Nd, ^{95}Nb and ^{95}Zr were quantitatively eluted first followed ^{99}Tc and finally U.

In Russia, SFE of uranium and transuanium (Np ,Pu, Am) from solid oxides and from solid surfaces has been extensively studied at the Vernadsky Institute of Geochemistry and Analytical Chemistry, Russian Academy of Science and at the Klopin Radium Institute. The research was specifically dedicated to investigate possibility of using SFE for spent nuclear reprocessing and decontamination purposes. In this paper, the SFE work by the Russian research group lead by M.D. Samsonov has been discussed upto year 2011[96]. According to Study, liquid CO_2 is as efficient as SC CO_2 in dissolving complexes of Uranium and Plutonium. Based on study a schematic flowsheet for SNF reprocessing using CO_2 as diluent was suggested. Based on the data from Russia, United States, Japan, United Kindom and India, Super-DIREX (Super Critical Fluid Direct Extraction, Mitsubishi)) process was suggested in Japan[97,98]. In Super-DIREX, SC-CO_2 containing TBP-HNO_3 adduct is fed to extraction column containing SNF dissolving U and Pu leaving behind undissolved fission products. Russian groups suggested RELICT process (reprocessing by liquid Carbon dioxide Treatment) [99,100]. In REFLECT is based on combing the operation of oxide SNF dissolution and actinide extraction with solution of TBP-HNO_3 adduct. Super-DIREX is performed at 200-300 atm and 298-318 K whereas RELICT is performed at 70 atm and 298-318 K . The RELICT was initially tested on simulated SNF. Also it was tested on real samples of spent fuel of RBMK-1000 and WWER- 1000 reactor [101,102].

Conclusion

Supercritical Fluid Extraction offers promising alternative to conventional solvent extraction process. It assumes significance in the extraction of actinides owing to its inherent potential of minimisation of radioactive liquid waste generation. SFE can be considered as high pressure extraction process. CO_2 is preferred choice because of its moderate critical constants, chemically inertness, radiochemically stability, nontoxic nature and easy availability. A thorough understanding of chemistry of compounds in SC- CO_2 is essential for designing SFE process for particular ion and matrix.

The whole SFE process is matter of choosing suitable complexing ligand which can

efficiently complex with metal ion. Solubility of ligand and metal complex in SC-CO_2 determine the outcome of extraction process.

Also instrumental parameters such as pressure, temperature, CO_2 flow rate, extraction mode static/dynamic , complexing mode online/in-situ, need to be optimised. A large number of ligands such organophosphorus compounds, β-diketones, macrocyclic compounds, amides, dithiocarbamates have been extensively investigated by many research groups. Super - DIREX (Super Critical Fluid Direct Extraction, Mitsubishi) process and RELICT process (Reprocessing by liquid Carbon dioxide Treatment) are proposed for reprocessing of Spent Nuclear Fuel. The RELICT process has been test on real samples of spent fuel from reactor. These are all lab scale demonstration. Commercial reprocessing plants are expected to become reality in future. The probable reason for hesitation for adapting on commercial scale might be the high pressure requirement. SFE of Uranium from ores appears promising and research need to be focused in this direction. SFE using ionic liquids is at infant stage and seems promising in future. Plant scale SFE for natural products exists. In nuclear field upscaling to plant level has still not matured. However SFE offers promising alternate to solvation extraction process and dedicated research in extraction of actines needs to be continued.

Acknowledgement

Figures :
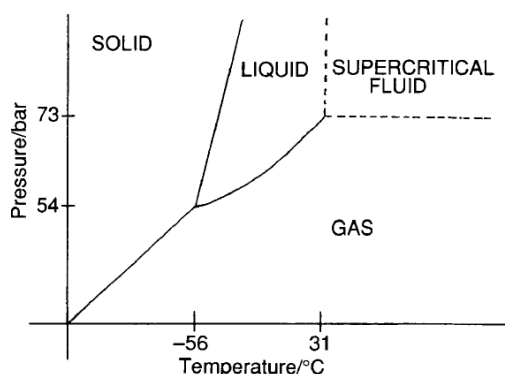
Fig. 1: Pressure –Temperature Phase Diagram for CO_2[38]
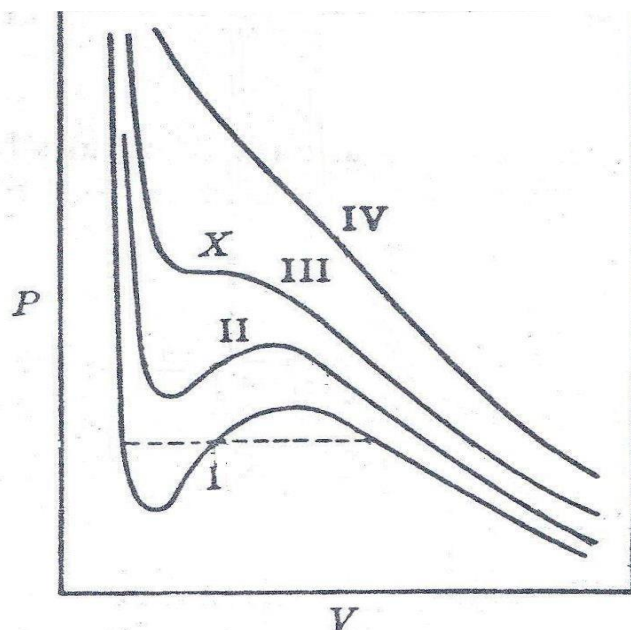
Fig. 2: Experimentally obtained P-V Isotherms for a Real Gas [4]
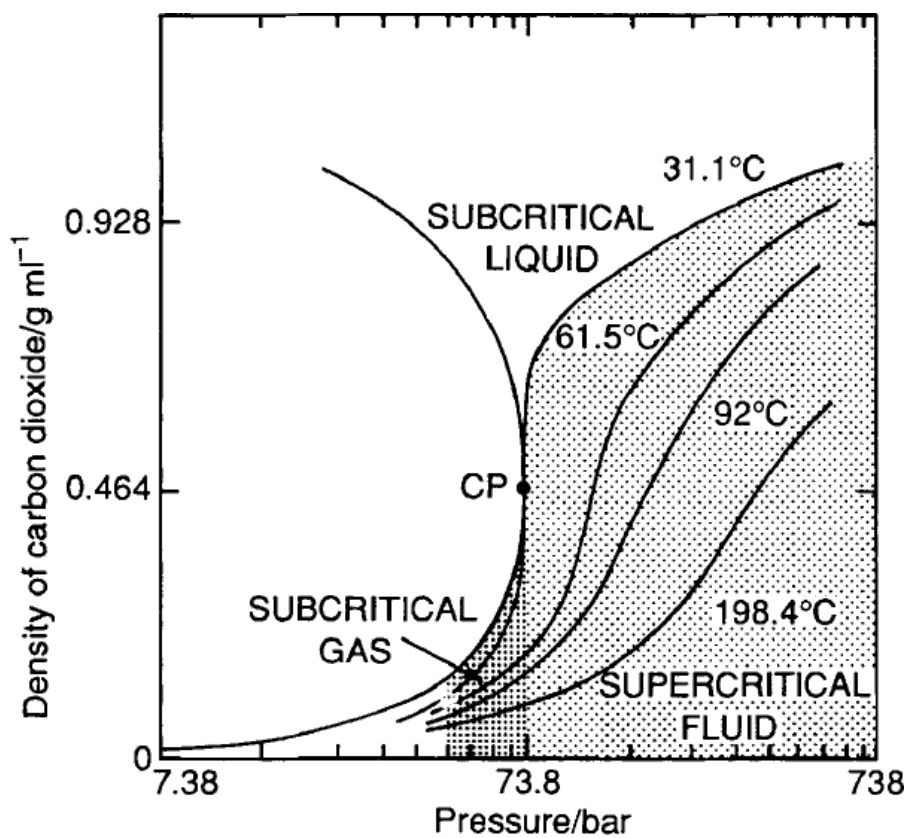
Fig. 3: Phase Diagram of supercritical and near supercritical CO_2 [38].
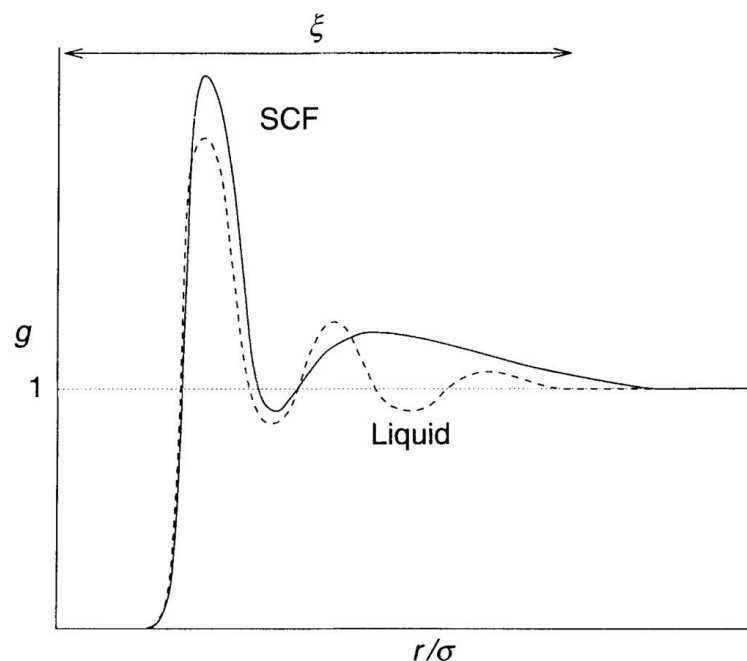
Fig. 4: Schematic representation of the pair correlation function in liquids and supercritical fluids. ζ is the correlation length, g is the ratio of local to bulk density at a distance r away from a molecule fixed at origin and σ is the molecular diameter[7].
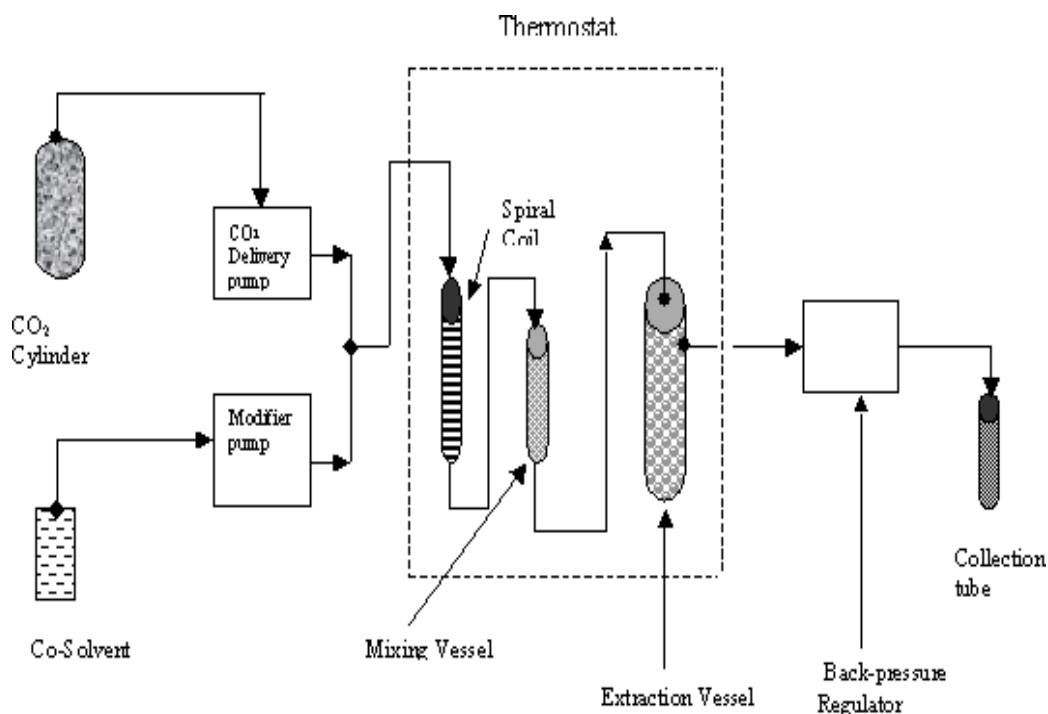
Fig. 5: A schematic diagram of SFE set-up[14]
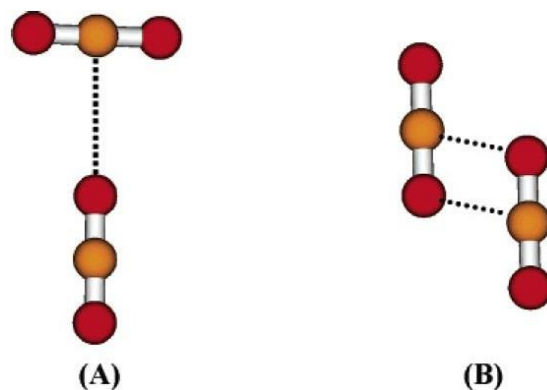
Fig. 6: Optimized geometries of the (A) T-shaped and (B) slipped parallel configurations of the CO_2 dimer[18].

$$H^+ + NO_3^- + TBP \longleftrightarrow H(NO_3).TBP$$

$$UO_2^{2+} + 2\,NO_3^- + 2TBP \longleftrightarrow UO_2(NO_3)_2.2TBP$$

$$CO_2 + H_2O \longleftrightarrow H_2CO_3 \longleftrightarrow 2H^+ + CO_3^{2-}$$
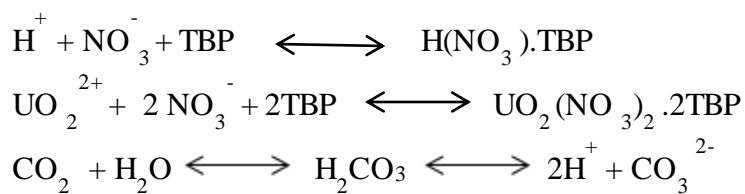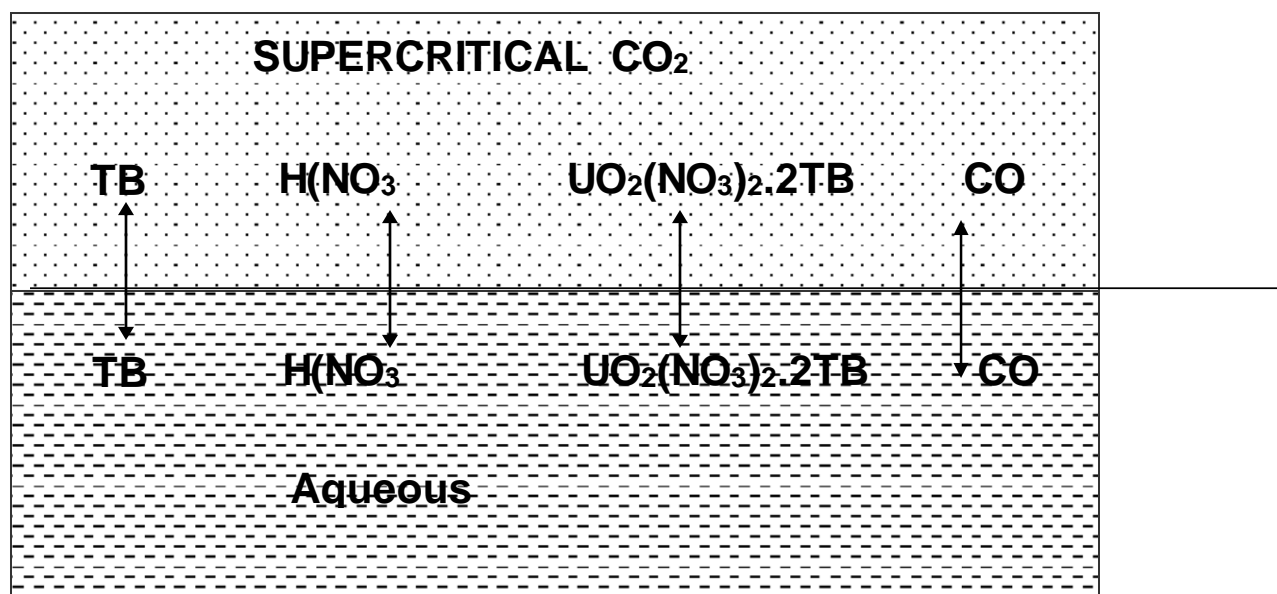
Fig. 7: Equilibria Involved in Extraction of UO_2^{2+} with Solvating Extractant [14]

Tables:

Table 1: Comparison of Physical Properties of Different States[14]
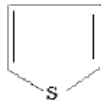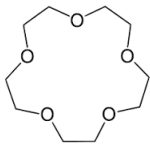
State	Density (g mL^{-1})	Viscosity (poise)	Diffusivity (cm^2 s^{-1})
Gas	10^{-3}	$(0.5-3.5)*10^{-4}$	0.01-1.0
Supercritical Fluid	0.2-0.9	$(0.2-1.0)*10^{-3}$	$(3.3-0.1)*10^{-4}$
Liquid	0.9-1.0	$(0.3-2.4)*10^{-2}$	$(0.5-2.0)*10^{-5}$
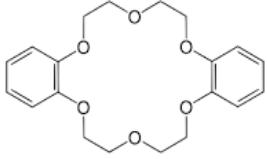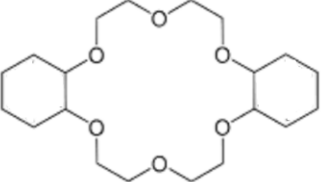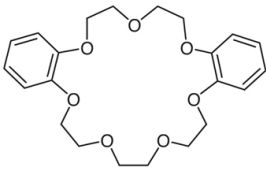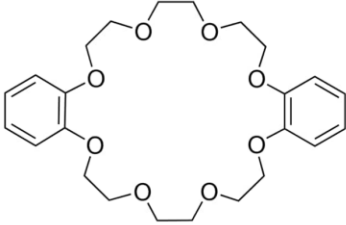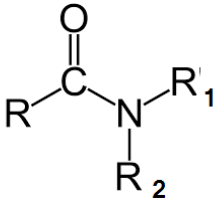
Table 2: Critical constants of some common Solvents used in SCF State[14]

Fluid	Critical Temperature T_c ($\Box$C)	Critical Pressure P_c (atm)	Critical Density (g/mL)	Density at 400 atm (g/mL)
CO_2	31.3	72.9	0.47	0.96
N_2O	36.5	72.5	0.45	0.94
NH_3	132.5	112.5	0.24	0.40
n-C_5	196.6	33.3	0.23	0.51
H_2O	374.2	217.6	0.27	--
SF_6	45.5	37.1	0.74	1.61
Xe	16.6	58.4	1.10	2.30
CCl_2F_2	111.8	40.7	0.56	1.12
CHF_3	25.9	46.9	0.52	--

Table 3: Chemical Structure of various compounds employed in the SFE of Uranium, Plutonium, Thorium

Tributyl Phosphate (TBP)	$(RO)_3$-P=O, R = C_4H_9
Triphenyl Phosphate (TPP)	(RO)3-P=O, R = C_6H_5
Trioctyl Phosphine Oxide (TOPO)	R_3-P=O, R = C_8H_{17}

Triphenyl Phosphine Oxide (TPPO)	R_3-P=O, R = C_6H_5
Tributyl Phosphine Oxide (TBPO)	R_3-P=O, R = C_4H_9
tri-isoamyl phosphate TiAP	(RO_3)-P=O, R= $(CH_3)_2CH(CH_2)_2$
tri-ethyl hexyl phosphate TEHP	(RO_3)-P=O, R= $(CH_3)_2(CH_2)_3CH(C_2H_5)CH_2$-
di-(2-ethylhexyl)phosphoric acid (DEHPA)	$(RO)_2POOH.$ R= $CH_3(CH_2)_3C(CH_3)CH_2$
Acetylacetone (AA)	R_1 =CH_3, R_2= CH_3
Trifluoroacetylacetone (TFA)	R_1 =CF_3, R_2= CH_3
Hexafluoroacetylacetone (HFA)	R_1 =CF_3, R_2= CF_3
Thenoyltrifluoroacetylacetone (TTA)	R_1=CF_3, R_2=
Heptaflurobutanoylpivaroylmethane (FOD)	R_1=C_3F_7 , R_2= $C(CH_3)_3$
15-Crown-5	

Dibenzo-18-Crown-6	
Ditertbutyldibenzo-18-Crown-6	
Dicyclohexano -18-Crown-6	
Dibenzo 21-Crown-7	
Dibenzo 24-Crown-8	
Fluorinated pentadecafluoro-n-octanoic acid (HPFOA)	$CF_3(CF_2)_6-\overset{\displaystyle O}{\overset{\displaystyle \|}{C}}-OH$
N,N-dialkyl amide	
N,N-dibutyl-2-ethylhexaanamide (DBEHA)	$R_1=CH_3(CH_2)_3(C_2H_5)CH$, $R_2,R_3 =C_4H_9$
N,N-dibutyl-3,3-dimethylbutanamide (DBDMBA)	$R_1=(CH_3)CCH_2$, $R_2,R_3 =C_4H_9$

N,N -dhexyloctanamide (DHOA)	$R_1=CH_3(CH_2)_6$, $R_2,R_3 =C_6H_{13}$
N,N-di-sec-butylpentanamide, DBPA	$R_1=CH_3(CH_2)_3$, $R_2,R_3 =CH(CH_3)(C_2H_5)$
N,N-dibutyloctnamide, DBOA	$R_1=CH_3(CH_2)_6$, $R_2,R_3 =C_4H_9$

Table 4: Major mile stones

1822	Supercritical Fluid was discovered by Cagniard de la Tour
1879	Hanny and Hogarth reported the solvating properties of supercritical fluids in the Royal Society meeting held at London.
1958	Lovelock suggested their use in chromatography as mobile phase enabling faster separation.
1962	Chromatography equipment came into existence by Klesper et al.
1992	Laintz and Wai were the first to report the SFE of metal ion, Cu^{2+}
1993	Lin et al. was successful in performing SFE of lanthanides and uranyl ion from solid materials
1994	Lin et al reported the SFE of thorium and uranium from solid and liquid materials with fluorinated β-diketones and TBP.
1996	Hong Wu et al$^{)}$ carried out SFE of uranium and thorium from nitric acid solution with organophosphorus reagents
1997	First review article on SFE of metal ions was publishes by Wai's group
2000	Erkey extensively reviewed the SFE of metal ions from aqueous solution including uranium and thorium.
2006	M.Koh et al. investigated Uranium SFE using diamide derivative.
2007	Pradeep Kumar et al. investigated Various organophosphorus reagentsfor SFE of thorium from simulated tissue paper matrix.
2007	Keskin et al. reviewed the ionic liquids towards supercritical fluid application.

2009	Pradeep Kumar et al. investigated supercritical fluid extraction of thorium from tissue paper matrix employing various β-diketones
2010	Pradeep Kumar et al., investigated various crown ethers for the SFE of uranium from acidic medium.
2010	Pradeep Kumar et al. investigated Supercritical fluid extraction of uranium from U3O8 powder granules, green pellet and sintered pellet using TBP–HNO3.
2010	P.K. Mohapatra's group studied for SFE of uranium and thorium from nitric acid medium and tissue paper matrix using various N,N-Dialkyl aliphatic amides.
2009-2021	N.Sivaramn' group extensively carried out research work on SFE of plutonium, uranium, thorium and Americium employing large variety of reagents such as TBP, TOPO,TTA, D2EHIBA, CMPO.
2012	Liyang et al. investigated the possibility SFE of uranium from TRISO- coated fuel particles
2014	L.Donna et al. investigated the feasibility of separating U from nitric acid solutions of mixed actinides U, Np, Pu, and Am using tri-n-butylphosphate (TBP)-modified SC-CO2.
2016	Supercritical Fluid Extraction (SFE) and purification of Uranium, from crude sodium diuranate (SDU) and rock phosphates ores
2002	Super-DIREX (Super Critical Fluid Direct Extraction, Mitsubishi)) process was suggested
2005	Russian groups suggested RELICT process (reprocessing by liquid Carbon dioxide Treatment) tested on real samples of spent fuel of RBMK-1000 and WWER- 1000 reactor
2009	B. F. Myasoedov, et al. Russian research group thoroughly investigated recovery of uranium and plutonium from simulated spent nuclear fuel(SSNF).
2011	M.D. Samsonov investigate possibility of using SFE for spent nuclear reprocessing and decontamination purposes using liquid CO2.

References:

1. C. Cagniard de la Tour, Ann. Chim. Phys. 21, 127, 1822.

2. C. Cagniard de la Tour, Ann. Chim. Phys. 22, 410, 1823.

3. T. Andrews, Philos. Trans. R. Soc. Lond. 159, 575, 1869.

4. S.Glasstone, "Thermodynamics for Chemists", Boston College, East-West Press Private Limited, 3rd edition.

5. L. Sangers, J.M.H. in Supercritical Fluids , Fundamnetal for application, 3-38 (NATO ASI Ser E), 273 Kluwer, Dordent ,(1994).

6. Sengers, J.V. & L. Sengers, J.M.H , Annu. Rev, Phy.chem 37,189, 1986 .

7. C .A. Eckert, B.L.Knutson & P.G. Debenedetti, Vol 383(26), 313, 1996.

8. J.B. Hanny, J. Hogarth, : Proceedings of Royal Soc. (London) 29, 324,1879.

9. J. Lovelock, : Private communication quoted in W. Bertsch, thesis, University of Houston, Texas, 1958.

10. E. Klesper, A. H. Corwin, D.A. Turner, J. Org. Chem. 27, 600, 1962.

11. R. M. Smith, "Supercritical Fluid Chromatography", University of Technology, Loughborough, The Royal Society of Chemistry, Burlington House, Picadilly, London (1988).

12. R. M. Smith,. J. of chromatography A, 856, 83, 1999.

13 .P.Kumar, A. Rao and K.L. Ramakumar, BARC news letter issue 202 , April 2009.

14. P. Kumar, A. Rao and K.L. Ramakumar, BARC report, BARC/2006/E/009.

15. P . Raveendran, S.L. Yikushima, L. Wallen Acc. Chem. Res. 38,478, 2005.

16. L.Reynolds, J.A. Gardecki, S. J.V. Frankland, M.L. Horng, M.Maroncelli, J.phys. Chem. 100, 10337,1999,

17. J . F . Kauffman, J. F. J. Phys. Chem. A., 105, 3433, 2001.

18. K. W. Jucks, Z. S.Huang, R. E.Miller, W. J. Lafferty, J. Chem. Phys., 86, 4341,1987.

19. M. J. Weida, D. J.Nesbitt, J. Chem. Phys. 105, 10210,1996.

20. P.Raveendran,S.L. Wallen, J. Am. Chem. Soc. 124,12590, 2002.

21. M. A. Blatchford, P. Raveendran, S.L. Wallen, J. Am. Chem. Soc. 124,14818, 2002.

22. D. J .Heldebrant, P.G. Jessop, J. Am. Chem. Soc., 125,5600,2003.

23. J. M. DeSimone, Z. Guan, C.S. Elsbernd, Science, 257, 945,1992.

24. J. B.McClain, D. Londono, J.R. Combes, T.J. Romack, D.A. Canelas, D.E. Betts, G.D. Wignall, E. T. Samulski,J. M. DeSimone, J. Am. Chem. Soc. 118,917,1996.

25. J. A. Darr and M. Poliakoff, Chem. Rev., 99,495, 1999.

26. P. Raveendran, Y. Ikushima and Scott L.Walle Acc. Chem. Res. 38, 478, 2005.

27. G.G.Yee, J. L. Fulton, R.D. Smith, J. Phys. Chem. 96, 6172,1992.

28. A.Dardin, J. M. DeSimone, E.T. Samulski, J. Phys. Chem B,102, 1775, 1998.

29. J.V.Sengetrs, Ann.Rev.Phys.Chem, 37, 189, 1986.

30. P.Diep, K.D. Jordan,J.K. Johnson, E.J. Beckman, E. J. Phys. Chem. A 102, 2231, 1998.

31. C.R.Yonker,B.J. Palmer, J. Phys. Chem. A 105, 308,2001.

32. M. Kanakubo, T. Umecky, C.C.Liew, T. Aizawa, K. Hatakeda, Y. Ikushima, 194, 859,2002.

33. P.Raveendran, S.L. Wallen, J. Phys. Chem. B, 107, 1473, 2003.

34. M.A. Blatchford, P. Raveendran, S.L. Wallen, J. Phys. Chem. A, 107,10311, 2003.

35. T. L. Chester, J. D. Pinkston, and D. E. Anal. Chem. 70, 301, 1998.

36. Y.Ikushima, N. Saito, K. Hatakeda, S. Ito, In Supercritical Fluid Processing of Food Biomaterials; Rizvi, S. S. H., Ed.; Blackie: New York, 150, 244, 1994.

37. C.H. Matthew and C. R. Yonker , Anal. Chem. 78, 3909, 2006.

38. M. Mukhopadhyay, "Natural Extracts using Supercritical Carbon Dioxide", Department of Chemical Engineering, Indian Institute of Technology, Mumbai, India, CRC press (2000).

39. J. Charastil, J. Phys. Chem. 86, 3016, 1982.

40. N.G. Smart, T. Carleson, T. Kast, A.A. Clifford, M.D. Burford, C.M. Wai, Talanta 44 , 137,1997.

41. K.E. Laintz , C.M.Wai, C.R.Yonker , R.D.Smith, J Supercrit Fluids;4, 194,1991.

42. W. Cross, A. Akgerman, C Erkey, Ind. Eng. Chem. Res. 35, 1765, 1996.

43. S. Keskin, Defne Kayrak-Talay, Ugur Akman, Oner Hortac, J. of Supercritical Fluids 43,150, 2007.

44. C. R. Yanker,S. L. Wallen, and J. C. Linehan , The Journal of Supercritical Fluids, 8, 250,1995 .

45. Y. Meguro, S. Iso, T. Sasaki, and Z. Yoshida , Anal. Chem. 70,774, 1998.

46. R. Schurhammer and G. Wipff, J. Phys. Chem. A, 109, 5208, 2005.

47. K.L. Toews, R.M.Shroll, C.M. Wai. And N.L smarty, Anal. Chem. 67, 4040, 1995.

48. Laintz, K. E., Wai, C. M., Yonker, C. R., Smith, R. D.: Anal. Chem. 64, 2875, 1992.

49. Lin, Y., Brauer, R. D., Laintz, K. E., Wai, C. M.: Anal. Chem. 65, 2549 ,1993.

50. Lin, Y., Wai, C. M., Jean, F. M., Brauer, R. D., Environ. Sci. Technol. 28, 1190, 1994.

51. Hong Wu, Yuehe Lin, N. G. Smart, and C. M. Wai, Anal. Chem. 68, 4072,1996.

52. R.Kumar, N. Sivaraman, T.G., Srinivasan, P. R. V. Rao, Radiochim. Acta 90, 141, 2002.

53. R.Kumar, N. Sivaraman, E.S. Vaidivu, T.G. Srinivasan, P. R. V. Rao, Radiochim. Acta, 91, 197, 2003.

54. C.M Wai , Shaofen Wang, J of Chromatography –A, 785,369,1997.

55. C. Erkey , Journal of Supercritical Fluids ,17,259,2000.

56. J.S. Wang, M.K. Koh, C.M Wai , Ind. Eng. Chem. Res. 43, 1580,2004.

57. C.M. Wai, S. Wang, Biochem. Biophys. Methods, 43, 273, 2000.

58. N. G. Smart, Thomas E. Carleson, Sadik Elshani, S. Wang, and C. M. Wai, Ind. Eng. Chem. Res. 36, 1819,1997.

59. M. Koh, J. Yoo, Y. Park, D. Bae, Kwangheon Park,* Hakwon Kim, and Hongdoo Kim, Ind. Eng. Chem. Res. , 45, 5308,2006.

60. Donna L. Quacha, B. J. Mincher b,, C. M. Wai, Journal of Hazardous Materials 274, 3600,2014.

61. A.Rao , B.S. Tomar, Separation and Purification Technology, 161, 159,2016.

62. L. Zhua,W. Duan, J. Xu, Y.Zhu, J. of Hazardous Materials, 241-242,456, 2012.

63. P. Kumar, A.Pal, M.K. Saxena and K.L. Ramakumar, Radiochimica Acta, 95, 701, 2007.

64. P. Kumar, A. Pal, M.K. Saxena and K.L. Ramakumar, Desalination, 232 ,71,2008.

65. A. Rao, P. Kumar and K.L. Ramakumar, Radiochimica Acta, 96 ,787,2008.

66. P. Kumar, A. Rao and K.L. Ramakumar, Radiochimica Acta, 97,105,2009.

67. A. Rao, P. Kumar and K.L. Ramakumar, Radiochimica Acta , 98, 403,2010.

68. A. Rao, P. Kumar and K.L. Ramakumar, J. of Radioanalytical and Nuclear Chemistry, 285, 245, 2010.

69. N.V. Rathod, A. Rao, P. Kumar, K. Lakshmi, Ramakumar and D. D. Malkhede, New Journal of Chemistry. online 21 aug,2014.

70. A. Rao, P. Kumar, B.S. Tomar, Separation and Purification Technology, 134 (25), 126, 2014.

71. N. V. Rathod, A. Rao, P. Kumar, K. Lakshmi. Ramakumar, and D. D. Malkhede, Industrial Engineering and Research, 54, 3933 , 2015.

72. P. Prabhat, A. Rao, P. Kumar, B.S. Tomar, Hydrometllurgy, 164,177, 2016.

73. P. Prabhat, A. Rao, Vivekchandra G. Mishra, D. J. Shah, P. Kumar and Bhupinder, S.Tomar, Radiochimica Acta 2020.

74. A. S. Kanekar, P. N. Pathak,P. K. Mohapatra, V. K. Manchanda , J of Radioanalytical and Radiochemsitry , 283,789,2010.

75. A. S. Kanekar, P. N. Pathak,P. K. Mohapatra, R,Acharaya , V. K. Manchanda, Desalination and Water Treatment 38(1-2), 199,2012.

76. A. S. Kanekar, P. N. Pathak, and P. K. Mohapatra, Separation Science and Technology, 50 ,471,2015,

77. T. Vincent, M. Mukhopadhyay , P.K. Wattal , Desalination 232 (1–3), 91, 2008.

78 .T.Vincent, M. Mukhopadhyay , P.K. Wattal , J.of Supercritical Fluids, 48,230,2009.

79 .R. Kumar, N. Sivaraman, K. Sujatha, T. G. Srinivasan∗ and P. R. Vasudeva Rao, Radiochim. Acta, 97, 443, 2009.

80. R. Kumar, R. Venkatakrishnan, N. Sivaraman, T. G. Srinivasan, and P. R. Vasudeva Rao, J. of Nuclear and Radiochemical Sciences, 6(2),127, 2005.

81. R. Kumar, N. Sivaraman, K. Sujatha, T. G. Srinivasan and P. R. Vasudeva Rao Radiochimica Acta, 95(10) 577, 2007.

82. K. Sujatha, K. C. Pitchaiah, N. Sivaraman, T.G. Srinivasan, P. R. V. Rao, American Journal of Analytical Chemistry, 3, 916,2012.

83. K. Sujatha , K.C. Pitchaiah , N. Sivaraman , K. Nagarajan , T.G. Srinivasan P.R. Vasudeva Rao, Desalination and Water Treatment, 52,470,2014.

84. K. C. Pitchaiah, K. Sujatha, C. V. S. Brahmmananda Rao, S. Subramaniam, N. Sivaraman and P. R. Vasudeva Rao, Radiochim. Acta 103(4), 245,2015.

85. K. C. Pitchaiah, K. Sujatha, C. V. S. Brahmmananda Rao, N. Sivaraman, T. G. Srinivasan, K. Nagarajan, P. R. Vasudeva Rao, International Journal of Analytical Mass Spectrometry and Chromatography, V2(2) , 32,2014.

86. K. C. Pitchaiah, N. Sivaraman, M. Joseph, P. K. Mohapatra & G. Madras, Separation Science and Technology, 52(14),2224 ,2017.

87. J. Deepithaa, K.C. Pitchaiaha, C.V.S B. Rao, G. Madrasb, and N.Sivaraman, Separation Science and Technology 54(10), 1650, 2019.

88. K.C.Pitchai, K.Sujatha, J.Deepitha, S.Ghosh, N.Sivaraman, J of supercritical fluids, 147, 194,2019.

89. J.Deepitha . K.C. Pitchaiah, G. Chandrasekhar,N. Sivaraman, Separation and Purification Technology , 2021

90. J.Deepitha,K.C. Pitchaiah, G. Chandrasekhar N. Sivaraman, J. of Supercritical Fluids.,176, 105318, 2021.

91. J. Deepitha a, K.C. Pitchaiah b, G. Chandrasekhar c, N. Sivaraman , Separation and Purification Technology 283,120174, 2022.

92. B. F. Myasoedov, Yu. M. Kulyako, T. I. Trofimov, M. D. Samsonov, D. A. Malikov, T. A.Mariutina and B. Ya. Spivakov, Radiochim. Acta 97, 473, 2009.

93. M.N.Litvina, D.A.Malikov,T.A. Maryutina, M.Y. Kulyako, B.F.Myasoedov p. 533,

The Royal Society of Chemistry,Spec. Publ. No 305 (Proc. of the conference Actinides 2005, Manchester, UK),RCS Publishing, Cambrige, UK, 20.

94. M. N. Litvina, D.A. Malikov, T.A. Maryutina, M.Y. Kulyako, B.F. Myasoedov, Radiokhimiya 49, 144, 2007. (in Russian).

95. B.F.Myasoedov, T.A. Maryutina,M.N. Litvina,D.A. Malikov,M.Y. Kulyako, B.Y. Spivakov, C. Hill, J.M. Adnet,M. Lecomte, C. Madic,. Radiochim. Acta, 93, 9, 2005.

96. M. D. Samsonov , A.Yu. Shardin, D.N. Shafikov, Yu M.Kulyako and B.F. Myasoedov, Supercrtical Fluid extraction in Modern Chemsitry , Radiochemsitry 53(2) , 111,2011.

97. T. Shimada, S. Orgumu , N .Ishihara , J Nucl. Sci. Technol, 3, 757, 2002.

98. Y. Enokida , Int Conf Supergreen , 2, 35,2002.

99. A. Shardin, A. Muzrin, V .Romanovsky et al, Proc . Int Conf Global 2005, Tsukuba (Japan), paper no 12, October , 2005.

100. M.Y. Kulyako, A Shadrin and B.F.Myasoedov , Ross KhimZh. (Zh, Ross Khim O-va im D.I.Mendeleva) 49(2), 97,2005.

101. A. Shardin, A Muzrin, V.Romanovsky, Int. Conf. Global, Tsubuka (Japan),128, Oct, 2005.

102.A. Shardin, A. Muzrin, A.Lumpov and V. Romanovsky , Solvent Extr. Ion Excah 26(6), 797, 2008.

Sorption of Eosine Y dye onto pre-treated hen feathers in aqueous solution

Madhavi Rahul Pawar

Chemistry Department, Pune University, Pune 411007, India

Email: madhavipawar11@gmail.com

Abstract

The present study reports Eosine Yellow (EosineY) dye removal by adsorption method. For this purpose hen feathers (HF) are used as sorbent. After optimization of various parameters, it was observed that 75.7% removal of dye (25ppm) occurs at pH 4, contact time 1 h using 1.25 g of adsorbent. Adsorption isotherm studies shows that Langmuir model is best fitted for sorption of the dye on selected sorbent. The kinetics and thermodynamics studies revealed that adsorption process follows pseudo second order kinetics and is exothermic in nature. Use of hen feathers for removal of Eosin Y is found to be efficient and cost effective.

Key words: Eosin Y, hen feathers, batch adsorption, kinetics, thermodynamics

Introduction

Effluents from dye industry affect flora and fauna to a greater extent. Number of methods are in use for treatment of these effluents[1,2]. Among all, adsorption is found to be the simplest, effective and environment friendly method. Survey of the literature shows that biosorption provides an economically viable sustainable technology for treatment of wastewater[3,4].

Use of waste biomaterial as sorbent (biosorption) is newly developed technique for removal of dyes due to its low initial cost, simple design, ease of operation and efficiency[5]. A large number of low cost bioadsorbents based on natural material such as rice husk[6], Mangrove bark[7], wool and cotton fiber[8], activated carbon prepared from pistachio nutshell[9], delonix regia pod[10], rice hull ash[11], have been investigated for removal of dyes from aqueous solution. Biological materials such as chitosan[12] bacterial biomass[13], yeast[14], fungi[15], have been used as bioadsorbent for removal of dyes from solution. Present study deals with the biosorption characteristics of hen feathers (HF) for removal of Eosine Y from aqueous solution. Amino acids in feathers have number of functional groups which render interesting

physicochemical sorption of inorganic and organic compounds[16]. Feathers are waste product generated in abundant amount in commercial poultry plants.[17]

Material and method

AR grade chemicals and Eosine Y (C.I. No. 45380, MF $C_{20}H_6Br_4Na_2O_5$) were used in the present work. The initial pH of the desired Eosine Y concentration was measured with pH meter and maintained using 0.01 M H_2SO_4 and 0.01M NaOH solution. Structure of Eosine Y is shown in Fig. 1.

Material development

Hen feathers collected from local market were washed several times with detergent and tap water. Feathers were dried completely in the oven at 100^0C. The barbs were cut into small pieces with scissor and middle rachis was removed. Dried sample was finely powdered in the mixer and stored until further use.

Characterization of Sorbent

Chemical analysis of hen feathers was done by SEM-EDS (scanning electron microscope with energy dispersive X- ray spectroscope) method of elemental analysis. Surface structure of the biosorbent was analysed using scanning electron microscope (JSM-6360 A, JOEL, Japan.) at an electron voltage of 20 kV.The SEM image (Fig. 2) of the bioadsorbent shows large surface area that could possibility entrap and bioadsorb Eosine Y by surface functional groups.

For FTIR analysis finely powdered sample of hen feathers was used. Scanning range was selected between wavenumber 4000-400 cm^{-1}. The FTIR spectrum of hen feathers (Fig. 3) shows the bands at 1,600 - 1,700 cm^{-1} (amide I) and 1,500-1,560 cm^{-1} (amide II). Band appears at stretching vibrations of C-H (2960 - 2874 cm^{-1}) and that of CO (2960 - 2874 cm^{-1} and 1159.26 cm^{-1}).

Batch Sorption

Batch adsorption technique was used for the removal of Eosin Y from its aqueous solution. Maximum removal of Eosin Y was achieved by optimization of different parameters Viz. pH, contact time, dosage, concentration of dye and temperature. For adsorption studies fixed amount of powdered HF was shaken with fixed volume (25mL) of dye at desired concentration in 100 mL RB flask on magnetic stirrer to achieve equilibrium. After acquiring

equilibrium condition, solution was filtered and concentration of the dye in filtrate was measured spectrophotometrically at λmax 517 nm.

Calculations

The following equation was used to calculate amount of residual dye per unit quantity of biosorbent

$$q_e = \frac{Co - Ce}{M} X \, V \qquad\qquad (1)$$

Where Co and Ce indicate initial and equilibrium dye concentration (mg L^{-1}) respectively, V is volume (L) of the dye solution and M is mass (g) of bioadsorbent. The Following equation is used to find % removal.

$$\% \, Removal = \frac{Ci - Ca}{Ci} X \, 100 \qquad\qquad (2)$$

Results and discussion

Effect of pH

Effect of pH on Eosine Y removal is shown in Fig.4. As can be seen, Maximum removal was found to be 60.69 % at pH 4 and then it decreases with pH reaching minimum removal (21.79 %) at pH 10. Hence pH 4 was selected as an optimum pH. At lower pH, adsorption increases as protonation increases which causes neutralization of negative charges at the surface of hen feathers. Lower pH is responsible for more degree of protonation causing neutralization of negative charges at the surface of adsorbent leading to more adsorption. Degree of protonation is less at higher pH causing preferential adsorption of dye on active sites and enhances the diffusion process. At higher pH, protonation decreases thus repulsive forces becomes operative, which retards adsorption and diffussion[18].

Effect of contact time

Fig. 5 shows variation of % removal of dye with contact time (1-4 h) at pH 4. Maximum removal of dye occurs in about 1 h. Initially, removal was found to be high but it reaches a constant value as contact time increases. This can be attributed to saturation of adsorption sites with time [19].

Effect of amount of adsorbent

The amount of adsorbent was varied between 0.25g - 1.25g at fixed pH and concentration. From the results (Fig.6) it is observed that % removal of Eosine Y increases with increase in adsorbent dosage. This may be due to the increased surface area with amount of adsorbent making more adsorption sites available[20]

Effect of initial dye concentration

Fig. 7 shows effect on initial dye concentration (5-25 ppm) on its removal. As can be seen from this Fig, percentage removal increases from 5ppm to 25ppm. This was expected due to fact that with higher initial dye concentration the driving force of the concentration gradient increases resulting in favorable condition for adsorption of dye[21].

Adsorption isotherm

In the present study, experimental data for Eosine Y - hen feathers equilibrium was examined with Freundlich and Langmuir isotherm models.

A Langmuir equation [22,23] is as follows

$$\frac{1}{q_e} = \frac{1}{a_b}\frac{1}{C_e} + \frac{1}{b} \qquad \textbf{(3)}$$

Where, qe = amount of dye per unit mass of HF (mg/g), a = constant related to affinity of binding sites (L/g), b = maximum amount of dye per g of HF (mg/g), C_e = equilibrium dye concentration. Plots of 1/qe vs 1/Ce gives straight line with slope of 1/ab and intercept 1/b (Fig.8).

Freundlich model can be expressed by following equation[24-26],

$$ogq_e = \frac{1}{n}\log C_e + logK_f \qquad \textbf{(4)}$$

Where, q_e = amount of dye per unit weight of adsorbent (mg/g) Ce = equilibrium dye concentration per unit weight (mg/g) K_f = Freundlich constant 1/n = Freundlich Isotherm constant related to adsorption intensity. A plot of log q_e vs log Ce is shown in Fig.9

For the adsorption of Eosine Y onto HF, the Freundlich constant K_f indicates the sorption capacity of adsorbent. The value of n (closer to1) indicates favorable adsorption process.

Correlation coefficients reveal that Langmuir model is better fitted than the Freundlich model. Experimental data is presented in Table 2.

Biosorption kinetics

The kinetics of adsorption process was studied by varying the contact time. In order to study adsorption process, it is necessary to establish most appropriate correlation for equilibrium data[27]. Kinetic data was examined in the light of pseudo first order equation[28] and pseudo second order equation[29].

Plot of t/qt against t is shown in Fig.10. The different values for pseudo first and pseudo second order kinetics are shown Table 3.The obtained data reveals that adsorption process obeys pseudo second order kinetics and overall process may be controlled by chemisorption [30, 31].

Thermodynamics studies

The various thermodynamic parameters were calculated using following equations[32,33],

$$K = \frac{q_e}{c_e} \tag{5}$$

$$\Delta G^0 = \text{-RT ln } K \tag{6}$$

Where all the symbols have their usual meanings. Positive ΔG^0 at all the temperatures indicates that adsorption of Eosine Y is not a spontaneous phenomenon and sorption of Eosine Y onto hen feathers may be due to physical process of diffusion[34].

The thermodynamics adsorption parameters ΔH^0 , ΔS^0 are calculated from Fig.11 using the equation:

$$log K = \frac{\Delta S^0}{2.303 R} - \frac{H^0}{2.303 RT} \tag{7}$$

ΔH^0 and ΔS^0 were calculated from Fig.12 and the obtained results are shown in Table 4.

The exothermic nature of adsorption is indicated by negative value of ΔH^0 and positive ΔG reveals non-spontaneous process of adsorption. Further, decreased disorder at the solid solution interface during adsorption is revealed by negative value of entropy change ΔS^0. With increasing temperature mobility of the dye molecules increases which is responsible for escape of adsorbent molecules from the solid phase causing decrease in the adsorption

capacity of Eosine Y. Similar results were reported by Mahanashi etal [35] for adsorption of E 120 dye onto activated carbon

Conclusion

Maximum removal (75.7%) of Eosine Y (25ppm) was seen at pH: 4, contact time: 1h, adsorbent dosage: 1.25 g and concentration: 25 ppm.Langmuir model is best fitted for the biosorption of Eosin Y on hen feathers. Adsorption of Eosine Y on HF can be described by pseudo second order kinetics model. On the basis of thermodynamic parameters it can be revealed that biosorption process is exothermic. As hen feathers are naturally available and cheap animal residue, proposed method can be considered as economical method for the removal of Eosine Y.

Acknowledgement

Figures:
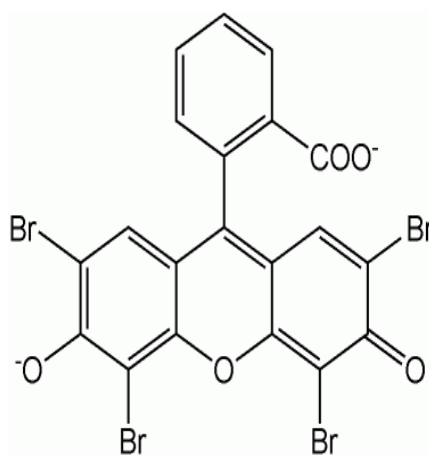
Fig.1: Chemical structure of Eosine Y
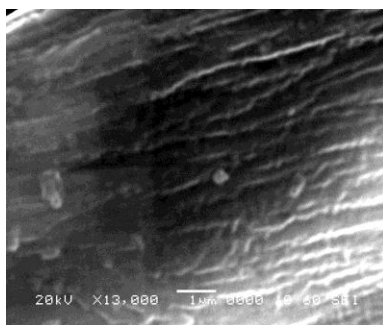
Fig.2: SEM of HF
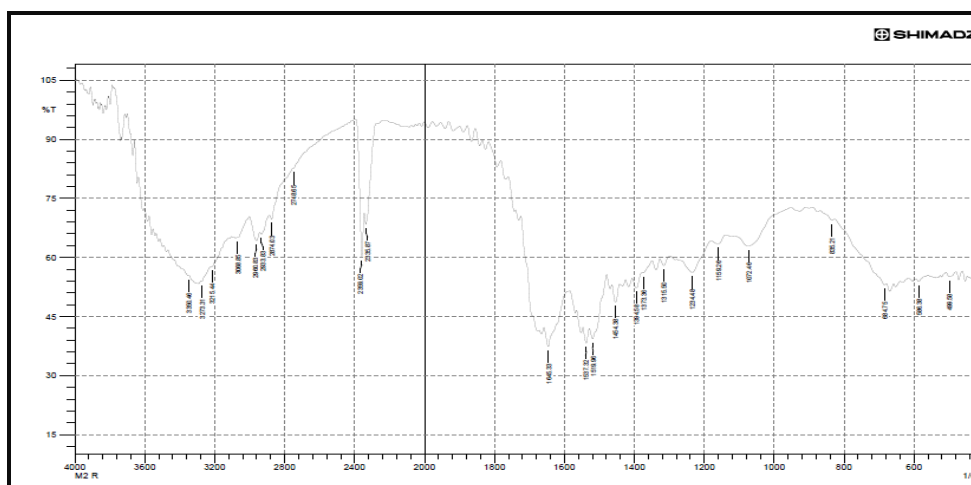
Fig.3: FTIR analysis of hen feathers
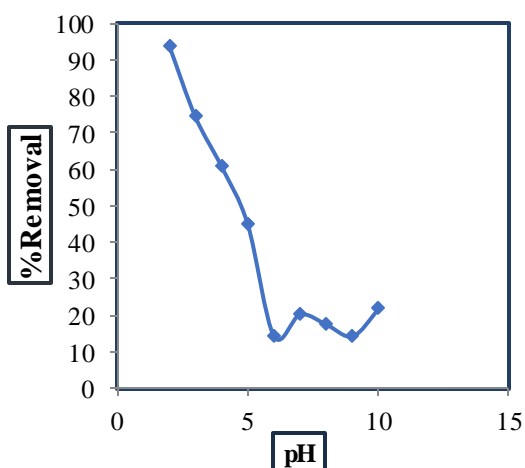
Fig. 4: Effect of pH on uptake of Eosine Y by HF (Experimental condition: Eosine Y concentration = 15 ppm, dosage =0.5 g, contact time = 1h)
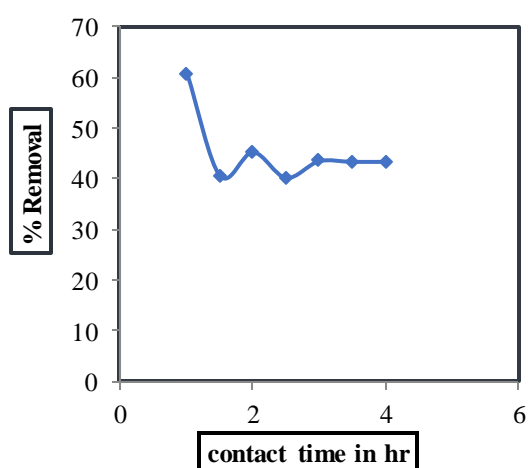
Fig.5: Effect of contact time on uptake of Eosine Y by HF (experimental condition: Eosine Y concentration = 15 ppm, dosage = 0.5 g, pH=4)
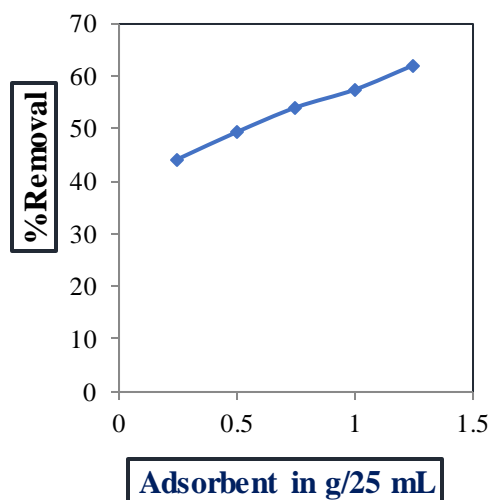
Fig.6: Effect of dosage on uptake of EosineY by HF (Experimental condition: Eosine Y concentration = = 15 ppm, contact time = 1 hr, pH = 4)
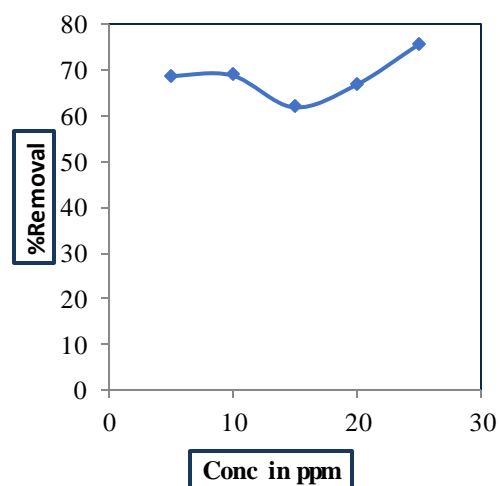
Fig.7: Effect of concentration on uptake of Eosine (experimental condition: contact time = 1 h, pH = 4, dosage =1.25 g)
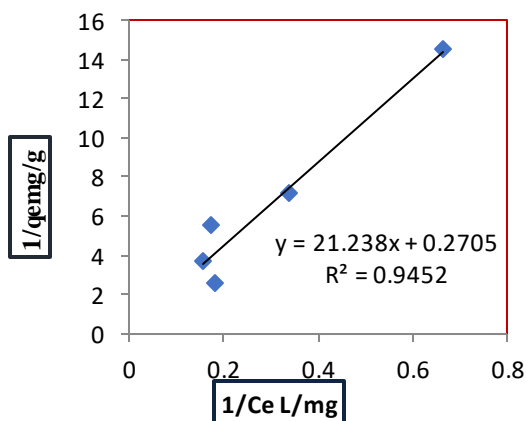
Fig.8: Langmuir plot for adsorption of Eosine Y onto HF.
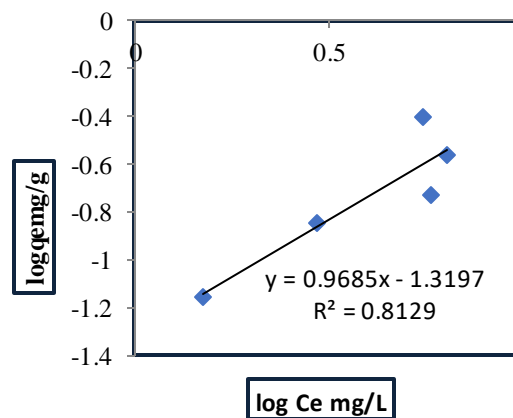
Fig.9: Freundlich plot for adsorption of Eosine Y onto HF
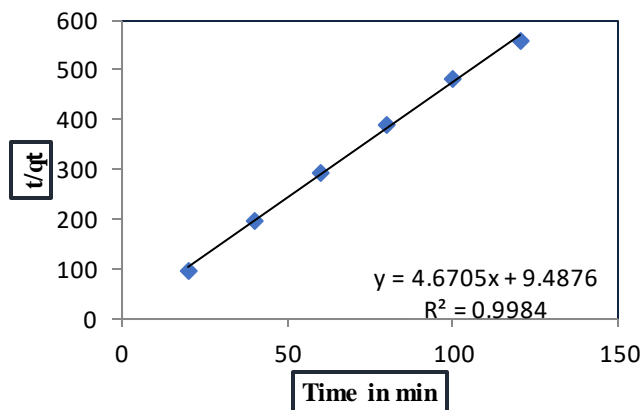
Fig.10: Pseudo second order plot of t/qt Vs time
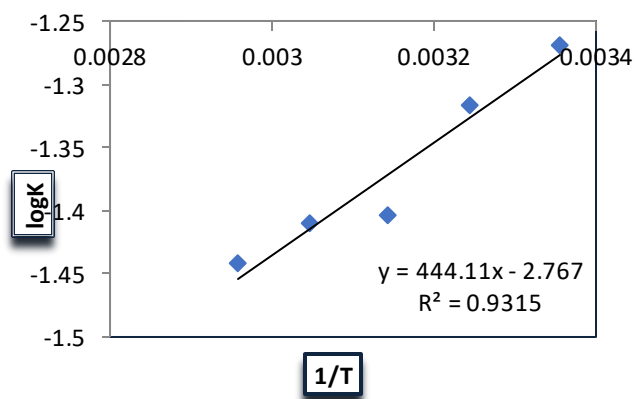
Fig. 11: Plot of log K vs 1/T

Tables:

Table 1: Elemental essay of feathers used in adsorption experiment,

Element	(keV)	Mass%
C K	0.277	35.09
N K	0.392	51.38
O K	0.525	4.41
S K	2.307	1.27
Cu K	8.040	3.07
Zr L	2.042	4.78

Table 2: Values of different constants for biosorption of Eosine Y by HF

Langmuir isotherm			Freundlich isotherm		
a(mg/L)	b(mg/g)	R^2	K_f	N	R^2
0.0127	3.703	0.945	0.047	1.033	0.812

Table 3: Kinetic parameters for adsorption of Eosine Y onto hen feathers

Pseudo first order kinetics				Pseudo second order kinetics		
q_{eexp}	q_{ecal}	K_1	R^2	qe_{cal}	K_2	R^2
(mg/g)	(mg/g)	Time		(mg/g)	g/mg/min	
0.2145	0.010	--	0.149	0.2141	2.342	0.998

Table 4: Estimated values of $\Delta G^0, \Delta S^0$ and ΔH^0 for adsorption of Eosine Y onto hen feathers.

ΔG^0					ΔS^0	ΔH^0
kJ/mol					kJ/(mol K)	kJ/mol
298K	308K	318K	328K	338K		
7.2	7.758	8.547	8.851	9.324	-0.052	-8.510

References

1. I. L Finar, The Fundamental Principles, Addison Wesley Longman Ltd, Organic chemistry, sixth ed, 890, 1973.

2. P.C. Vandevivere, R. Bianchi, W. Verstraete, J. Chem. Technol. Biotechnol., 72, 289, 1998.

3. K. Al-sabti, Ecotoxicol. Environ. Saf., 47 (2), 149, 2000.

4. S. Chowdhury, S. Chakraborati, P. Saha, Col. Surf B Bio Interfaces, 84 (2), 520, 2011.

5. S. Chowdhury, P. Das Saha, Appl. Water Sci, 2(3), 209, 2012

6. R Uma, Lakshmi, V. Chandra, Srivastava, Deo M., D. Lataye, J. Environ. Manage., 90, 710, 2009.

7. L. S. Tan, K.Jain, C. Rozaini, J. Appl. Sci. in Environ Sanita., 5 (3), 283, 2010.

8. A. Rasheed Khan, Tahir H, Uddin Hameed, J. Appl. Sci. Env. Manage., 9, (2), 29, 2005

9. P. Vijayalakshmi, K.V. Sathya Selva Bala. P.Thiruvengadaravi , M. Palanichamy, S. Sivanesan Sep.Sci. Technol., 46 (1), 155, 2010.

10. H.Yuh-Shan, R. Malarvizhi, N. Sulochana J. Env. Prot. Sci., (3), 111, 2009.

11. A.Gang Chen, S.Shuang, S.Ting Liu, P. Zhang, A. Zhang, Jie Sun, Ying Ye, Sep. Sci. Technol., 47, 147, 2012

12. Kamari, W. Saime, Wan N, L.Ken, Liew. J. Environ. Sci. 21. 296, 2009.

13. S.W. Won, SB Choi, SB Chung, D.Park, JM Park, Y.S.Yun, Ind. Eng. Chem. Res. 43 7865, 2004.

14. M A Martins , M H Cardoso, M J Queiroz, M T Ramalho, A M Campos, Chemosphere, 38(11), 2455, 1999.

15. K.Selvam., M. Shanmuga Priya. Inter. J. Environ. Sci. 2 (4), 1938, 2012

16. A.Villarreal, B.Petriciolet, H.Montoya, MAMontes-Moran, HE Reynel-Avila, Chem. Eng. J. 167, 67, 2011.

17. A Mittal, V. Thakur, V. Gajbe, J. Environ Sci Pollut Res., 20, 4602, 2013.

18. A.Mittal, V. Thakur, V. Gajbe, Environ Sci Pollut Res., 20, 260, 2013.

19. P. Martin, Solomon, J. Samu, Env. Sci. Pollut. Res Int., 1(2), 201, 2011.

20. V. K .Garg, R. Gupta, A.B. Yadav Kumar, Bioresourse Techno, 89, 121, 2003.

21. M.S.Chiou, Li J. Hazard. Mat., B 93, 233, 2002.

22. K Elass, A. Laachach, A.Alaoul, A. Azzi, Appl. Eco. Env. Res. 8 (2), 153, 2010.

23. Zheng W, Li XM, Wang F, Yang Q, Deng P, Zeng GM. J. Hazard. Mater. 157 (2), 490, 2008.

24. S. Chatterjee S, Chatterjee. Das AR, Guha AK J. Colloid Interface Sci., 288(1), 30, 2005.

25. A.Safa Özcan, Adnan Özcan, J. Colloid Interface Science276 (1), 39,2004.

26. Freundlich, H.M.F., Uber die adsorption in losungen. Z. Phys. Chem., 57, 385. 1906

27. B. Karima, B. Mossab, M. A.Hassen International Renewable Energy Congress, Sousse, Tunisia 360, Nov-2010.

28. N.S. Rajurkar, D. Mahajan J. Appl. Chem., 4 (4) 1206 2015.

29. Y.S Ho, D.A.J Wase and C.F. Forster, Environ. Technol., 17 (1), 71, 1996.

30. G McKay Y.S. Ho. Process, Biochem. Elsevier science Ireland ltd., 34, 452, 1999.

31. G McKay Y.S. Ho Water Res., 33 (16), 578, 1999.

32. C. Namasivayam, R.T.Yamuna Environ. Pollut., 89, 1, 1995.

33. G.C Catena, F.V. Bright, Anal. Chem., 61, 905, 1989.

34. H. Beak, C. Ijagbemi, and S. Dong. J. Environ. Sci. Health Part A, 44, 536, 2009.

35. M. H Mahnashi, S. S. Abu-Alrub, M. W Amer, A. O Alqarni, Tropical J. of Pharmaceutical Res., 20 (3), 1596, 2021

Advanced Oxidation Processes for the Degradation of Organochlorine Pesticides

Kavita Gandhi[1]*, Noor A. Khan[2], Kanchan Singh[1], and Neeta Thacker[1]

[1]Pesticide Residue Laboratory, Sophisticated Environmental Analytical Facility and

[2] Delhi Zonal Centre,

CSIR-National Environmental Engineering Research Institute, Nagpur, India

Email: kn_gandhi@neeri.res.in

Abstract

Advanced Oxidation Processes (AOPs) are a group of treatment technologies, which aim at efficient decomposition of pollutants. The AOPs are based on oxidation of pollutants using various single or combinational techniques generating free radicals, thereby leading to oxidative degradation and complete mineralization of pollutants. Conventional AOPs based on ultraviolet (UV) irradiation are commonly used for destruction of microorganisms in the household filters. These techniques have also been used to remediate conventional and upcoming pollutants like pesticides, Pharmaceuticals etc., which are normally persistent in nature. The various combinations used for generating reactive radicals in AOPs are fenton, photofenton, ozone, UV radiations, sonolysis etc.

In the present study, degradation using various AOPs and different pesticides was performed for the organochlorine group of pesticides. It was found to be effective for degradation of the targeted pesticides which are otherwise, persistent in nature. The response of the studied pesticides was different for all the AOPs used, which include, UV photolysis, H_2O_2 degradation, UV-H_2O_2, fenton's etc. Studies have been performed in the aqueous matrix and degradation rates are determined for the different reactions. The rate of degradation was found to be significantly enhanced in presence of H_2O_2 and fenton's reagent with UV irradiation rather than UV alone.

Keywords: Advanced Oxidation Processes, Organochlorines, Pesticides, UV, Fenton's reagent

Introduction

Pesticides and fertilizers play a substantial role in enhancing the crop productivity. However, the use of pesticides goes parallel with its residues in water and soil due to its indiscriminate use. The pesticides after being used in the fields, enter the environment through surface run-offs, aerial sprays etc. and some of persistent pesticides may bind with the soils and also get deposited in the sediments.

Humans may be exposed to pesticides by direct and indirect routes of exposure like dermal contact, inhalation etc. The exposure to these compounds may lead to acute and chronic health issues.

The pesticides can be classified into various classes depending upon their chemical composition, applications, origin etc. Under chemical classification, pesticides are categorized according to the chemical nature of the active ingredients. The various categories include Organochlorines (OCPs) Synthetic Pyrethroids (SPs) Organophosphate (OPPs) etc.

Of these, the OCPs is the most persistent of the group. They are synthetic organic compounds with five or more chlorine atoms. They have been used significantly in agriculture and mosquito control in the past. Some important representative compounds of this group are dichlorodiphenyl-trichloroethane (DDT),Hexachlorocyclohexane (HCHs), aldrin, dieldrin, chlordane, endosulphan etc.[1,2]

OCPs have a high bioaccumulation potential, toxicity, and persistence in the environment [3].

A good number of pesticides, particularly organochlorines, can also be seen among the Persistent Organic Pollutant list of Stockholm convention[4]. A share of about 40% of all the pesticides used belonged to organochlorines in the past[5].

The various studies carried out on pesticide concentrations in the environment, indicate their presence not only in environmental matrices but also at various food chain levels.

During 2005-2007, 16 bird species in more than 100 samples were collected from Ahmedabad after being killed with kite flying threads. All carcasses were detected with pesticide contamination during the study, which makes the situation more alarming[6]. The blood plasma samples of Vultures collected from Ahmedabad indicated the presence of organochlorine pesticides (OCPs) and polychlorinated biphenyls[7] .

Some studies have also been carried out in the Cauvery river[8] in the water, sediment, shrimps and fish samples indicate the presence of OCPs in these samples.

Another review[9] reported OCPs in the Cauvery river which include compounds like hexachlorocyclohexane (HCH), dichloro-diphenyltrichloroethane (DDT), endosulfan, aldrin, dieldrin, heptachlor epoxide etc. The concentrations of HCHs, DDTs and endosulfan residues in water were observed up to 2.3microg/L, 3.6 microg/L and 15.4 microg/L, respectively.

Fate of pesticides

The fate of pesticide in environment depends on the chemical and physical properties of the pesticides, its environmental interactions and abiotic and biotic characteristics of the receiving matrix. Pesticides are degraded or immobilized through processes like, hydrolysis, photolysis, soil adsorption, degradation through microorganisms and plant uptake.

The distribution of pesticides in the environmental matrices is dependent on physico-chemical characteristics of pesticide like solubility, partition coefficient, half-life and photolysis, etc.[10]. The immobilized pesticides can remain in the soil/sediment till they are degraded by the soil microbes or other reactions. Mostly, the more hydrophobic pesticides tend to get locked in soil/sediment.

Due to potential water contamination by these pesticides there is a need to develop techniques for destruction of these compounds in water. Advanced Oxidation Processes (AOPs) have been recently studied as a promising techniques for many applications[11].

AOPs are relatively cleaner in context of environmental applications. They use various combinations of oxidants, UV irradiation and some catalysts for hydroxyl radical (OH$^\bullet$) generation in solutions. This radical is non-selective and strong chemical oxidant that can react rapidly with most organic compounds. AOPs have also been successfully used to remove, upcoming pollutants like pharmaceuticals and other endocrine disrupting chemicals[12].

The organic pollutants are oxidized by free radicals and can be ultimately mineralized to water, carbon dioxide and mineral salts. Ozonation alone or oxidation of organic compounds through H_2O_2 may or may not completely oxidize organics to CO_2 and H_2O in many cases. Supplementing the reaction with UV radiation would aid in the reaction completion[11].

Process efficacy is dependent on the rate of hydroxyl radical generation and their contact with the contaminant molecules. Earlier studies have been performed on the removal of Lindane

from soil and water using certain AOPs[13-16]. Lindane is reported to be difficult to degrade by ozonation and requires addition of oxidant like H_2O_2 for efficient degradation[16].

A few studies have reported photolytic degradation of endosulphan using UV irradiation[17] and biodegradation of endosulphan[18-19].

A study[11] on comparative operating costs of some of the AOPs reported a high oxidant cost in the ozonation/UV and ozonation /H_2O_2 process. In the present study we have not used ozonation but attempted to degrade the studied pesticides using UV irradiation, H_2O_2, fenton's reagent and a combination of both, that is, UV/H_2O_2 and UV/Fenton. These five AOPs are optimized to achieve maximum degradation of lindane and endosulphan isomers.

Lindane and Endosulphan are persistent pesticides and are listed amongst POPs (Persistent Organic Pollutant) in Annexure A under the Stockholm Convention[4]. Lindane (1,2,3,4,5,6-hexachlorocyclohexane) is an organochlorine pesticide with a broad-spectrum of activities and was commonly used for a wide range of soil-dwelling and plant-eating insects. It was previously used on numerous crops, as a seed treatment. Another common use of Lindane is treatment of scabies and lice in humans[4]. Throughout the world, it had been used for agricultural applications as a mixture of technical grade HCH or in pure form, since 1940s. The effective component of technical grade HCH is lindane[20].

Lindane has the potential for long-range environmental transport, tendency of bioaccumulation and carcinogenic characteristics[4] . Hydrolysis of lindane happens in alkaline pH and it reduces to its half concentration in nearly 50 hours at pH 9, it is reported to be completely stable at pH 5 [21]. Due to widespread use during earlier times and resistance to degradation, lindane and other HCH isomers occurred frequently in soils and groundwater all over the world causing environmental issues[22]. Due to its toxicity and non-biodegradability in the environment, most of the countries have restricted its use [20].

Endosulphan is chlorinated- cyclodiene insecticide with broad spectrum activities. Technical grade Endosulphan consists of two stereoisomers, α and β endosulphan in an approximate ratio of 7:3[18]. In the environment, it hydrolyzes to a less toxic species, endosulphan diol, due to O-S double-bond breakage .It can also be oxidized to a more persistent compound that is endosulphan sulphate which requires degradation; Photolysis produces endosulphan diol[17]. Endosulphan is toxic to aquatic organisms [23-24]. The lethal concentration 50 of endosulphan is relatively higher than DDT [25].

Due to the persistence of these two organochlorines and their extensive use in the previous times, they were selected as model compounds for studying the degradation of pesticides through AOPs.

Materials and Methods

Chemicals

All the solvents (Merck) used for standard preparation and sample extractions were of HPLC grade. FeSO$_4$ (Loba) was used as received. Neat Standards of Lindane, Alpha and Beta Endosulphan were procured from Sigma Aldrich. A working solution of 5 ppm was prepared from the stock. The stock and working solutions were prepared in n-hexane.

The composition of Fenton's reagent used was 1mM FeSO$_4$ + 10mM H$_2$O$_2$ for most of the experiments unless otherwise mentioned.

Photochemical Experiments

The laboratory scale photodegradation experiments were performed in an immersion well quartz reactor of 650 mL capacity. The photochemical reactor was cylindrical in shape with a water recirculation arrangement to maintain the temperature close to 25^{0}C. It was irradiated using a 400 W medium pressure mercury lamp (SAIC, India), which emits radiation at various wavelengths ranging from 200nm-400 nm.

Batch experiments were performed using individual pesticide solutions (lindane and endosulphan isomers) of 5 ppm (200 mL) prepared in ultrapure water (Millipore). The reaction solution was continuously stirred with a magnetic bar during reaction.

For light reactions, the time of turning on UV lamp was turned time zero for light experiments and addition of hydrogen peroxide was the beginning time for dark.

Analytical Method

After completion of irradiation time, the sample was removed from the photoreactor and methanol was immediately added to it to stop further reaction[16]. The sample was extracted thrice using dichloromethane (10 ml each) by vigorous manual shaking for 5 min and then removing the organic layer after separation. The collected organic phase was combined and dried with a small amount of anhydrous Na$_2$SO$_4$. The extract was concentrated before injecting into the gas chromatograph. Final sample concentrate was made up in n-hexane.

Concentration was quantified using gas chromatograph with ^{63}Ni electron capture detector (Perkin Elmer, Clarus 500). Fused-silica capillary DB-5 column (30m x 0.25mm x 0.25 μm film thickness) was used for analysis. Nitrogen was used as a carrier gas.

The recovery of γ-HCH was 81-95%, α and β-Endosulphan was 80-85% obtained in the working range for three replicates. The detection limits for these compounds were 0.1±0.02 μg/l.

Results and Discussion

The purpose of this study was to obtain maximum degradation of critical POP lindane and other persistent pollutants, α and β Endosulphan. The degradation rates of three pesticides were different for all the studied AOPs.

Lindane showed a slower degradation under UV irradiation as compared to endosulphan isomers. The degradation rate of lindane was enhanced in presence of H_2O_2. Lindane also gave faster degradation using fenton's and fenton's /UV process. However, fenton's reagent did not play a significant role in the degradation of α and β Endosulphan. Also, in presence of H_2O_2, α and β Endosulphan did not show a significant degradation as compared to lindane. The individual degradation processes are detailed in the following sub-sections.

Degradation using UV Irradiation

A number of organic contaminants absorb UV radiation in the range of 200–300 nm and get decomposed either due to direct photolysis or indirectly through radical generation. On irradiation of solutions containing lindane and endosulphan isomers, photolytic degradation of both the compounds occurred.

Fig. 1 shows the trends of photolytic degradation of lindane and endosulphan isomers. It can be observed that the degradation of lindane in presence of UV alone was slow as compared to endosulphan. Complete degradation was observed in 300 min of irradiation with an observed rate constant of 2.2 x 10^{-4} s^{-1} (r^2 = 0.83) as shown in Table 1. The initial degradation rate of lindane was slow upto 90 minutes and then the reaction proceeded at a faster rate, indicating that isomerization of lindane occurred in 90 minutes and finally a complete degradation of breakdown products occurred in 300 minutes of irradiation. No significant peak was observed in the chromatogram by the end of reaction.

Alpha endosulphan degraded faster than beta isomer. In 240 min, 96% of α and 89% of β Endosulphan was degraded. A photolysis study [26] of α-endosulphan and β-endosulphan was

performed in aqueous solution and in hexane reported that α-endosulphan and β-endosulphan were more stable under UV light in aqueous solution than in hexane. Also, the degradations of both the isomers in both matrices were of first-order kinetics. The observed rate constant in the present study was   2.3 x 10^{-4} s^{-1} for α and 1.5 x 10^{-4} s^{-1} for β endosulphan (r^2 =0.99). An earlier study[19] reported that 38% of alpha and 25% of beta degraded by UV irradiation in 30 min.   Similar values were obtained in this study for the two pesticides in 30 minutes irradiation. It is also reported [17] that the major product of UV irradiation of endosulphan is endosulphan diol which is a less toxic species. Also, endosulfan is fairly resistant to phototransformation particularly in air but its degradation products endosulfan sulfate and endosulfan-diol are susceptible to photolysis[27]. This will lead to a complete degradation of the endosulphan molecule with a possible pathway of formation of endosulphan sulphate or endosulphan diol and then complete dissociation of these breakdown products. These trends were also confirmed by the chromatograms obtained in the study, which showed no significant peak of endosulphan sulphate, by the end of reaction.

Degradation using UV/H$_2$O$_2$

To improve the reaction rate, H$_2$O$_2$ was added as an oxidizing agent to the aqueous solution of lindane. Initially, dark experiments (without UV irradiation) were performed in presence of H$_2$O$_2$.

The direct photolysis of hydrogen peroxide leads to the formation of 2 OH$^•$ radicals [28]:

$$H_2O_2 \xrightarrow{hv} 2OH^•$$
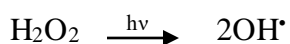
In the absence of UV irradiation, 36.7% degradation of lindane was observed in 30 min for a 2mM of H$_2$O$_2$ concentration. On increasing the concentration of H$_2$O$_2$ to 10mM, a three-fold increase (90%) was observed in same time period indicating an increase in the number of hydroxyl radicals generated.

On irradiating the solution of 5 ppm of lindane with 2mM of H$_2$O$_2$, the reaction became even faster. Rate constant of 5.3 x 10^{-4} s^{-1}.was observed with 97% degradation in 90 min (Fig. 2). The suggested mechanism for photolysis in presence of H$_2$O$_2$ follows breakdown pathway of the molecule with two OH$^•$ radicals generated with each quantum of radiation absorbed [29].

On addition of H$_2$O$_2$, no significant dark degradation was observed for endosulphan isomers. Fig.2 shows the degradation trends for UV-H$_2$O$_2$ (2mM) reactions. 49.2% of alpha and 46% of beta endosulphan was degraded in 90 min of UV irradiation in presence of H$_2$O$_2$ with a

rate constant of 1.1×10^{-4} s^{-1} and 0.97×10^{-4} s^{-1} respectively. It has been reported [30] that endosulphan isomers and endosulphan sulphate show no appreciable reaction with $OH^\bullet$ radicals produced by H_2O_2 photolysis in air matrix. The endosulphan degradation seems to be proceeding more through direct photolysis rather than being mediated by hydroxyl radicals. It is also reported that UV based photolysis and hydrogen peroxide synergistic reaction will be useful only for the contaminants, which need comparatively higher oxidation conditions due to higher activation energies [31]. Endosulphan isomers are reported to have low activation energies. (Around 44 to 59 KJ/mol) [25].

Reverse is observed for lindane. Presence of H_2O_2 drastically improved degradation of lindane. During UV/H_2O_2 treatment, during which $OH^\bullet$ radical is generated rapidly, the $OH^\bullet$ radical attack of lindane is majorly observed than direct photolysis or reaction with H_2O_2 as the initial reaction step.

Degradation in Fenton's and Photo-fenton's process

To improve the process further, fenton's oxidation using a mixture of ferrous ion and H_2O_2 was used. Free radicals could be generated from a catalytic reaction of Fe salt with H_2O_2 either in absence or presence of UV light. The use of Fe(II)/H_2O_2 as an oxidizing agent for water treatment is useful due to abundance and non-toxicity of iron and easy handling of environmentally benign hydrogen peroxide [11].

Degradation of lindane using fenton's reagent (1mM $FeSO_4$ + 10mM H_2O_2) is given in Fig. 3. Complete degradation of lindane was obtained in 120 min in dark. The basic reaction for the fenton's process can be described as follows [32]:

$$Fe^{2+} + H_2O_2 \longrightarrow Fe^{3+} + OH^- + OH^\bullet$$

In the photofenton process greater numbers of hydroxyl radicals are generated in comparison to the conventional Fenton method or photolysis, thus promoting faster rates of degradation of organic pollutants.

The basic reactions for the Photofenton process at pH 3 lead to the formation of Fe $(OH)^{2+}$ complex because of the acidic environment [11]:

$$Fe^{3+} + H_2O \longrightarrow Fe(OH)^{2+} + H^+$$
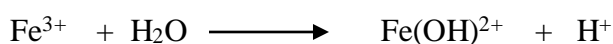
Further UV exposure leads to the complex being decomposed as follows:

$$Fe(OH)^{2+} \xrightarrow{h\nu} Fe^{2+} + OH^\bullet$$
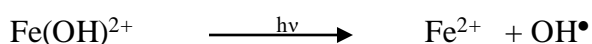
On UV irradiation in presence of Fenton's reagent, 92% degradation was obtained in 60 min of irradiation with an observed rate constant of 6.3 x 10^{-4} s^{-1}. pH of reaction is an important factor affecting photo–Fenton degradation. Oxidation is much favorable at strongly acidic pH. The effect of like Bicarbonate and carbonate ions have a negligible activity as radical scavengers under the acidic conditions [31], in the present study the operating pH was 2.5 for fenton's reactions.

On changing the concentration of $FeSO_4$ in fenton's reagent, no noticeable change was observed in the degradation rate. However, on changing the concentration of H_2O_2, faster degradation rates were achieved as depicted in Fig.4. Ninety-six percent degradation was observed in 30 min of time in double and triple H_2O_2 concentration in fenton's reagent. The first order rate constant was increased to 7.8 x 10^{-4} s^{-1} for 20 mM of H_2O_2. For 30mM of H_2O_2, similar rate constant value was observed indicating saturation.

The effect of iron content in the fenton's reagent did not play a major role, indicating that the used millimolar concentration of iron was sufficient for catalyzing the reaction.

Alpha and beta endosulphan did not show significant degradation in presence of fenton's reagent.

Conclusions

The major conclusions from the above study are:

More than 95% of Degradation of lindane was observed for all the AOPs used (UV,H_2O_2, UV/H_2O_2, fenton's reaction, UV/fenton). The degradation rate was significantly enhanced in presence of H_2O_2. The photo- fenton's process produced the highest reaction rate 6.3 x 10^{-4} s^{-1} of all the five AOPs studied.

Significant degradation of α and β-endosulphan (96% and 89% respectively) was observed on UV irradiation in absence of any additive. No significant dark degradation was observed for endosulphan isomers on addition of H_2O_2, which increased to 49.2% of alpha and 46% on UV irradiation. No significant degradation was observed in presence of fenton's reagent.
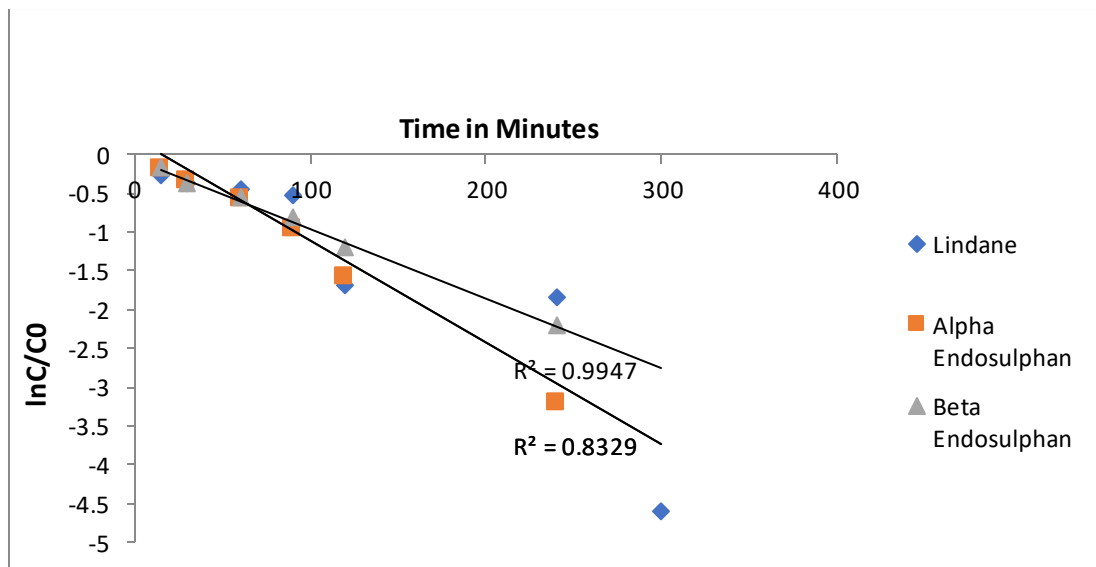
Of all the AOPs studied, UV/H_2O_2 can be suggested as an efficient technique for degradation of lindane as it does not generate any byproduct (viz. iron sludge in fenton's reactions) and the cost of oxidant (H_2O_2) is also low. For endosulphan isomers UV irradiation is the suggested as an efficient AOP.

Acknowledgement
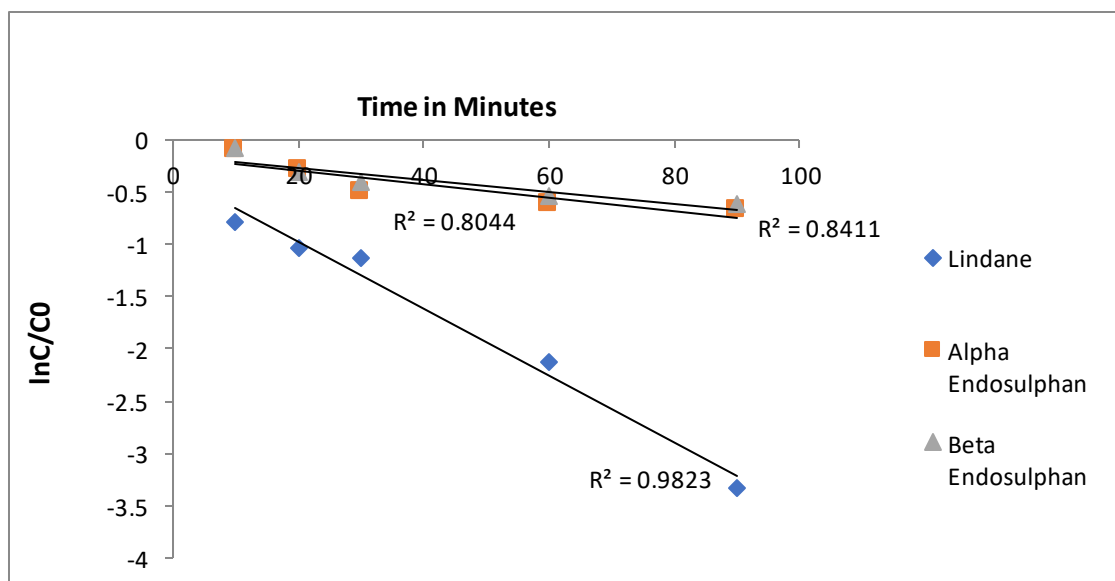
Figures:

Fig. 1: First Order Kinetics for Pesticide Photodegradation with UV

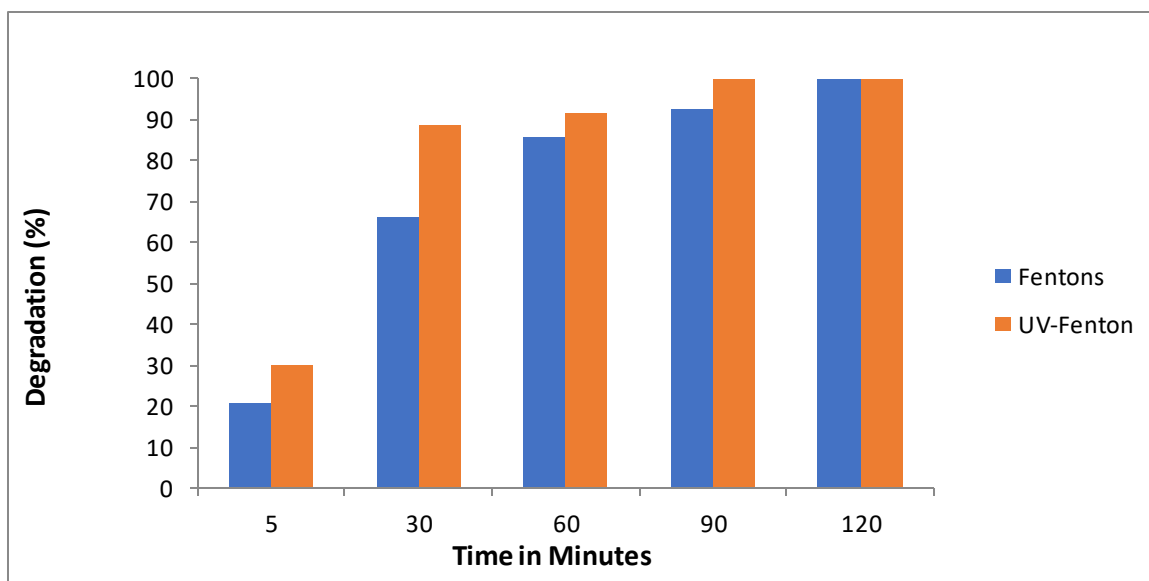**Fig. 2:** First Order Kinetics for Pesticide Photodegradation with UV-H2O2

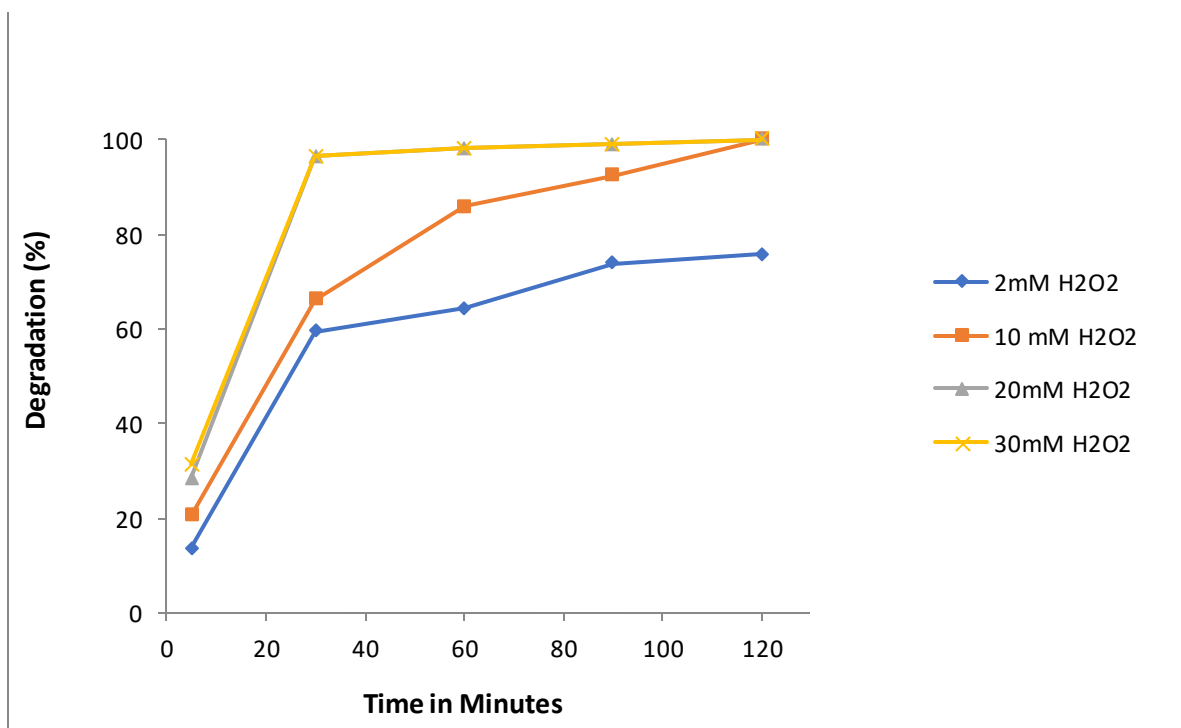**Fig. 3:** Degradation of Lindane using Fentons and UV-Fentons Process

Fig. 4: Effect of H2O2 concentration on photodegradation of Lindane

Table:

Table 1: First order rate constants (s^{-1}) for pesticide degradation using various Advanced Oxidation Processes

Pesticide	UV	UV/H_2O_2	Fenton's	UV/Fenton
Lindane	2.2×10^{-4}	5.3×10^{-4}	4.6×10^{-4}	6.3×10^{-4}
α -endosulphan	2.3×10^{-4}	1.1×10^{-4}	-	-
β- endosulphan	1.5×10^{-4}	0.97×10^{-4}	-	-

References

1. R. Jayaraj, P. Megha, and P. Sreedev, Interdiscip. Toxicol., 9(3-4), 90, 2016.

2. A.K. Chopra, M.K. Sharma and S. Chamoli, Environ. Monitoring and Assessment, 173 (1-4), 905, 2010.

3. S.U. Park, J.G. Kim, M.J Jeong and B.J. Song, Arch. Environ. Contam. Toxicol., 60(4), 576, 2011.

4. UNEP: Retrieved July 15, 2020 from

   http://www.pops.int/TheConvention/ThePOPs/TheNewPOPs/tabid/2511/Default.aspx

5. P.C. Abhilash and N. Singh, J Hazard Mater., 165(1-3), 1, 2009.

6. V. Dhananjayan, Environ. Sci.and Pollut. Res., 20(5), 3149, 2013.

7. V. Dhananjayan, S. Muralidharan, and P. Jayanthi, Environ. Monitoring and assessment, 173(1-4), 803, 2011.

8. A. Begum, S. HariKrishna, and I. Khan, International J. of Chem. Tech Research, 1(2), 237, 2009.

9. N. N. Patil, K. K. Selvaraj, V.K. Krishnamoorthy, A. Elaiyaraja, and B.R. Ramaswamy, Organochlorine Pesticide Contamination in the Kaveri (Cauvery) River, India: A Review on Distribution Profile, Status, and Trends. Water Challenges and Solutions on a Global Scale, Chapter 7, Vol. 1206, 115, 2015.

10. V. Jan, and T. Březinová, Environment International, 75, 11, 2015.

11. R. Munter, Proc. Estonian Acad. Sci. Chem., 50(2), 59, 2001.

12. S. Esplugas, D.M. Bila, L.G.T. Krause, M. Dezotti, J. of hazard. Materials, 149(3), 631, 2007.

13. H. Fu, X. Quan, Z. Liu and S. Chen, Langmuir, 20, 4867, 2004.

14. H. Fu, X. Quan, H. Zhao, J. Photochem. and Photobio. A: Chem., 173, 143, 2005.

15. A. Zaleska, J. Hupkaa, M. Wiergowski, and M. Biziuk , J. Photochem. and Photobio. A: Chem., 135, 21, 2000.

16. A.M. Nienow, J.C. Bezares-Cruz, I.C. Poyer, I. Hua, and C.T. Jafvert, Chemosphere, 72, 1700,2008.

17. M.H. Barcel ´o-Quintal, M.C. Cebada-Ricalde, A.R. Trejo-Irigoyen, R.B. Rend´on-Osorio and J.A. Manzanilla-Cano, J. Environ. Sci. Health Part B, 43, 120, 2008.

18. N. Awasthi, A. K. Singh, R. K. Jain, B. S. Khangarot, and A. Kumar, Deg Appl. Microbiol Biotechnol., 62, 279, 2003.

19. J. H. Kim, J. of Korean Ind. & Eng. Chem., 10(1), 30, 1999.

20. Y.F. Li, Sci. Total Environ., 232, 121, 1999.

21. A., Hiskia, A. Mylonas, D. Tsipi and E. Papaconstantinou, Pestic. Sci., 50, 171, 1997.

22. S. Dutchak, V. Shatalov, M. Mantseva, O. Rozovskaya, N. Vulykh, M. Fedyunin, M. Aas, K. Breivik and D. Mano, Status report 3. Cooperative Programme for Monitoring and Evaluation of the Long-Range Transmission of Air Pollutants in Europe, 2004. Retrieved July 15, 2020 from http://www.msceast.org/reps/3_2005.pdf.

23. W.W. Walker, Development of a fate/toxicology-screening test. EPA Report No. EPA-600/4-84-074; (1984). U.S. Environmental Protection Agency, Environmental Research Laboratory, Gulf Breeze, FL.

24. K.H. Khan, International Journal of Biosciences, 2(1), 9, 2012.

25. S. Hengpraprom and C. Lee, from http://www.ces.clemson.edu/ecl/caseStudy/case2.pdf , 2020.

26. N. C.Singh, T.P. Dasgupta, E.V. Roberts and A. Mansingh, J. Agric. Food. Chem., 39, 575, 1991.

27. ATSDR: Toxicological Profile For Endosulfan, U.S. Department Of Health And Human Services Public Health Service Agency for Toxic Substances and Disease Registry. Retrieved from https://www.atsdr.cdc.gov/ToxProfiles/tp41.pdf, July 15, 2020.

28. E. Simonenko, A. Gomonov, N. Rolle and L. Molodkina, , Procedia Engineering, 117, 337,2015.

29. P. Stepnowski and A. Zaleska, J. Photochem. and Photobio. A: Chem., 170, 45, 2005.

30. Endosulphan Monograph, Volume 3 Chapter 8, Environmental Fate and Behavior, (1999). Retrieved July 15, 2020 from http://chm.pops.int/Portals/0/Repository/Endosulfan2008/UNEP-POPS-POPRC-END-08-EU-V3-8.English.PDF.

31. P. R. Gogate and A. B. Pandit, Advances in Environmental Research, 8, 553, 2004.

32. G. Lyngsie, L. Krumina, A. Tunlid, and P. Persson, Scientific Reports 8:10834, 2018.

Is ultraviolet Radiation a Confounding Variable for COVID-19 in India?

Suvarna Tikle[1]* and Gufran Beig[2]

[1]*Indian Institute of Tropical Meteorology, Pune-411008, Ministry of Earth Sciences, India

[2]National Institute of Advanced Studies (NIAS), Indian Institute of Science (IISc) Campus, Bangalore-560012, India

Email: sstikle@gmail.com

Abstract

The current global Coronavirus disease (COVID-19) became a pandemic due to its contagion nature and rapid spread throughout the world. The pandemic caused a lockdown resulting in a large decline in the level of anthropogenic emissions of tiny aerosol particles that altered the solar irradiance and decreased the quantity of aerosol, which opposes global warming. This study first demonstrates that surface ultraviolet radiation (UV) increased significantly during the lockdown period in four major Indian mega cities, whose magnitude varies based on city demography. Results shows that the correlation between the high rate of increase in Ultraviolet irradiance (UV-irradiance) on mortality and morbidity. Although there are numerous confounding factors for the pandemic, UV-irradiance could be one of the factors supporting the hypothesis that increased solar UV dose may increase rate of disinfection as radiation warps the structure of genetic material of the virus and deactivates it. Another factor which also have potential to add up increase of Vitamin D3 production per minute of exposure due to UV-irradiance resulting in an increased human immune system to fight COVID-19 more effectively. However, it is cautioned here that a high dose of direct UV exposure to humans may be fatal leading to skin damage and melanoma cancer. Hence, the harmful impact of UV-Irradiance on the human body and its application to possible disinfectant to virus deactivation should be understood in a proper perspective.

Introduction

The COVID-19 pandemic is perhaps the greatest challenge the world is facing since World War-II. It has infected millions of people and taken many lives. It is caused by SARS-CoV-2

virus and has an extremely high transmission rate by droplet spray from coughing and sneezing and by a direct human to human contact[1]. The SARS-CoV-2 is not unique; but a new variant in the beta coronavirus family[2,3]. To fight the pandemic, many countries around the world implemented a lockdown. Although, India officially declared the first phase of countrywide lockdown from 24th March 2020 for about 3 weeks, the curfew-like situation started even a week before (18th March 2020) as the death count started to mount. The country-wide closure decreased almost all anthropogenic activities such as industrial emission and severely reduced car, bus, truck, and airplane traffic. The Satellite imagery of the Earth Observatory of NASA, reported that the aerosol levels have dropped significantly since the COVID-19 lockdown began in India[4]. It is known that anthropogenic aerosols negatively impact the environment and can cause everything from warming to cooling, to deadly air pollution. Recent studies report that the climate effects of aerosols have masked and countered some of the warming induced by greenhouse gases. The term called "solar dimming" happens when these aerosols absorb solar energy or reflect it into space. The result is a reduction in the amount of global direct irradiance at the Earth's surface[5]. These cooling temperature effects may appear beneficial but are almost certainly overwhelmed by aerosol's negative health impacts. UV radiation plays multiple roles. Excessive direct UV exposure is harmful for human beings, has the potential for damage to the skin and eye with an increase in UV radiation. It also suppresses the immune system[6]. According to the World Health Organization (WHO), annually around 1.5 million DALYs (Disability-adjusted life years) are lost through excessive UV exposure globally. Furthermore, environmental levels of UV radiation may suppress cell-mediated immunity and can enhance the risk of infectious diseases. However, on the other hand, UV radiation is needed for vitamin D production which plays an essential role in human immune system[7] and is particularly useful at destroying pathogen genetic material prevents viral particles from making multiple copies of themselves[8]. A recent study also stated that deficiency of vitamin D may increase the risk of severe COVID-19 due to reduced natural vitamin D synthesis[7]. Ultraviolet light has been demonstrated to be capable of destroying viruses, bacteria, and fungi in many studies[8].

UV radiation wavelengths ranges from 200 to 440 nm[9]. UV-A and UV-B ranges from 400 to 315 315 to 280 nm. According to the erythemal action the UVB radiation causes more sunburn than UVA radiation, Mie scattering is not strongly wavelength dependent however Rayleigh scattering is more effective at short wavelengths[10]. UVA spectrum portion does not damage SARS-CoV-1 was demonstrated by previous study[11]. It has been observed that

SARS-CoV-2 can be rapidly inactivated by exposure to UVC light (254-nm) from a low-pressure mercury vapor (germicidal) lamp[11,12] however inactivation amount depends on the dose for inactivation by sunlight. According to[13] UVC range can inactivate many viruses and bacteria in times less than minute depending upon the dose. Ultraviolet light can be an effective measure for decontaminating surfaces that may be contaminated by the SARS-CoV-2 virus[3]. The usage of concentrated forms of UV-C radiation was on the front line in the fight against Covid-19 in China. In China blue light had been used for disinfection of buses, UV-emitting robots for cleaning floors in hospitals, UV-radiations to disinfect money in banks[14]. Meteorological parameters are important factors influencing infectious diseases such as severe acute respiratory syndrome (SARS) and influenza outbreaks[15]. Past studies demonstrated that absolute humidity had significant correlations with influenza viral survival and transmission rates[14,16]. Recently, it has been reported that COVID-19 counts decreased with the increase in temperature[17], but their effects on mortality have been sparsely reported. Influenza viruses have shown that their survival period on certain surfaces may reduce when exposed to high temperatures or high UV radiation. Although earlier studies have shown that UV radiation can be used against other corona viruses, such as SARS[18], no results have been reported in so far providing evidence relating Covid-19 related mortality with UV radiation.

The objective of the present study is to investigate the impact of reduction in emissions during the COVID-19 lockdown of 2020 in the UV-irradiance. For the purpose we compute the variability between year 2020 and that of averaged value of year 2017-2019. We also hereby report the relationship of COVID-19 related mortality /morbidity with that of relative increase in UV irradiation during year 2020 with that of past years based on experimental data. The observational data used in the present study is taken from four major cities of India namely, Delhi, Mumbai, Ahmedabad and Pune (Fig. 1).

Methodology

This work uses data obtained under the project- "System of Air Quality and Weather Forecasting and Research (SAFAR)" of the Ministry of Earth Sciences, Government of India that is also adopted as a pilot project of the World Meteorological Organization (WMO)[19]. The SAFAR data is used for 4 Indian cities, namely, Delhi, Mumbai, Ahmedabad and Pune. The measurements of UV-radiation have been taken continuously by UVS-E-T radiometer deployed under the project (Fig.1). The UVS-E-Tare is designed for precise measurements of atmospheric ultraviolet radiation in three different spectral ranges. It measures global UV-irradiance, i.e. the sum of direct solar radiation and the radiation that has been scattered by

particles or molecules in the air. The angular response follows the cosine of the zenith angle as with an ideal Lambertian surface. The UV index has been calculated quantitatively by multiplying the UVE radiation value by 40 m²/W[20]. The calculated value is presented in an integer. For example, 0.25 W/m² of UVE represents a UV Index of 10. This is the value used for public health information. The calibration of instrument has been done as per recommendation of WMO at the time of installation of instrument. For instruments designed to measure erythemally weighted UV, the radiation amplification factor (RAF) should match the RAF for erythema (e.g. RAF= 1.21 at 30 SZA and 300 DU)'[21]. According to the spectral mismatch details, a unique software program for post-processing and analysis of UV data 'the UVIATOR program' had been developed by Kipp & Zonen. It performs automatically a number of UV measurement corrections and thereby improves the measurement quality significantly. To achieve the most accurate measurement result with broadband UV radiometers the spectral mismatch error correction is based on the calibration and correction method described in the WMO Report 141 and 164[21,22]. First the raw signal of the instrument (in units of Volts) has to be transformed into an irradiance (in units of W/m2) then irradiances have correct for the spectral mismatch error with 'conversion factors', determined using modeled UV irradiances as a function of various total Ozone column densities and solar zenith angles[20]. The measurement conditions for which correction factors are calculated are obtained by varying the solar zenith angle, _0, and the total Ozone column density. The solar zenith angles, _0, are varied between 0° and 85°. Applying these corrections improves the accuracy by a factor of 2 or more. Yearly calibration of UVS-E-T Radiometer is performed with a Xe lamp system, a monochromator (ORIEL Cornerstone MS257), and a calibrated Si-photodiode detector. The measurement with Si-photodiode is used to determine the UVS radiometer-weighted irradiance and finally radiometric calibration factor is obtained according to $r=U_{UVS}/E_{UVS}$ and to account spectral mismatch error the min sensitivity (%) also determined.

We have used the peak value of the day in this work as we feel that the highest signal would be a better marker to understand the day to day variability for comparison purpose and correlative study. It is stated here that we have performed the analysis based on 4 city data and derived the correlation because we were constrained with the data available only for 4 cities. The standard deviation also obtained during the study period for cities.

We hereby introduce another terminology which is known as Ultraviolet Index (UVI) in this paper. The WHO recommended the use of UVI in order to evaluate and increase the awareness of the risks connected to exposure of UV-irradiance. The UVI is a simple and informative indicator to alert the general public about health risk exposure. The UVI can be adopted for the evaluation of the UV dose, even as prediction tools [23] to reduce the threat of skin cancer like diseases[24]. UVI is a unit less measure of the level of solar UV irradiance at the earth's surface. The UVI values are grouped into exposure categories as shown in Fig. 1. The values of the index range from zero upward - the higher the UVI, the greater the potential for damage to the skin and eye. However, it may be noted here that UVI may not be a good indicator for the risk of UV-induced ocular disease[25] as ocular exposure was approximately 1/10 that to the crown and effects of exposure also varies with different meteorological condition[26]. It may shows the maximum impact on eye only when the sun is directly at the front at approximately 40° of solar altitude.

It has been also correlated with peaks of influenza virus activity during year 2010-2018 in northern Europe[27] and with transmission of COVID-19 during year 2020 in Chinese cities[28]. The clear-sky UVI is the erytherrmally weighted UV irradiance (1 unit equals 25 mWm−2) reaching the Earth's surface modified by the McKinlay and Diffey (1987) action spectrum for the susceptibility of Caucasian skin to sunburn (erythemal) and it is valid for cloud-free conditions[30]. UVI data has been measured for the period from 20th February to 10th April 2020 to cover the period before and after the lockdown. The data for the identical period of previous three years (2017-19) have been averaged for the comparison. We have used the peak UVI value of the day in this work as we feel that the highest signal would be a better marker to understand the variability for comparison purpose.

Result and Discussion

The peak index in tropical Indian cities is observed during the day between 12 noon to 4PM. Our analysis covers 2 regimes- (a) Normal (Before lockdown): Business as usual scenario during February 20th to 18th March; (b) Lockdown period (between 19 March to 10th April). Fig. 2 (a-d) shows the comparison of peak value of UVI in all 4 cities for the above 2 regimes of 2020 and that of averaged values of past 3 years (2017-2019) for the identical period. A vertical line separating the normal and lockdown period is shown in Fig. 2 on 19th March. Due to the much reduced emission activities and movement of people, levels of air pollutants declined significantly [31] in India leading to sudden cleansing of the atmosphere, which not

only affected the ground pollution but also the major part of the troposphere. A comparison of 2020 with past years (Fig. 2) shows that the UVI was comparable before the lockdown but immediately after the imposition of lockdown, a significant upward jump is observed and the magnitude of UVI during 2020 continued to remain elevated as compared to previous years. The total irradiations are likely to increase due to less scattering /reflection in presence of less thick layers of aerosols in the troposphere under lockdown that otherwise remain thick[4]. The presence of aerosols during normal days acts as a solar radiation reflector by scattering mechanism[14,32]. The reduction in aerosols during lockdown must have resulted in increasing ultraviolet radiation as shown in Fig.2.

Fig. 2a shows the daily distribution of the peak value of UVI over Pune city. It was observed that UV index steadily increases after the lockdown from 5-6 to 7.5 during the lockdown which falls under the "High Risk" category. The UVI was in the range of 3.9 to 6.1 before lockdown. The city was exposed to a high risk level of exposure for 18 days (nearly 37% in 2020 during the lockdown period of 20 days as compared to last three years average UVI during the same period. The steady increasing trend was observed in Ahmedabad (Fig. 2b) where UVI increased from 6 to 8from normal to beginning of lockdown period. Although a slight declining trend in UVI is noticed in the later part of 2020 lockdown but magnitude of UVI in 2020 continued to remain higher than that of past years. It crossed from moderate risk category level to high-risk category immediately after lockdown. High-risk means continuous exposure to sun rays for more than an hour can cause sunburn to Indian skin type and eye irritation. In Mumbai, a sudden jump in UVI is observed immediately after the lockdown and this elevated level was maintained throughout the lockdown period. However, level of UVI in 2020 was found to be consistently higher than that of previous three years average as evident from Fig. 2c. Fig. 2c also shows that the city recorded the peak UVI level of 6.5 in 2020 as compared to an average level of 5.6 in the last three years. The overall magnitude of UVI in Mumbai is found to be lowest among all 4 cities. Mumbai is surrounded by sea from 3 sides and the reflectivity index is relatively high from the water surface as compared to land except for specular reflection. Fig. 2d shows the time series for the peak value of UVI for Delhi which shows a maximum jump in UVI after the lockdown. Further, it can be noted that UVI values prominently altered within the range of 6-7 during the lockdown period. The highest level of UVI was recorded during 6-7th April 2020 when the UVI touched ~7.3 which falls in the high-risk category. The UVI was in the moderate level (3-5) during normal period in Delhi. It is noticed that the magnitude of UVI in 2020 was significantly higher when compared with last three years. It is noteworthy to mention here that citizens of Ahmedabad

were exposed to the highest UVI values but in spite of elevated level as compared to past 3 years during lockdown, a slight declining trend is noticed, probably due to the fact that it has already touched a maximum level. The UVI has indicated a minimal increase for Mumbai in 2020 as compared to the previous three years average. There are various meteorological confounding factors which affects the morbidity and mortality of COVID-19[33]. According to[34], relative humidity and absolute humidity showed a moderate positive correlation with the daily COVID-19 cases in few cities of India. Despite many studies, there is inconsistencies in findings[35] due to impacts of regional factors like geographical locations and population[36].

Percentage variability in day to day UVI during the lockdown period for 2020 with respect to averaged UVI of past 3 years in all 4 SAFAR cities are shown in Fig. 3a. In Pune, it is found to vary from 2% to a maximum of 50%. The % increasing trend in UVI of Ahmadabad varied from a minimum of 6% to a maximum of 43% on 3rd April 2020. At the same time, UVI at Mumbai showed a fluctuating pattern and reached to its peak at 37%. The % increase in UVI for Delhi was 5% immediately after the lockdown which shot to ~ 42% towards the end of lockdown period. Average percentage variability in UVI during 2020 as compared to past 3 years are also provided in Table 1. The standard deviation (SD) from the mean for all the 4 cities is also shown in Table-1. The SD is found to be highest in Pune ($\pm$ 14) followed by Delhi ($\pm$ 13), Mumbai ($\pm$ 13) and Ahmadabad ($\pm$ 9).

Fig. 3b and 3c show the cumulative growth in percentage variability of UVI during lockdown period of 2020 as compared to past 3 years along with mortality and mortality in all the 4 cities. The cumulative value of UVI is obtained by averaging the peak values of UVI over the lockdown period of 19th March to 10th April for 2020.

The percentage increase in cumulative UVI is calculated by comparing it with the cumulative value of the same period of the previous three years. The cumulative increase in UVI in 2020 w.r.t past 3 years are found to be 27%, 22%, 20% and 18% for Pune, Ahmedabad, Delhi and Mumbai respectively. The correlation coefficient is also derived to understand the association between UVI and COVID-19 related deaths and infection counts among 4 cities during the lockdown period which is found to be anti-correlated. The correlation coefficient of UVI with mortality and morbidity is found to be -56% and -86% respectively. In general it is found that higher rate of increase in UVI is associated with the lower death counts. Similar results are also observed by[33]. The anticorrelation established the fact that in a city like Ahmedabad, the number of mortality counts is found to be lowest because % growth in UVI is highest (22%). In the case of Mumbai, the growth in UVI w.r.t a normal level is found to be lowest (18%)

but the rate of mortality is highest. In Pune, UVI increase was highest (27%) and COVID infection counts were found to be lowest 182 as compared to other cities. In Mumbai city, a sharp increase of 1241 infection cases is found which relates well with lowest growth rate of 18% in UVI. However, it may also be argued that a strong correlation may be a combined effect of above factor and that of additional production of Vitamin-D3 because UV-irradiance is capable of producing Vitamin D and other compounds in the human body[37,38]. This may enable the human immune system to fight COVID-19 more effectively by preventing the rapid development of the SARS-CoV-2[39]. This has limitation for protection against worsened COVID-19 outcomes as a supplementation of vitamin D is due to lack of genetic evidence[40].

Although the present study is reported for summer season when temperature remain high but such factor may play a significant role in higher latitudes, especially considering the relatively cold spring time when people are still indoors, where the ambient UV cannot disinfect the Corona virus. Hence, it is pertinent to mention here that future study may also focus on the possibility of mitigating COVID-19 deaths via sensible sunlight exposure or vitamin D intervention[41].

Conclusion

Covid-19 pandemic caused a lockdown forcing major emission activities to be seized leading to thinning the aerosol layer in the entire troposphere[42–44]   thereby, increasing the level of UV irradiation. The highest increase of UVI in 2020 with respect to past years is found in Pune, as it is located in the relatively higher altitude. Mumbai is surrounded by sea from 3 sides and radiations tend to get attenuated leading to least variability in UVI. This may also be due to combine impact of meteorological factors and high specific heat of water. Due to which sea surface absorb heat slowly and also loses heat slowly which influences the adjacent land temperature and ultimately affects the changes in daily UVI of coastal city. The critical finding of the present study is twofold- (1) to demonstrate that COVID-19 lockdown resulted in a rapid increase in UVI over Indian mega cities, whose magnitude depends on the geographical location and climatology of the city; (2) although there are numerous confounding factors for the pandemic, increase in UV-irradiation is found to have positive and favorable impact on COVID-19 cases. A strong anti-correlation with COVID-19 infection rate (-86%) tends to suggest that the rate of increase in UVI was found to be beneficial in spreading COVID-19.

A decrease mortality count due to Covid-19, may also be attributed to an additional production of Vitamin D and other compounds in the human body which leads to enhanced human immune system to fight Covid-19 more effectively. However, more evidence and research need to be done to fully understand the relationship. The difference between negative effect of UV-irradiance exposure and its positive impact towards disinfecting and reducing severity of Coronavirus needs to be properly understood and cautious approaches need to be adopted for achieving the maximum benefit. Any misconception needs to be explained and rectified concerning its useful application to disinfect regions of high risk without exposing the Human body which could be counterproductive.

The result from this analysis suggest that further studies are needed for confounding influence of UV radiation on COVID-19 mortality and morbidity by considering other weather parameters like rainfall, wind speed, and so forth. It shall provide additional information to mitigate the epidemic by carefully considering robust modeling.

Acknowledgments

Figures:
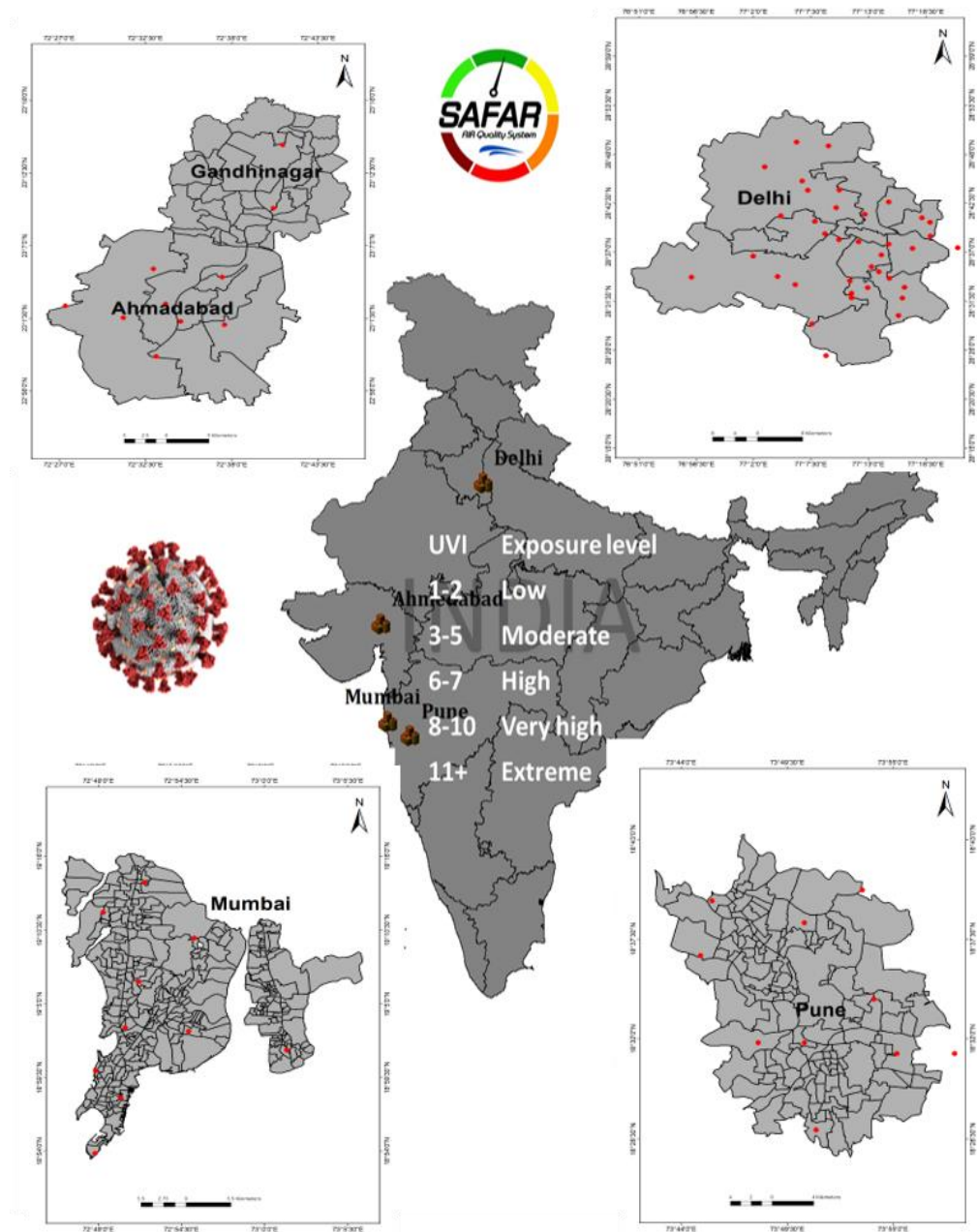
Fig. 1: The location of 4 Indian mega cities and the table indicating the UVI (Ultra-Violated Index) and associated health risk.
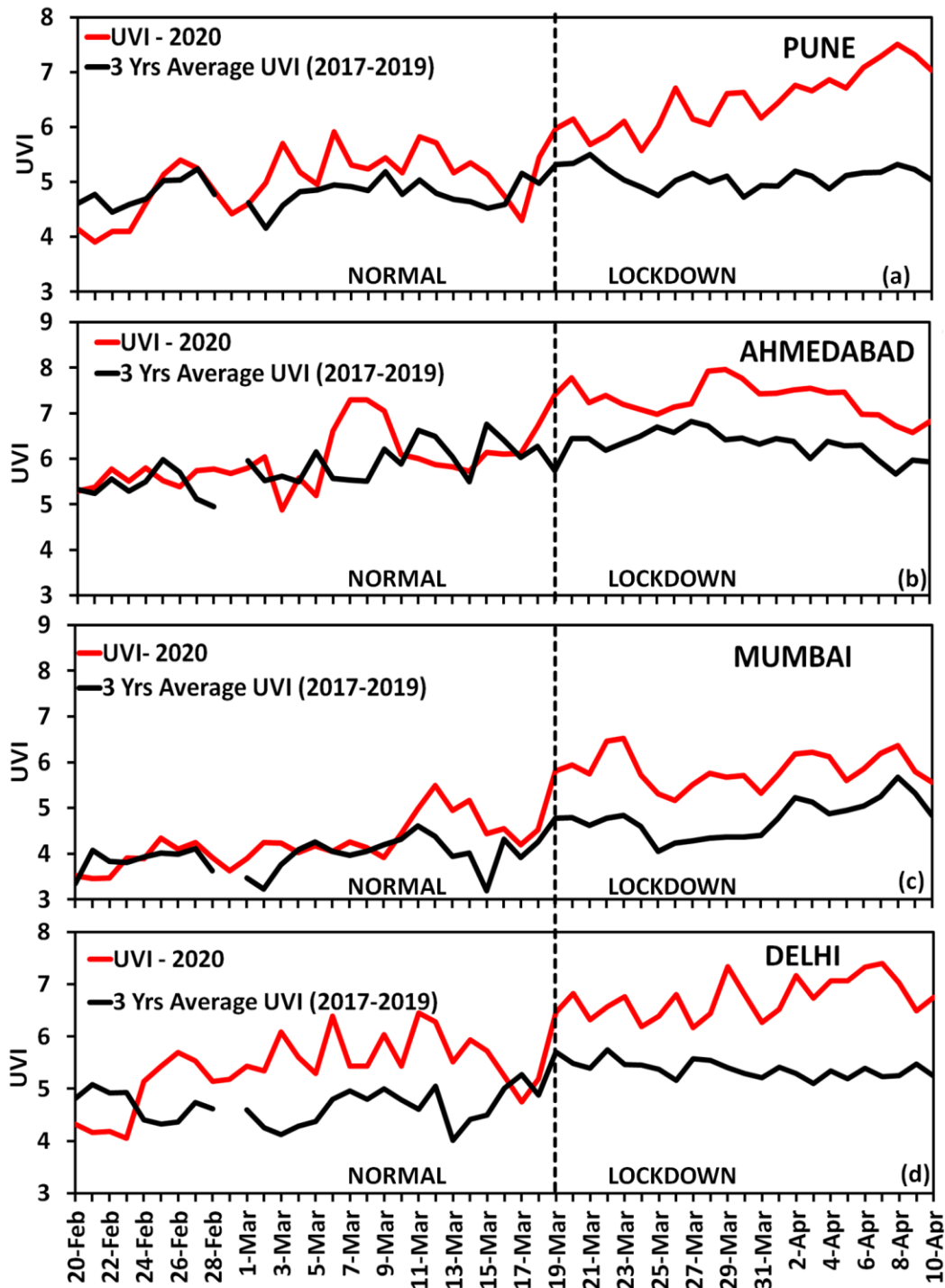
Fig. 2: A comparison of the peak value of UVI during the lockdown period of 20th February to 10th April 2020 with averaged values of past 3 years (2017-19) for the identical period in all four cities of Pune, Ahmedabad Mumbai and Delhi.
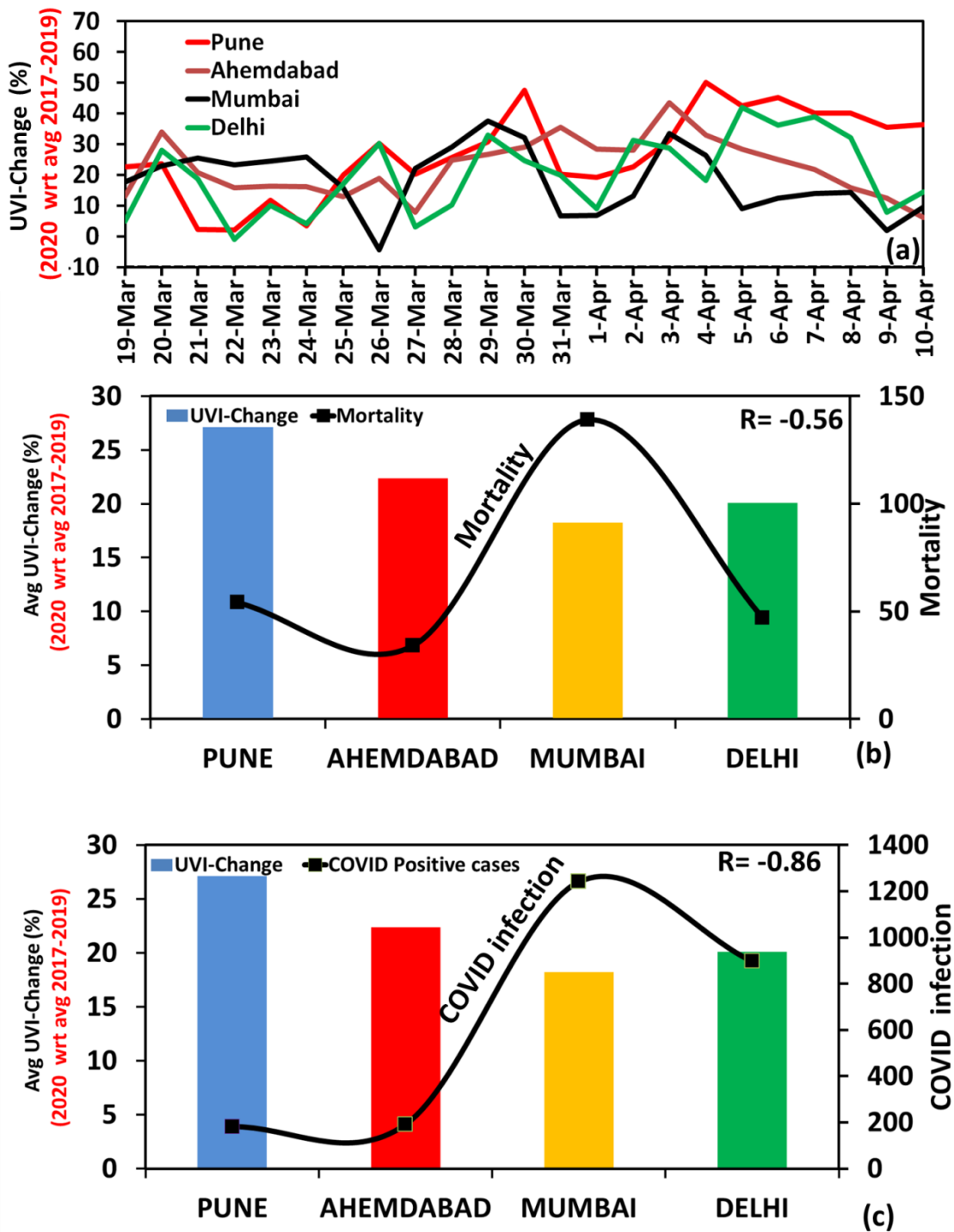
Fig. 3: (a) Percentage change in cumulative value of UVI averaged over the lockdown period (19th March to 10th April) of 2020 as compared to the averaged value of UVI of the past 3 years (2017-19) for the identical period in all 4 SAFAR cities. The correlation of % change in cumulative UVI in 2020 wrt average 2017-2019 with (b) mortality and (c) infection rate per lakh.

Tables:

Table 1: The percentage variability in peak daily value of UVI during lockdown period of 2020 as compared to averaged values of past 3 years (2017-19) for the identical period in all four cities as per Figure 3a.

Date	Pune (%)	Delhi (%)	Mumbai (%)	Ahmedabad (%)
19-03-2020	23	5	18	13
20-03-2020	24	28	23	34
21-03-2020	2	19	26	21
22-03-2020	2	-1	23	16
23-03-2020	12	10	25	16
24-03-2020	3	4	26	16
25-03-2020	20	17	16	13
26-03-2020	30	30	-4	19
27-03-2020	20	3	22	8
28-03-2020	26	10	29	25
29-03-2020	31	33	37	27
30-03-2020	48	25	32	29
31-03-2020	20	20	7	36
01-04-2020	19	9	7	28
02-04-2020	23	31	13	28
03-04-2020	31	29	34	43
04-04-2020	50	18	26	33
05-04-2020	42	42	9	28
06-04-2020	45	36	12	25
07-04-2020	40	39	14	22
08-04-2020	40	32	14	16
09-04-2020	36	8	2	12
10-04-2020	36	15	9	6
Standard Deviation	(± 14)	(± 13)	(± 11)	(± 9)

References

1. Y. Zhu, J. Xie, F. Huang, L. Cao, Sci. of Total Environ., 727, 138704, 2020.

2. D. Fisher, D. Heymann, BMC Med., 18–20, 2020.

3. W. J. Kowalski, T.J. Walsh, N. York, P. Hospital, V. Petraitis, Technical report, 2020.

4. J. G. P. et al., https://earthobservatory.nasa.gov/images/146596/airborne-particle-levels-plummet-in-northern-india, 2020.

5. A. Giannini, A. Kaplan, Clim. Change, 152, 449, 2019.

6. C. Heckman, C.J. Heckman, K. Liang, M. Riley, Prev. Med. (Baltim), 123, 71, 2019.

7. H.K. Biesalski, NFS J., 20, 10, 2020.

8. W. Kowalski, Ultraviolet Germicidal Irradiation Handbook, Springer, New York, 2009.

9. T. Carleton, J. Cornetet, P. Huybers, K.C. Meng, J. Proctor, Proc. Natl. Acad. Sci. U. S. A. 118, 1, 2020.

10. K. Wai, P.K.N. Yu, K. Lam, PLOS ONE, 20(8), e0135562, 2015.

11. S.Ratnesar-Shumate, et al., J. Infect. Dis.,222, 214, 2020.

12. J. Herman, B. Biegel, L. Huang, Air Qual. Atmos. Heal, 14, 217, 2021.

13. C.D. Lytle, J.L. Sagripanti, J. Virol., 79, 14244, 2005.

14. Z. Gorvett., https://www.bbc.com/future/article/20200327-can-you-kill-coronavirus-with-uv-light, 2020.

15. J. Tan, et al., J. of Epidemiology & Community Health, 59 (3), 186, 2005. doi:10.1136/jech.2004.020180.

16. J.A. Metz, A. Finn, J. Inf. Secur. 71, S54 (2015).

17. B. Oliveiros, L. Caramelo, N.C. Ferreira, F. Caramelo, 2020, doi:10.1101/2020.03.05.20031872.

18. M.E.R. Darnell, K. Subbarao, S.M. Feinstone, D.R. Taylor, Journal of Virological Methods, 121,85, 2004.

19. G. Beig, et al. GAW Report No. 217, vol. 41, 2015.

20. Kipp & Zonen, Broadband UV Radiometers, www.kippzonen.com, 1–4, 2018.

21. G. Seckmeyer, A. Bais, G. Bernhard, M. Blumthaler, C.R. Booth, K. Lantz, R.L. McKenzie, WMO report No 164, Part 2, 1, 2008.

22. WMO. Report No. 141: Report of the LAP/COST/WMO Intercomparison of Erythemal Radiometers, 2000.

23. G. Salvadori, F. Leccese, D. Lista, C. Burattini, F. Bisegna, Environ. Res. 183, 109274, 2020.

24. P. Gies, E. Van Deventer, A.C. Green, C. Sinclair, R. Tinker, Health Physics, 114, 84,

2018.

25. N. Hatsusaka, et al., Transl. Vis. Sci. Technol. 10, 1 , 2021.

26. D. H. Sliney, J. Photochem. Photobiol. B Biol., 64, 166, 2001.

27. Ianevski, A. et al., Viruses, 11, 207, 2019.

28. Y. Yao, et al., Eur Respir J., 55(5), 2000517, 2020.

29. A.F. McKinlay, B.L. Diffey, CIE J. 6, 17–22, 1987.

30. A.S. Panicker, G. Pandithurai, G. Beig, D. Kim, D. Lee, Advances in Meteorology, 1, 2014.

31. S. Sharma, M. Zhang, J. Gao, H. Zhang, S. Harsha, Sci. Total Environ. 728, 2020.

32. Z.Li, J. Clim., 11, 5, 1998.

33. M. R. Kalippurayil, medRxiv 2020.

34. V. Anand, N. Korhale, S. Tikle, M.S. Rawat, G. Beig, Earth Syst. Environ. , 0123456789, 1-10, 2021.

35. Á. Briz-Redón, Á. Serrano-Aroca, Prog. Phys. Geogr., 44, 591, 2020.

36. A. Gupta, B. Pradhan, K.N.A. Maulud, Earth Syst. Environ., 4, 523, 2020.

37. G. Isaia, H. Diémoz, F. Maluta, I. Fountoulakis, D. Ceccon, Sci. Total Environ., 757, 143757, 2021.

38. P. B. Whittemore, J. Infect. Control, 48, 1042, 2020.

39. F. Mitchell, Lancet Diabetes Endocrinol., 8, 570, 2020.

40. G.Butler lporte, et al., PLoS Med., 18, 1, 2021.

41. R.K. Moozhipurath, L. Kraft, B. Skiera, Sci. Rep., 10, 1, 2020.

42. S.K. Sahu, P. Mangaraj, G. Beig, B. Tyagi, S. Tikle, V. Vinoj, Urban Clim., 38, 100883, 2021.

43. R.Latha, et al., Sci. Total Environ. 759, 144299, 2021.

44. G.Beig, et al., Curr. Sci., 119, 1178, 2020.

About ISAS

The Indian Society of Analytical Scientists (ISAS):

****

The Indian Society of Analytical Scientists (ISAS), born in 1983 at Bhabha Atomic Research Centre (BARC) Mumbai, has now expanded into a 4000 plus strong Indian National Multidisciplinary Professional Forum of Experts In Analytical Sciences, spread over its 10 Chapters (Kerala, TN, Bangalore, Belagavi, Nagpur, Pune, Jaipur, Hyderabad, Baroda and Delhi) with its members making dynamic contributions to the entire cross section of multidisciplinary development activities all over our Nation, that include all industries, academic and R&D institutions, power stations, agricultural and health sectors, environmental and ecological conservation.

Over the past 39 Years, ISAS has organized more than 36 National and International Conferences, and during 2020-2021, organised 75 Weekly Webinars on various topics of interest to the scientific community, which were all very well attended by leading professionals from India as well as abroad.

The main goal of ISAS is to Promote Excellence, Relevance, and Right Direction, in routine and innovative work, by providing top-level analytical expertise in Analytical Sciences, Technology and Management. ISAS is committed to the dissemination of knowledge, expertise, and improved Scientific Temperament of the entire community of analytical scientists, academicians, and students. Almost all the leading scientific and technical institutions in India have been proudly recognizing the positive activities of ISAS by participating and spontaneously supporting all the programs organized by it.

During the past, many leading scientists from various National Laboratories in India, have been the proud recipients of The Prestigious Saastra Pitamaha (Dr. R.Chidambaram), Saastra Tejas Award (Dr Anil Kakodkar), Aatma Nirbharata Award (Dr. K.N. Vyas, Dr A.K. Mohanty, Dr. B. Venkataraman, Dr. Unnikrishnan Nair), Life Time Achievement Awards, Honorary Fellowship Awards, Best Paper Awards conferred by ISAS as a recognition for their Professional Excellence. ISAS has also instituted an Analytical Scientist of The Year Award, starting from 2019.

From 2022, ISAS has started Awarding Indian Manufacturers/ Importers and Innovators working on Analytical Instrumentation.

ISAS is the only National Premier Expert Forum of Analytical Scientists and Technologists in India.

ISAS is now embarking on an Electronic Journal, to promote publication of good quality R&D work so that the information is disseminated amongst the Indian Professionals, Researchers and Students to benefit and impact the national development activities.

Positive Ideas

- Plant Safety Boards/Stickers
- Vertical Rack Product Job Card Board
- SS Metal Name Tag
- Acrylic Sandwich Boards
- Acrylic Product Display
- Event Flex Banners/Boards
- Conference Material
- Gift Articals
- Memento/Souvenir
- Product Display
- Exhibition Banners
- Table Top Banners
- Roadside Tent
- Calendars
- Brochures
- E-Invite

& more....

Call : 93 77 13 20 26
Jayendra Vora
positiveideas@gmail.com

Agilent ICP-QQQ

10 **Years**
of enabling
industry advances

Know Your Results Will Be Accurate at All Levels, Whatever the Sample Type

Powerful, flexible ICP triple quad (ICP-QQQ) supports MS/MS mode for advanced interference control

The Agilent triple quadrupole ICP-MS (ICP-QQQ) is the world's most successful and widely used tandem ICP mass spectrometer. Available in a range of configurations to cover applications from routine contract analysis to advanced research and high-purity materials analysis, the Agilent ICP-QQQ redefines ICP-MS performance, delivering results you can trust. Let the 8900 ICP-QQQ take control of your interferences and put your results beyond doubt.

www.agilent.com